

Masakazu Matsumoto

Topology and Dynamics of Hydrogen Bond Network in Liquid Water

*Department of Structural Molecular Science
School of Mathematical and Physical Science
The Graduate University for Advanced Studies*

1995

Acknowledgments

First of all, I wish to express my gratitude to Prof. Koichiro Nakanishi, Prof. Iwao Ohmine, and many staff of the Graduate University for Advanced Studies (GUAS), for the kindnesses of accepting me after the time limit of entrance application.

This study has been carried out under the direction of Prof. Iwao Ohmine at the Institute for Molecular Science (IMS) and Nagoya University since 1992. Molecular dynamics simulations, normal mode analysis and quenching programs are based on Dr. H. Tanaka's and more than 600 programs are newly developed for analyzing the simulation results. Most analyses were held on HP9000 series 735.

I'd like to express my heartfelt thanks to Prof. Iwao Ohmine for his valuable suggestions and stimulating discussions throughout the study. I also thank for his continuous encouragement and financial supports.

I am greatly indebted to Prof. Masaki Sasai and Dr. Hideki Tanaka. Prof. Sasai gave me a lot of suggestions for water. I was also influenced by Dr. Tanaka, who encouraged me and gave me his philosophy as well as many suggestions. I also thank Dr. Ken'ichiro Kouga for his valuable suggestions and fruitful discussions. My research is no doubt affected by their insight into water.

I wish to thank Dr. Tamiki Komatsuzaki, Dr. Shinji Saito, Dr. Akira Shudo, Dr. Shoji Takada, Dr. Tooru Yoshida, Mr. Masakatsu Ito, Mr. Yuji Michihiro, with whom I took issue on every topic all night long when I was at IMS. I was learnt there "what a profession the researcher is". The days I spent with them in Okazaki were truly worthwhile.

I would like to thank Mr. Kousuke Douga, Mr. Yoshihiro Hirata, and other members of our laboratory at Nagoya university, who made my life in Nagoya comfortable. I am glad to get acquainted with them. These skillful students also assisted me and reduced my system administration tasks.

My best appreciation is given to my parents, Kenji and Akiko, for their unchangeable supports. I also wish to thank from my heart the people who rescued and helped my family at the time of Kobe Earthquake.

Nagoya
Nov. 1995

Masakazu Matsumoto

Contents

1	General Introduction	9
2	Simulation Methods	16
2.1	Molecular Dynamics	16
2.2	Inherent Structure of Water	17
2.3	Voronoi Polyhedra	17
3	Static Properties of Hydrogen Bond Network	19
3.1	Hydrogen Bond	19
3.2	Structure	21
4	Dynamic Properties of Hydrogen Bond Network	29
4.1	Collective Motions in Water	30
4.1.1	Hydrogen Bond Rearrangement Map	30
4.1.2	Distance Matrix	30
4.1.3	Network Distance Matrix	32
4.1.4	Indices for Collective Motions	33
4.1.5	Global Topological Indices	34
4.2	Local Structure and Dynamics	38
4.2.1	Topological and Dynamic Parameters	38
4.2.2	Graphical Analysis	46
4.2.3	Lattice Model	51

4.2.4	Discussion	55
4.3	Some Other Analyses and Remarks	58
4.3.1	Survey of the Potential Hypersurface	58
4.3.2	Probabilistic Automaton, Spinglass and Water	60
4.3.3	Comparison with Random Bond Percolation	61
5	Conclusions	100
A	Defect Motion on Sparse Network	102
B	Heterogeneity Index	106
C	Simulation Methods and Algorithms	108
C.1	Voronoi Polyhedra Tessellation	108
C.2	Voronoi Grid Tessellation	109
C.3	Number of n -rings in the Network	110
C.4	Block Diagonalization of the matrix	113
C.5	Visualization	115

List of Tables

4.1	Various indices for global network structure rearrangement	36
4.2	The simultaneous correlation of various global topological indices	37
4.3	Various topological indices	39
4.4	Various indices of structure rearrangement.	39
4.5	Various correlation between two topological indices at 240K	41
4.6	The correlation between two topological indices at 300K	41
4.7	Various correlations between topological index and dynamic index at 240K	42
4.8	The correlations between topological index and dynamic index at 300K	43
4.9	Various correlation between two dynamic indices at 240K	45
4.10	The correlation between two dynamic indices at 300K	45
4.11	The probabilities of disconnecting a hydrogen bond (HB)	49
4.12	The defect propagation probabilities	56

List of Figures

3.1	First hydration shell	23
3.2	The pair interaction distribution	24
3.3	The oxygen-hydrogen RDF	25
3.4	The decomposed RDF	26
3.5	The second and third hydration shell	27
3.6	The decomposed PID	28
4.1	The hydrogen bond rearrangement map	64
4.2	Distance matrices of liquid water at 248K	65
4.3	Distance matrices of liquid water at 273K	66
4.4	Partial distance matrices at 240K	67
4.5	The Hamming distance <i>vs.</i> Euclidean distance	68
4.6	Hamming distance matrices	69
4.7	The coherency index	70
4.8	Power spectra of various local topological indices at 240K	71
4.9	Power spectra of various local topological indices at 300K	72
4.10	The separation scheme of the HB network	73
4.11	The state transition diagram of a node	74
4.12	Three types of defect motion	75
4.13	The HBR frequency in various time and temperature	76
4.14	Energy fluctuations in the model lattice systems	77

4.15	The HB lifetime distribution obtained for the models	78
4.16	The heterogeneity index	79
4.17	The potential energy profile in the quenching process from an instantaneous structure at 240K.	80
4.18	The potential energy profile in the quenching process from an instantaneous structure at 300K.	81
4.19	The potential energy profile in quenching processes from successive instantaneous structures at 240K.	82
4.20	The potential energy profile in quenching processes from successive instantaneous structures at 300K.	83
4.21	The distance matrices in quenching process	84
4.22	The survived hydrogen bond cluster	85
4.23	The average diameter of σ -clusters in liquid water	86
4.24	The average diameter of clusters in random bond lattice model	87
4.25	The cluster size distribution of the random bond lattice model	88
4.26	The size distribution of the σ -clusters in liquid water	89
4.27	The size distribution of the α -clusters in liquid water	90
4.28	The diameter distribution of the size=6 cluster in random bond lattice model with various lattices.	91
4.29	The diameter distribution of the α_6 -clusters in liquid water	92
4.30	The diameter distribution of the σ_6 -clusters in liquid water	93
4.31	The diameter distribution of the size=7 cluster in random bond lattice model with various lattices.	94
4.32	The diameter distribution of the α_7 -clusters in liquid water.	95
4.33	The diameter distribution of the σ_7 -clusters in liquid water.	96
4.34	The diameter distribution of the size=8 cluster in random bond lattice model with various lattices.	97

4.35	The diameter distribution of the α_8 -clusters in liquid water	98
4.36	The diameter distribution of the σ_8 -clusters in liquid water	99
A.1	Possible motions of a defect on the network	104
C.1	The cavity in liquid water	116
C.2	Low and high density Voronoi polyhedra	117

Chapter 1

General Introduction

Water is the most omnipresent material on earth as well as the most indispensable element for all living things. Its physical properties are very different from other liquids.[F 72a] For example, most liquids expand by about 10% on melting, while water shrinks about 10% on melting and has the density maximum at 4°C. Its boiling and melting points are about 1.5 times higher than those of other hydrides in the same family. These are ascribed to the hydrogen bonding (HB) but are by no means unique, as other hydrogen bonding liquids show similar tendency. The uniqueness of water among hydrogen bonded molecular liquids is due to the fact that water forms the three-dimensional HB network structure. The structure and dynamics of liquid water are strongly controlled by the HB network. The latent heat of melting, about 1.43kcal/mol, means that only 10% of HB are broken, while 90% of them are retained, upon melting from ice to liquid water. Water thus can be regarded as the mixture of the normal component and the anomalous component. The latter anomalous component, arising from three-dimensional HB formation, dominates in the low temperature. For most liquids, the isothermal compressibility χ_T , which is proportional to the density fluctuation, decreases with decreasing temperature. This is also true for water at high T , but χ_T has a minimum at 46°C and actually increases as T decreases.[F 72b] In addition, the constant-volume specific heat C_v , which is proportional to the energy fluctuation, is extremely large in case of liquid water.

Dynamical properties of liquid water show also the dramatic difference from normal

liquids. The self diffusion coefficient becomes almost 10^5 times larger when melting, and this ratio is 10 times larger than argon.[F 72a] Moreover, the self diffusion coefficient decreases as the density is lowered on the contrary to normal liquid motion.

These anomalies of water become distinct at low temperature, especially at supercooled region. Numerous studies on supercooled liquid water has been made and found divergence of various thermodynamic properties, including isobaric specific heat,[AST 73] density,[AST 73, RM 73] isothermal compressibility,[SA 76] velocity and absorption of sound,[RLC 77] relative permittivity,[HS 76, HA 78] density fluctuation, [BTS 81], structural relaxation times of shear viscosity[H 63] or spin-lattice relaxation time[LH 82]. Angell indicated that these properties are going to diverge at unreachable temperature $T_a \simeq -45^\circ\text{C}$, and assumed there is a phase transition from fragile liquid to strong liquid at the temperature. [A 82, SA 76, A 93]¹

Each water molecule is binded to about four water molecules, forming very directive HBs. The HB network in water is well percolated but topologically distorted. Strong and weak HB regions are marbly mixed in the network and its distribution alters in time. In the short time scale (about pico second order), water is found to yield intermittent collective motions and large energy fluctuations associated with HB network rearrangement (HBNR).[OTW 88, TO 89] It is of the current interest to explore the physical origin of these cooperative motions.

Many models have been proposed to describe the properties of water from spectroscopic and thermodynamics data. Bernal and Fowler studied the irregular tetra-coordinated structure in liquid water by the X-ray diffraction analysis of liquid water, and constructed the pseudo crystalline model.[BF 33] X-ray diffraction data by Morgan and Warren clearly

¹There are also negative observations by Xie *et al* [XLMHS 93] and Dings *et al* ,[DME 92] where small angle X-ray diffraction results show that the density fluctuation does not diverge at T_a and concluded that there is no spinodal line or critical point. The discrepancy between the experiments are arisen from the fact that water is very difficult to be supercooled. Any observation under deeply supercooled condition is made in small micropore, where the surface effect may not be negligible.

showed the tetrahedral order in liquid water, which led to the filling-in model.[MW 38] Pople treated the structure of liquid water as the distorted hydrogen bond network in his continuum model[P 51] and Bernal extended his model to the random bond model.[B 64] While Némethy and Sheraga extended the idea of flickering cluster model by Frank and Wen[FW 57, F 58] and proposed their 5 state description.[NS 62] There have been many other n -state description used by experimental chemists.[B 78, GLS 88, GLS 86, HS 90, AR 84] These models are, however, mainly based on phenomenological assumptions.

Rahman and Stillinger's computer simulation marked a new epoch in the theory of liquid water.[RS 71, RS 73, SR 74] Their Molecular Dynamics (MD) study clarified many essential features of the dynamic properties as well as the structure of liquid water. It was shown that HBs are strongly deformed and there do not exist distinctive cluster structures in liquid water. It was also found that some kinds of cooperative molecular motions are involved in liquid water. However, it has not been clear what are the spatial, time and energy scales of the cooperativity involved in the dynamics. The main difficulty in dealing with liquid dynamics is how to extract the core structural changes in dynamics (e.g., the fundamental changes in the hydrogen bond network rearrangement in liquid water), which is buried in the thermal noise (*ie* vibrational movements). Stillinger and Weber introduced the concept of inherent structure and exposed the intrinsic dynamics of simple liquids and clusters.[SW 83a] They regarded the dynamics of the system as the motion of phase point on the potential hypersurface, and separated the motion into two components, the intrinsic reaction path from one minimum to another minimum and the vibration perpendicular to the reaction coordinate. The structures at those minima are called inherent structures. This inherent structure analysis was applied to water by Tanaka and Ohmine[TO 89], where water potential hypersurface was surveyed and its undulation was discussed.

The origin of the large local energy fluctuation in liquid water was investigated by Tanaka *et al* .[TO 87, OTW 88, OT 93, O 95] Although the binding energy per hydrogen bond is as strong as -20kJ/mol , the hydrogen bond is sometimes easily disconnected and make

another connection with a neighboring water molecule. The cooperative molecular motion requires less total energy to rearrange the hydrogen bonds. By this mechanism, energy is quickly transferred from one molecule to another. They termed this energy transfer mechanism “flip-flop mechanism”. Their observations extract another layer of collective dynamics, where tens of water molecules move intermittently and collectively.² Sasai *et al* connected these intermittent structural rearrangement with $1/f$ type energy fluctuation in liquid water.[SOR 92] On the other hand, Giguère called the series of rearrangement motion via bifurcated hydrogen bond as the collective motion.[G 87]³

The effect of the collective dynamics is very important for the chemical reaction in the aqueous solution.[BGWH 86, GBWLH 86, GWH 88, WL 88] Ohmine pointed out that the vibrational energy dissipation of a photoexcited solute in liquid water is very fast and the excess energy of the solute molecule is quickly transferred to surrounding solvent water molecules.[O 86] Such a quick energy dissipation is due to the existence of strong energy exchange mechanism of the flip-flop type and the large energy fluctuation in water.

The recent progress in the theory of liquid also backs up in studying liquid water and aqueous solutions. Particularly, the extended RISM (Reference Interaction Site Model) and its derivatives are applicable for many static phenomena in liquid water.[HR 81, HRP 83] Its dynamic extension is also proposed by Hirata.[H 92]

Water has been a prototype liquid, where a lot of approaches are applied for. The idea of percolation is introduced to liquid water by Geiger *et al* .[GSR 79] Stanley *et al* applied the site percolation model to show that the icelikeness in liquid water are arisen from the four bonded patches in the hydrogen bond network and the homogeneous distribution of hydrogen bond results in the inhomogeneous distribution of patch.[ST 80, GS 82]

Speedy *et al* discussed the stability of five-membered ring structure in the hydrogen bond

²Jump diffusion of water molecule is detected by Bellissent-Funel *et al* using inelastic incoherent neutron diffraction.[MBCLT 93] It may be an evidence of intermittent structural rearrangement.

³The definition of the collective motion is not united. For example, Green *et al* regarded that the extension of the tetrahedrally hydrogen bonded region in the hydrogen bond network is detected as the magnitude of collective band in the Raman spectroscopy.[GLS 88, GLS 86, HS 90]

network.[S 84, SM 85, SMJ 87] ⁴

Grunwald first paid attention to water molecule with five hydrogen bonds.[G 86] Giguère pointed out the existence of the bifurcated hydrogen bond from X-ray diffraction data, and showed that when liquid water is supercooled, the ratio of bifurcated bond comes to zero around -45°C . [G 87] Stanley *et al* regarded that the five-coordinated water molecule works as the catalyst on rearranging the hydrogen bond network.[SGS 91]

A large number of computer simulations have been performed for supercooled water. [MSG 87, P 92, PSES 93, PSGSA 94, R 83, S 90, SPSH 90, S 84, SAEHPF 94, S 80, SW 83a] Poole *et al* did enormous computation to determine the phase diagram. They predicted the coexistence of low- and high-density amorphous states, and the existence of the second critical point in water phases.[PSES 93, PESS 93, SAEHPF 94, P 92]⁵ By computer simulations, however, it is difficult to reproduce the behavior near the critical point or glass transition, where very long time or large scale fluctuation are very important. Many lattice models are also proposed to reproduce the phase diagram of water. Sasai applied a lattice model utilizing the method of polymer physics to reproduce the water phase diagram at low pressure⁶. [S 90, S 93] Stanley *et al* also proposed a lattice gas model and discussed the existence of spinodal and the second critical point.[SSS 93] Many more intense studies are being made for the supercooled state of water.

Ruocco *et al* defined the index of asphericity of the Voronoi polyhedron and analyzed the relationship of the shape of the polyhedra to the structure [RSV 92, SSM 94] and to the dynamics [RSTV 93] of the hydrogen bond network. They indicated that the four-coordinated water molecule diffuses slower than three- or five coordinated molecules. [RSTV 93] This is one of the known most reliable evidences of relationship between the local structure and the local dynamics.

⁴Mausbach *et al* could not find any evidence of special properties in the ring structure. [MSG 87]

⁵Tanaka recently made very long time simulation at supercooled state and pointed that the second critical point should be placed at negative pressure region. [T 95] It is an issue of current debate.

⁶As far as our knowledge concerns, we do not know any model to deal with water under higher pressure, where many polymorphs of ice appear.

These topological indices are determined from the instantaneous structures and indicate the topological inhomogeneity in the hydrogen bond network. Describing this type of correlation between local structure and local dynamics is, however, not sufficient to understand the water dynamics because there is no information of cooperativity in it. We rather need to know the method to analyze the collective motions directly. By treating the water system as the dynamic network system, we can extract the essential information of the structure and dynamics of water. Many methods and theories of the network systems have already been developed in the fields other than chemistry; especially useful are the theories of graph, information, percolation and probabilistic automaton.

In this thesis, we have mainly focused on the relationship between the motions of individual water molecules and the dynamics of the hydrogen bond network. Experimental results can provide us with only a distant view of the microscopic dynamics, whereas the molecular dynamics simulation gives us much detailed information. The raw information obtained is, however, too complicated to understand the essential element of the dynamics. Although the statistical mechanics and the theory of liquids have been developed for several decades, there are only few theories directly dealing with the multidimensional dynamics.

Chapter 2 describes the methods used in the present work, the simulation and the analysis methods, including the molecular dynamics method, the quenching, and the Voronoi polyhedra tessellation. Detailed algorithms are also given in Appendix C. In Chapter 3, the static properties of liquid water are re-examined from the view point of network topology. Roles of the molecules in the first, second and farther coordination shells are clearly assigned assuming the network topology. The dynamic properties of liquid water are examined in Chapter 4. In Section 4.1, we introduce various indices of collective motion to show how the collective motions occur in liquid water. In Section 4.2, the local and short time rule of the hydrogen bond network rearrangement is extracted from the molecular dynamics calculation. Based on the rule, the network defect is defined, and then the collective motions are simply represented by the motions of network defects. This rule

is further used to construct a lattice dynamics model which reproduces the hydrogen bond rearrangement. The last section of this chapter describes the various other models and methods applied for water dynamics.

Chapter 2

Simulation Methods

The simulation methods utilized for this work are overviewed in this chapter. In order to determine important topological indices expressing the hydrogen bond rearrangement dynamics, we have first performed the molecular dynamics (MD) calculations for supercooled water systems.

2.1 Molecular Dynamics

The simulation is mainly performed for the system with 216 water molecules contained in a cubic box.¹ The periodic boundary condition is applied for the simulation cell. To keep the pressure of the system constant, Andersen's constant-pressure method [A 80] is implemented. The temperature is also kept constant by Nosé's constant-temperature method [N 84]. The trajectory calculation is done by integrating the Newton-Euler's equations of motion for rigid body. There are many choices for the integration method. In this work, Gear's Predictor-Corrector method is used.[G 71] In the molecular dynamics simulations, the calculation of the force is usually the most CPU consuming step. Popular integration methods like Runge-Kutta method or symplectic integration method requires many force calculations to advance one step of the simulation. On the contrary, in Gear's algorithm, the calculation of the forces is only once at a step. TIP4P potential function [JCMIK 83]

¹Some calculations are performed for 64-particle system.

is used and the intermolecular interactions are smoothly truncated at around 9Å. Any correction for long range interaction (*ie* Ewald sum) is not applied. Trajectories are recorded for about 100 to 1000 ps, depending on temperature.

2.2 Inherent Structure of Water

An instantaneous structure of the system is expressed by a phase point in the configurational space. The trajectory runs on the potential hypersurface, which consists of many potential wells. By quenching the system, any instantaneous structure in the same basin comes to one local minimum energy structure, called inherent structure. Stillinger and Weber first introduced the concept of inherent structures to analyze the liquid dynamics.[SW 83a] By projecting the instantaneous structure into each inherent structure, the dynamics of the system is easily understood as the repetition of stagnation and transition. In applying the inherent structure to water dynamics, most “bifurcated” or “half-binded” hydrogen bonds are assigned to the distinct hydrogen bonds and the ambiguity of the structure is removed. Tanaka and Ohmine applied Elber and Karplus’s method[EK 83] to determine the reaction coordinate between the successive inherent structures and calculate the barrier height distribution of the transition states.[TO 89]

In our calculation, the quenching is performed by the steepest descent method solving the equation

$$\mathbf{m} \frac{\partial \mathbf{r}}{\partial s} = - \frac{\partial \phi(\mathbf{r})}{\partial \mathbf{r}}, \quad (2.1)$$

which denotes the overdamped motion on the potential hypersurface. s is the virtual time variable.

2.3 Voronoi Polyhedra

When a set S of N points in space is given, we can always make a region around a point p_i in which any point is closer to p_i than any other points in the given set S .

Take a set of points which are nearer to a molecule i than to any other molecules. Such a set of points form a polyhedron around the molecule i . The polyhedron is called the Voronoi polyhedron (VP) of the molecule i .

VP is equivalent to Wigner-Seitz cell in the crystal and includes all information of neighborhood relations. As the tessellation is determined only by the positions of points, it is useful to understand the local structure on the molecular system.

There have been a lot of applications of Voronoi polyhedron for the analysis of the simple liquid with topological randomness,[F 70, HR 79a, HR 79b, CFW 81, T 86, NY 86, WT 87] and some for liquid water and ice.[RSTV 93, R 83, RSV 92, SSM 94]

The detailed algorithm to determine the Voronoi polyhedra in the system with periodic boundary condition is given in Appendix.

Chapter 3

Static Properties of Hydrogen Bond Network

Liquid water and ice form three dimensionally percolated network of the hydrogen bonds. Each water molecule is binded to four adjacent water molecules on the average. This number of the first neighbor molecules is much smaller than that of a simple liquid (about ten). Two of them, on the average, are ‘donating’ or ‘outgoing’ hydrogen bonds (*ie* hydrogen atom is donated to create a hydrogen bond with oxygen atom of another water molecule), and the other two, on the average, are ‘accepting’ or ‘incoming’ hydrogen bonds (*ie* hydrogen atom of another water molecule is accepted to create a hydrogen bond).

The spatial distribution of neighboring molecules around a water molecule is depicted in Fig. 3.1. The neighborhood molecules occupy tetrahedral positions. The distribution lobes at oxygen side of the central water molecule are broadened.

The static structure of the hydrogen bond network has been well investigated by many authors. In this chapter, the characteristics of the static structure is briefly introduced.

3.1 Hydrogen Bond

Before discussing the detailed structure of the hydrogen bond network, the definition of the hydrogen bond should be given. The short range structure of a water molecule is tetrahedral. The criteria for the hydrogen bond should, therefore, satisfy the condition so

that each water molecule has about four hydrogen bonds under normal thermodynamic condition. There are various possible definitions of the hydrogen bond satisfying such a criteria. Following are the examples:

- Belch and Rice[BR 87]
 1. Hydrogen-Lone Pair distance $< 2\text{\AA}$
 2. Suitable configuration of two molecules
 3. If there are some combinations for hydrogen and lone pair, most linear bond is chosen and other choices are neglected.
- Geiger/Mausbach/Stanley/Teixeira[BSGM 84]
 1. Pair interaction energy $< V_{\text{HB}}$
 2. Oxygen-oxygen distance $< 3.5\text{\AA}$
 3. Upper limit of the number of hydrogen bond is 4
- Rahman/Stillinger[RS 73]

Pair interaction energy $< V_{\text{HB}}$
- Speedy[S 84]
 1. Pair interaction $< V_{\text{HB}}$
 2. Upper limit of the number of hydrogen bond is 4
 3. Hydrogen bonds are searched iteratively so as not to bind more than four hydrogen bonds at a water molecule.

Among these, we have chosen the simplest definition in this study; two water molecules are hydrogen bonded if their interaction energy is lower than V_{HB} , and the value of V_{HB} is determined to -10kJ/mol from the distribution of the pairwise interaction energy shown

in Fig. 3.2. This threshold value is nearly equal to the value obtained from Raman spectroscopy and other experiments.[WC 91, WFHW 86, WI 66, W 72] Such a definition of the hydrogen bond gives rise to “bifurcated” hydrogen bonds. By quenching, the hydrogen bonds are assigned more definitely; these bifurcated bonds reduce to either of the hydrogen bonded or not. The pair distribution function between the hydrogen and oxygen shows the sharp separation of the hydrogen-bonded peak in Fig. 3.3.

3.2 Structure

Let us now analyse the static structure in terms of the hydrogen bond network. Local configuration of a water molecule is tetrahedral, that is, molecules in the first coordinate of a water molecule occupy only four of the eight vertices of a cube and other four vertices are vacant. It is of interest here to know how the cavity in liquid water are structurized. A water molecule in ice makes four large Voronoi faces with first neighbor molecules and small faces with third and fourth neighbor molecules, but does not make Voronoi face (*ie* is not adjacent) with the second neighbor molecules¹; a molecule is surrounded solely with four water molecules and four large cavities. The radial distribution function (RDF) of water is shown in Fig. 3.4. In the figure, RDF is decomposed into peaks according to the path length (*ie* n -th neighbor) along the hydrogen bond network. RDF of ice has sharp distinct first peak and well-separated layers of hydration shell. The wide gap between the first and the second peak shows the existence of the cavity. On the other hand, each RDF component forms asymmetrically broadened peak in liquid water, that is, the cavities around the central molecule are distorted and the third and fourth neighbor molecules approach. These configurations arise from the distortion of the O-O-O angle in water.

The spatial distribution of the water molecules classified by the path length along the hydrogen bond network is shown in Fig. 3.5. In ice Ic, the second neighbor (*ie* path

¹It is the case of hexagonal ice (ice Ih). There is no face with fourth neighbor molecule in ice Ic. The degree of neighbor is here defined along the hydrogen bond network.

length= 2) molecules are located at the symmetric 12 positions. The distribution is slightly broadened by the libration of the central molecule. On the other hand, the distribution lobe of the second neighbor molecules in liquid water forms continuous tori around the four axes through the first neighbor molecules. The outline of the third neighbor lobe is more ambiguous. The distribution of the third neighbor still holds high anisotropy.

The pair interaction distribution has been already shown in Fig. 3.2. A separated peak exists at -20kJ/mol , which represents the hydrogen bonded pairs. There seem to exist two shoulders at the both side of this main peak. In order to obtain further information, the pair interaction distribution is classified by the path length along the hydrogen bond network as shown in Fig. 3.6. It looks that the second neighbor molecules mainly contribute to the shoulders, *ie* some of pairwise stable configurations unstabilize the second neighbor. In the case of ice, the distribution of the pair interaction with the second neighbor forms definite peaks at the both side of the ordinal. The spatial distribution of the second neighbor molecules with the positive interaction energy coincide with the distribution of the whole second neighbor molecules.² The third and further neighbor molecules yield only small contribution.

As a summary, the roles of the pairwise interactions are clearly classified by the path length along the hydrogen bond network. The first neighbor molecules are no doubt important for the stability of the central molecule, and the second neighbor molecules also affect to the stability of the central water molecule.

²Li and Ross showed that there are two types of configuration for a hydrogen-bonded pair of water molecule in ice, where a configuration is twice as strong as the other.[LR 93] In our calculations, however, Only a slight constriction at the hydrogen bond peak (left peak) is found and such a dramatic difference in the first neighbor interaction cannot be seen in Fig. 3.6.

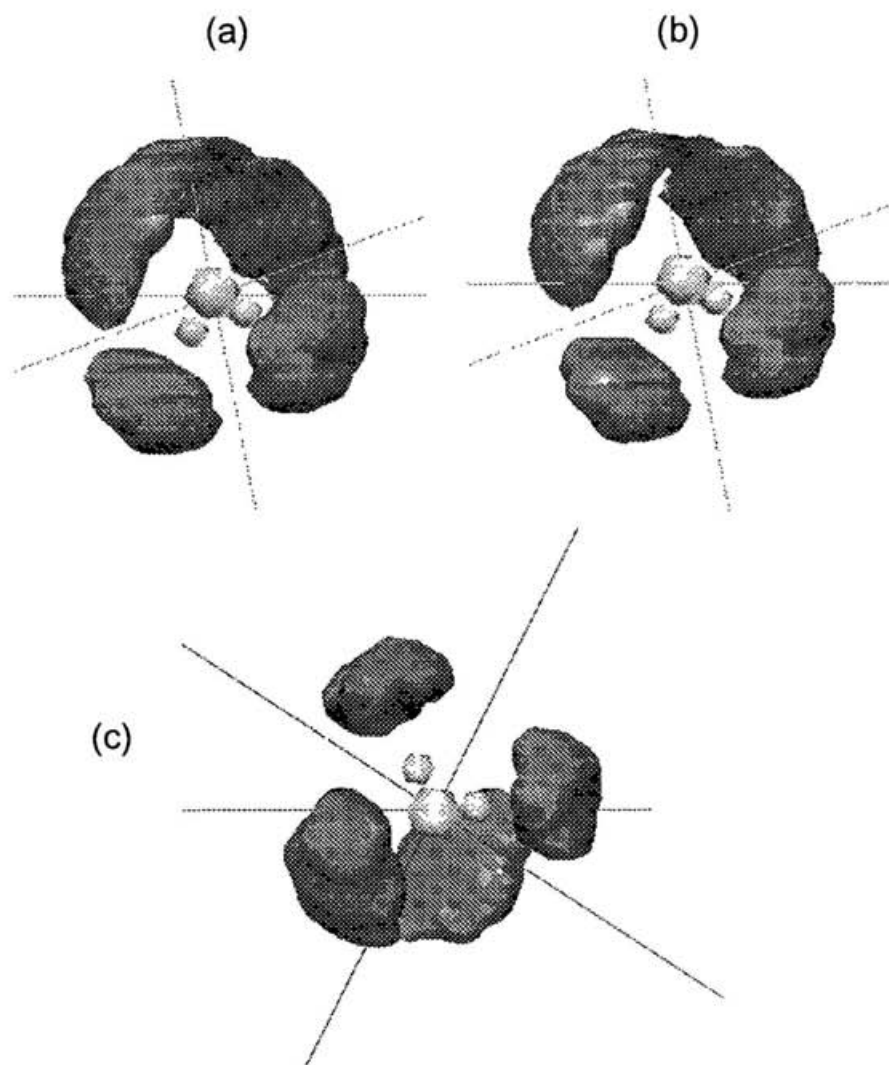


Figure 3.1: Illustrations of the water molecule distribution around a water molecule by molecular coordinate. Relative density threshold is 1.0 (*ie* the region where relative density is higher than the average is filled). (a) Liquid water at 300K; (b) Supercooled water at 240K; (c) Ice Ic at 240K. Only the first hydration shell is shown.

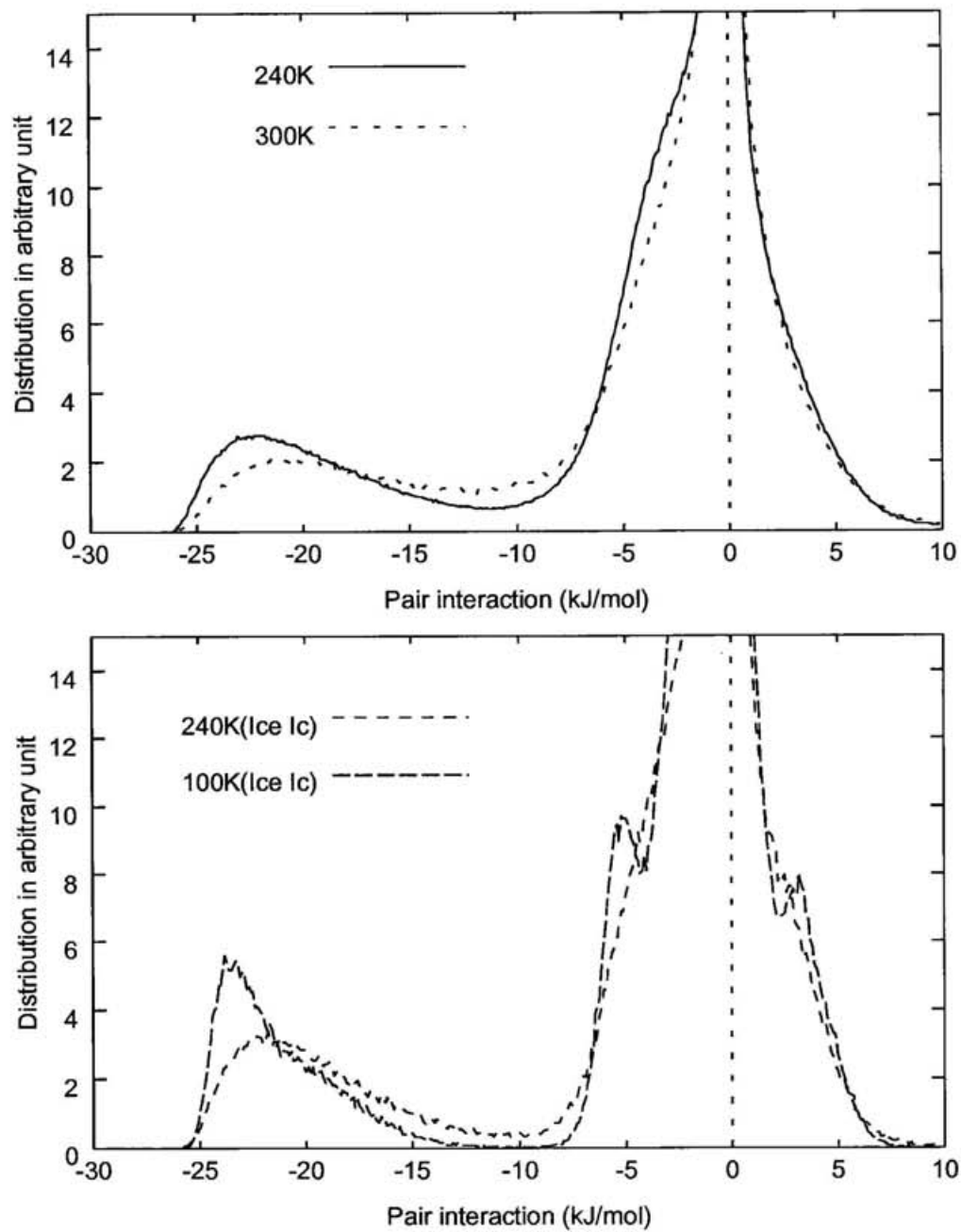


Figure 3.2: The pair interaction distribution for water; upper: liquid state at 240K and 300K; lower: ice at 240K and 100K. Second peak around -20kJ/mol corresponds to hydrogen bond.

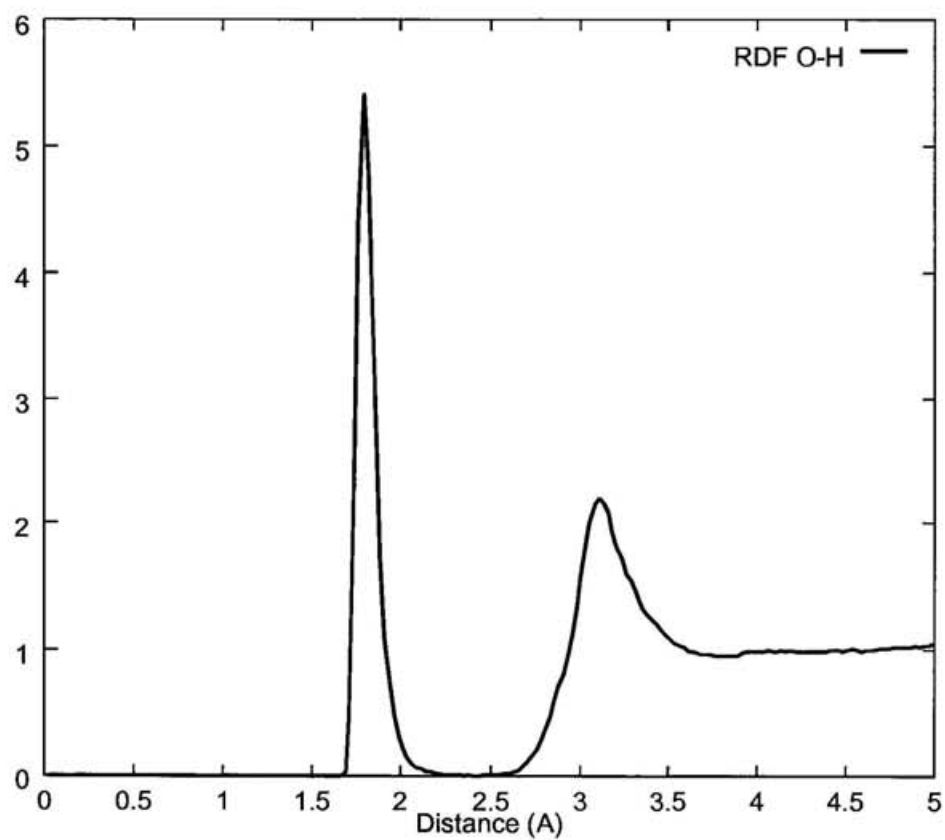


Figure 3.3: The radial distribution function of oxygen-hydrogen pair quenched from liquid state at 298K.

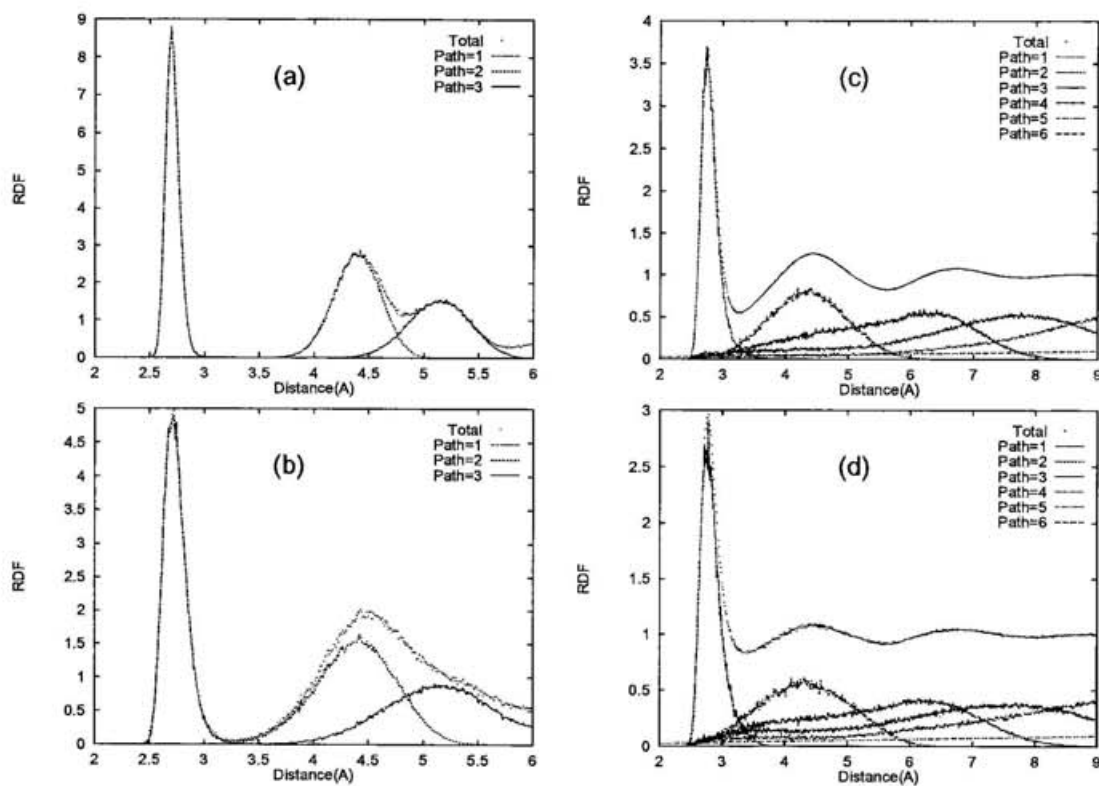


Figure 3.4: The radial distribution function between centers of mass of (a) ice Ic at 100K, (b) ice Ic at 240K, (c) liquid water at 240K, (d) liquid water at 300K. The distribution is decomposed into path length along the hydrogen bond network.

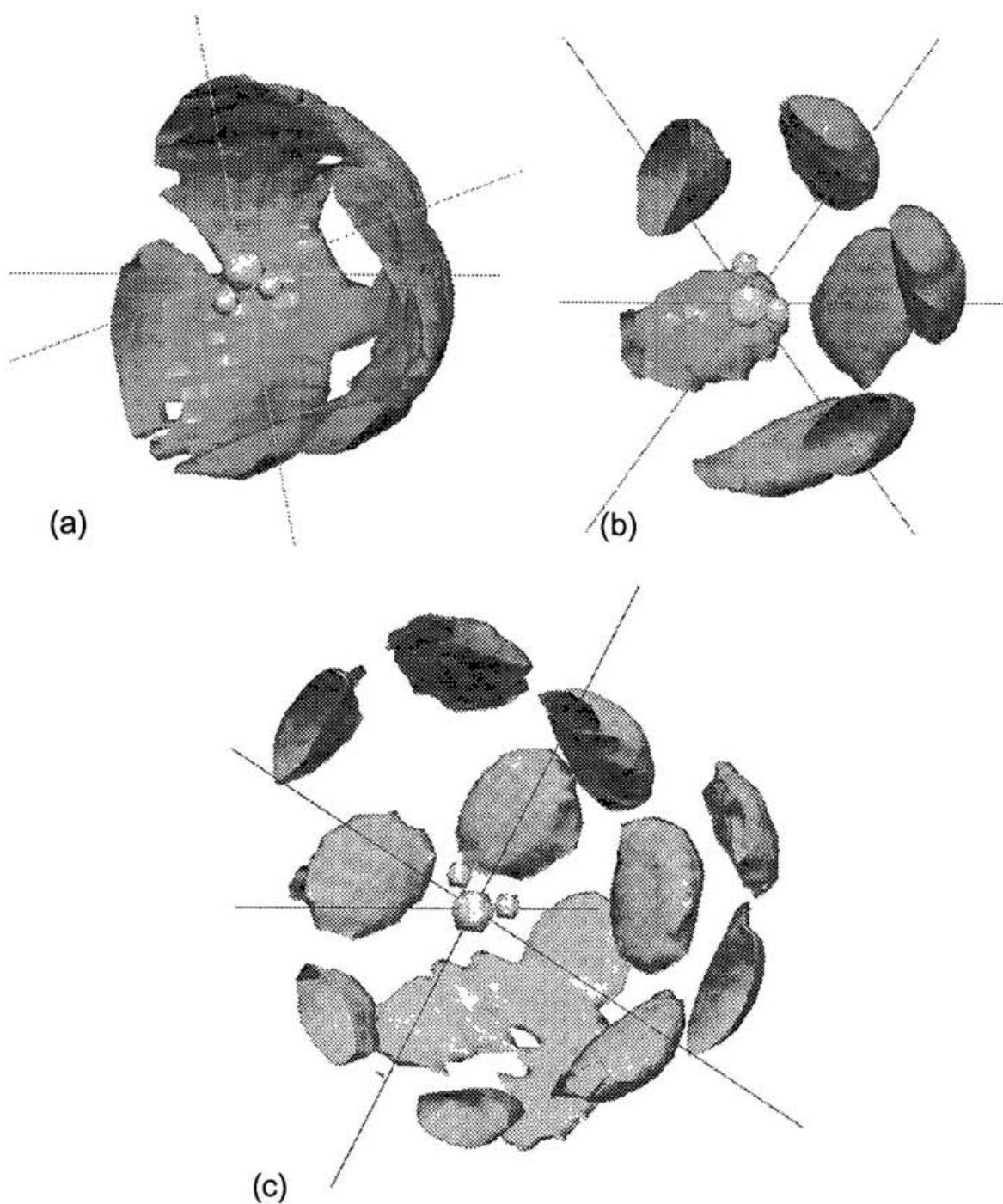


Figure 3.5: The spatial distribution of the hydration shell. The lobe indicates the higher probability region than average. (a) second neighbor in liquid water at 240K; (b) second neighbor in ice Ic at 240K; (c) third neighbor in ice Ic at 240K. The distribution is split in the molecular plane of the water and a half is displayed.

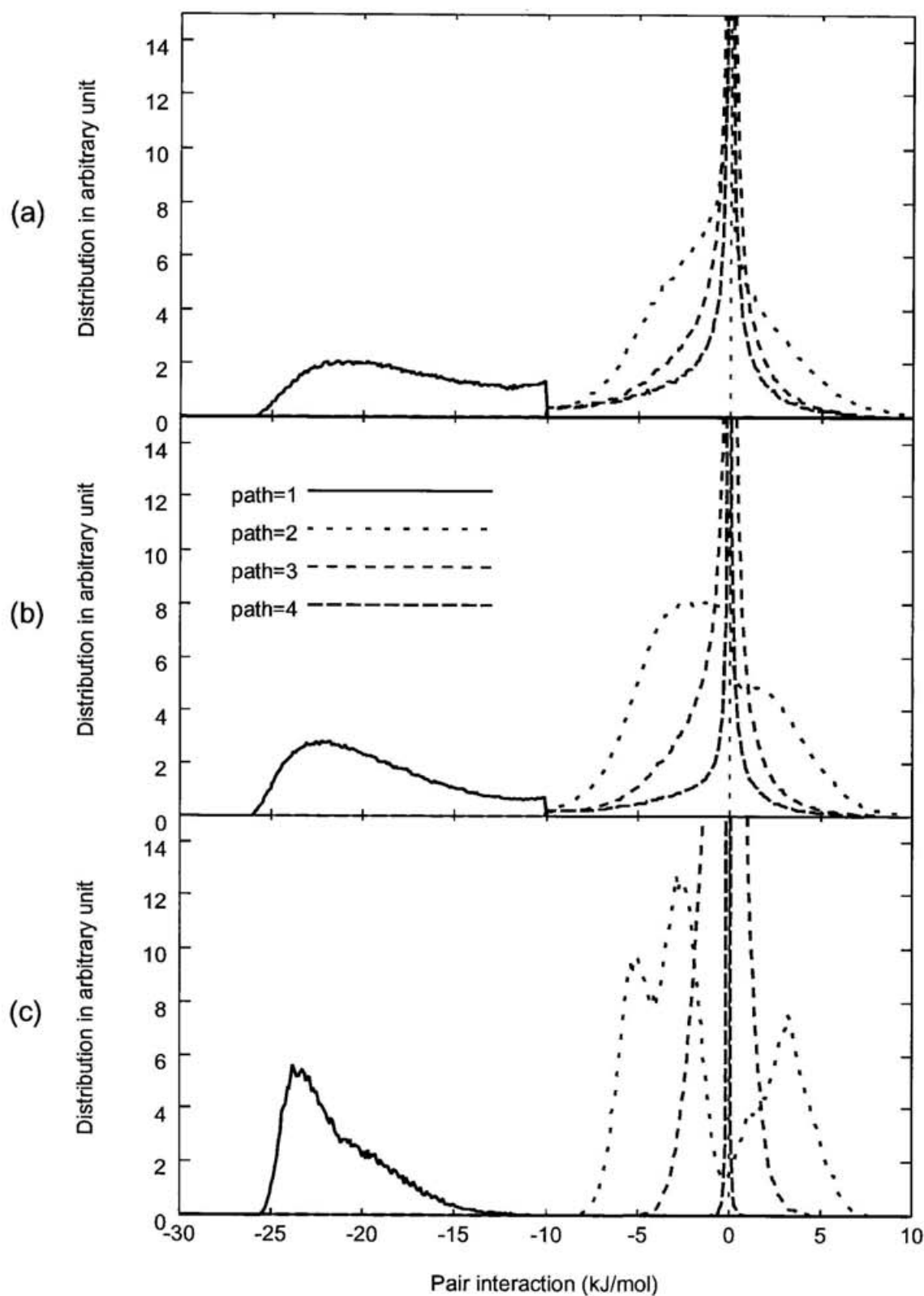


Figure 3.6: The pair interaction distribution classified by the path length along the hydrogen bond network in (a) liquid water at 300K; (b) liquid water at 240K; (c) ice Ic at 100K.

Chapter 4

Dynamic Properties of Hydrogen Bond Network

The motion of water molecules is described by the motion of a phase point in a $12N$ dimensional phase space, where N is the number of molecule.¹ In order to deal with the dynamics with very many degrees of freedom as in the present case ($N = 216$ in our study), it is essential to separate the fundamental motions from other stochastic motions.

Many ideas of understanding high dimensional motion have been proposed. Traditional thermodynamics gives the viewpoint of regarding the high dimensional motion as the motion of phase point in the $6N$ dimensional configuration space. The motion of the phase point is ruled by the undulation of the potential energy hypersurface. The stagnation and the transition of the phase point are detected as the intermittent structure rearrangement. To explain the motion of the phase point, it is required to characterize the profile of the potential energy hypersurface.

Despite of its fluctuating nature of water, the network appears to be homogeneously distorted. Many efforts have been thus made to describe the relationship between local structure and its dynamics in liquid water.

In Section 4.1 of this chapter, we will show how the water molecules move collectively, introducing various indices of collective motion. In Section 4.2, local rules for network motion

¹Degrees of freedom of intramolecular vibration are not included in our calculations.

is carefully extracted and a new approach to describe the rearrangement of the hydrogen bond network is suggested, where the transport mechanism of the network frustration is related to the collective dynamics of water. The last section is spent for describing various methods applied on related topics.

4.1 Collective Motions in Water

In this section, various indices are introduced to define the collective motions in liquid water. The cooperative nature of water is distinctly described by these indices. The motion of water molecules is diffusive in long time, but intermittent in short time around tens of pico second. These intermittent motions occur everywhere in the system. The spatiotemporal relationship of local motions in the large systems should be clarified.

4.1.1 Hydrogen Bond Rearrangement Map

The most primitive point of view of the intermittent molecular motion may be given by listing the frequency of hydrogen bond forming-breaking at each molecule. The HBNR map is indicated in Fig. 4.1, where ‘#’ is put when any hydrogen bond of a water molecule i is rearranged (*ie* connected or disconnected) at time t . The vertical white gap implies that the molecule is not active for a long time. The simultaneous appearance of ‘#’ marks on the horizontal line indicates how many water molecules are simultaneously rearranged their hydrogen bonds. As the total number of molecule is relatively larger (216 molecules) than the cluster size of the collective motion, the intermittency is hard to be seen in this map.

4.1.2 Distance Matrix

To understand the molecular motions in liquid, the “distance” between two configurations at different times is a very useful measure. Euclidean distance is defined by

$$D(t, t') = \left(\sum_{i=1}^N |\mathbf{r}_i(t) - \mathbf{r}_i(t')|^2 \right)^{\frac{1}{2}}, \quad (4.1)$$

where $\mathbf{r}_i(t)$ is the position of the center of mass of i th water molecule at time t . The element d_{ij} of the distance matrix denotes the distance between time t_i and t_j , that is, the change of the system. If the structure of the molecular system changes continuously, the distance matrix forms band structure. It is case for gas or simple liquids well above the melting point. On the other hand, the island structure appears as the intermittent change in the system.[TO 89]

The distance matrices of the liquid water with 64 molecules are shown in Fig. 4.2-4.3.² There exist clear island structures at supercooled region, that is, the system keeps a similar structure for few tens of pico second and then suddenly change its structure. As the temperature rises, or as the system becomes larger, many rearrangements occur simultaneously in the system. Even individual structure rearrangements occur intermittently in different regions forming the independent island structures, these island structures are overlaid in the overall (*ie* total system) distance matrix, and the total distance matrix seemingly yields the band structure expressing the diffusive molecular motion.

In order to extract the localized rearrangement of the structure embedded in the band structure, we define the “partial distance”, *ie* the measure of the structure change in the partial volume of the system:

$$D(t, t') = \left(\sum |\mathbf{r}_i(t) - \mathbf{r}_i(t')|^2 \right)^{\frac{1}{2}}, \quad (4.2)$$

where the summation is taken over the particles which are in the partial volume at time t . In this definition, the distance matrix is no longer symmetric. In Fig. 4.4, the partial distance matrices of one eighth of the system with 216 molecules are depicted. Each system includes 27 molecules in average. Although the original distance matrix looks totally diffusive, we can clearly see the island structure in the partial distance matrices indicating that the structure change is localized and intermittent. Overlaying the 8 partial distance matrices reduced to the original distance matrix.

²In this context, no quenching is applied. Intermittence of structure change therefore becomes a little ambiguous.

4.1.3 Network Distance Matrix

In order to understand the collective motions and relate them to the hydrogen bond rearrangement, it is very useful to redefine the distance matrix based on the topology of the network.

The instantaneous topology of the HBN in the system with N water molecules can be expressed as the binary $N \times N$ symmetric adjacency matrix, where each element $\{i, j\}$ gives 1 if molecule i is bonded with molecule j and 0 otherwise.³ We define the state of the system by the adjacency matrix. Suppose there are only three water molecules a , b and c in the system. The total number of states is $2^\nu = 8$, where $\nu = N(N - 1)/2$. Thus the state of the system can also be expressed by ν bits binary sequence, *ie* a vertex of ν dimensional hypercube. The change of the network is identical to the walk on the ν dimensional hypercube.

Then the ‘‘Hamming distance’’, a term from information theory, can be defined as the path length of the walk along the hypercube, *ie* number of different elements between two adjacency matrices as

$$D_H(t, t') = \sum_{i \neq j} |a_{ij}(t) - a_{ij}(t')|, \quad (4.3)$$

where the value of $a_{ij}(t)$ is 1 if the nodes i and j are connected by a bond at time t and otherwise 0. The correlation between Euclidean distance and Hamming distance in Liquid water is shown in Fig. 4.5. We can see in the figure that they are mutually linear for wide range of temperature.

The island structures similar to those in the Euclidean distance matrix are reproduced in Hamming distance matrix as seen in Fig. 4.6 The partial Hamming distance matrix can be defined by restricting the summation over the nodes in the partial volume at time t .

³Here the hydrogen bond network is treated as a undirected graph without multiply connected nodes, *ie* direction of the hydrogen bond or illegally connected hydrogen bonds are not considered.

4.1.4 Indices for Collective Motions

The collective motion is characterized by the size, shape or coherence of the group of molecules. Following are two indices proposed to characterize the collective motion.

Moment ratio

Suppose all molecules diffuse by a jump motion. The total square displacement, say D_2 , of the molecules in short time Δt is denoted by the product of the number of jumped molecules n and the square average jump distance J^2 as

$$D_2 = \sum_i \Delta \mathbf{r}^2 = n \cdot J^2. \quad (4.4)$$

The equation could be rewritten in quadratic form

$$D_m = \sum_i \Delta \mathbf{r}^m = n \cdot J^m, \quad (4.5)$$

where N stands for the total number of molecules. Thus the number of jumped molecules in short time Δt is simply written as

$$n = \frac{D_m \cdot D_m}{D_{2m}}, \quad (4.6)$$

which is also denoted by the averaged form

$$\frac{n}{N} = \frac{\langle |\Delta \mathbf{r}|^m \rangle \langle |\Delta \mathbf{r}|^m \rangle}{\langle |\Delta \mathbf{r}|^{2m} \rangle}. \quad (4.7)$$

For the case of $m = 2$, the equation coincides to the moment ratio of displacement.[SW 83a] Rigorously, it is not the scale of collectivity but rather the scale of simultaneous motions. Moreover, this index should be used carefully because it sometimes fails to measure the scale when no molecule jumps.

Coherency index

In order to extract the magnitude of the local structure rearrangement, another index of collective motion is introduced. The procedure is enumerated as follows:

1. Pick up a pair of adjacent water molecules⁴ and calculate their displacement, say \mathbf{v}_1 and \mathbf{v}_2 , in the short time, say Δt .
2. If the inner product of the displacement vectors is larger than the threshold value, *ie*

$$\mathbf{v}_1 \cdot \mathbf{v}_2 > r_{threshold}, \quad (4.8)$$

they are regarded to move coherently, and connect the two water molecules by a bond.

3. Repeat the procedures above for all pair of the molecules in the system. The bonds form cluster. The magnitude of collective motion in Δt is defined by the size of the connected graph, say “coherency index”.

The threshold should be chosen appropriately. Too small threshold will cause percolation of coherent cluster, while too large threshold will miss any collective translational motions.

An example is shown in Fig. 4.7. The structure rearrangements of the system with 64 water molecules at 240K are visualized for 600ps. The large rearrangement around 200ps can be seen in the distance matrix, which are detected by the coherency index clearly, where about half of the water molecules are moved collectively. The stagnation around 100ps, 300ps, and 500ps are also detected as the blank in the coherency index.

As this index indicates, the structure rearrangement in liquid water occurs intermittently and locally. The simultaneous rearrangements in the large system can be separated by this index. The definition of this index is very heuristic but gives a quite clear sign of the collective motion.

4.1.5 Global Topological Indices

The time scale of the network rearrangement cannot be directly inferred from the shape of island structures in the distance matrices. We thus need to introduce some topological

⁴Practically, the two water molecules are regarded as adjacent if they are closer than 4.0Å

indices of the total network, which are determined by the global network structure at an instance. The long time fluctuation of the network is expected to be seen as the time dependence of these topological indices. Many topological indices are proposed for QSAR (quantitative structure-activity relationship).[LMD 91, R 92]. Their physical meanings have been examined by some authors,[LMD 91] but the analyses on these indices are still very heuristic. We enumerate some topological indices in Table 4.1. To clarify the relationship between physical properties and these indices, the following correlation is calculated. The simultaneous correlation coefficient between two time sequences $\{x(t_1), \dots, x(t_i), \dots, x(t_N)\}$ and $\{y(t_1), \dots, y(t_i), \dots, y(t_N)\}$ is defined by

$$\begin{aligned} C(\{x\}, \{y\}) &= \frac{\frac{1}{N} \sum x(t_i) \cdot y(t_i)}{(\frac{1}{N} \sum x(t_i))(\frac{1}{N} \sum y(t_i))} \\ &= \frac{\langle x \cdot y \rangle}{\langle x \rangle \langle y \rangle}. \end{aligned} \tag{4.9}$$

This coefficient indicates the strength of linear correlation between two sequences and has a value between -1 to 1 . Correlations of these indices with the potential energy fluctuation are shown in Table 4.2. There are only weak correlations between them. The larger number of hydrogen bonds implies the larger topological indices. This is trivial and does not bring us any new information.

Table 4.1: Various indices for global network structure rearrangement. We denote the element of the distance matrix $\mathbf{D}(G)$ of the graph G as d_{ij} and adjacency matrix $\mathbf{A}(G)$ as a_{ij} . The “distance matrix” here means the matrix whose $\{i, j\}$ th element denotes the length of the path along the network between node i and j . This should not be confused with the Humming or Euclidean distance matrix defined before.

The polarity number, n -step number	The polarity number, p_3 , is defined as the total number of $d_{ij} = 3$ elements, <i>ie</i> the number of node pairs which take 3 hops to reach along the network. n -step number, p_n , is the general extension of the polarity number to any natural number n .
Wiener index	The Wiener index,[W 47a, W 47b] w , is given by
$w = \frac{1}{2} \sum_{i,j} d_{ij}, d_{ij} \in \mathbf{D}(G). \quad (4.10)$	
Complexity	<p>The summation is over the number of edges between all pairs of vertices in G.</p> <p>The complexity, $C(G)$, of a graph G is defined as the number of spanning tree, <i>ie</i> partial graph of the graph G, which is spanning over all nodes and has the form of a tree.</p> <p>The complexity of a graph G is easily counted by the following theorem:[T 89]</p> <p><i>Theorem:</i> The complexity $K(G)$ is equal to the cofactor of the matrix M, which is the adjacency matrix whose diagonal elements are replaced by d_i(<i>ie</i> adjacency number of node i) and the signs of all off-diagonal elements are inverted.</p>
The information content(I)	The information content, I_D^W , and the mean information content, \bar{I}_D^W , on the realized distances in G are:
$I_D^W = w \log_2 w - \sum_i i g_i \log_2 i \quad (4.11)$	
and	
$\bar{I}_D^W = \frac{I_D^W}{w} \quad (4.12)$	
The information content(II)	<p>where g_i indicates the incidence of distance i in G.</p> <p>The information content, I_D^E, and mean information content, \bar{I}_D^E, on the distribution of distances in G are defined as</p>
$I_D^E = \frac{n(n-1)}{2} \log_2 \frac{n(n-1)}{2} - \sum_i g_i \log_2 g_i, \quad (4.13)$	
and	
$\bar{I}_D^E = - \sum_i \frac{2g_i}{n(n-1)} \log_2 \frac{2g_i}{n(n-1)} = I_D^E / \frac{n(n-1)}{2}, \quad (4.14)$	
where n stands for the number of vertices in G .	

Table 4.2: The simultaneous correlation of the total potential energy E with various global topological indices.

Topological index	Correlation with E
Total number of incoming hydrogen bonds	0.163
Total square displacement of centers of mass	-0.129
Wiener index	0.219
Complexity	0.211
1-step number (total number of hydrogen bonds)	-0.187
2-step number	-0.193
3-step number	-0.230
4-step number	-0.143
Information contents(I), I_D^W	0.219
Average information contents(I), $\overline{I_D^W}$	-0.170
Information contents(II), I_D^E	0.211
Average information contents(II), $\overline{I_D^E}$	0.211

4.2 Local Structure and Dynamics

As mentioned above, the structure rearrangements occur intermittently and locally, where several molecules move cooperatively. In this section, we introduce some localized indices of structure and motion, and inspect how the structure and dynamics are coupled in short time dynamics of the hydrogen bond network.

4.2.1 Topological and Dynamic Parameters

In order to analyse the HBN rearrangement, topological indices of the network should be defined. They might be “rings” [S 84] or “polyhedra” [S 80] of the HBN. However, these indices defined with more than two molecules are difficult to trace and may cause ambiguity. We thus choose only unimolecular topological indices, as the structural indices. Examples are listed in Table 4.3. We here use a right arrow (\rightarrow), to indicate a donating (*ie* “outgoing”) hydrogen bond of the specified water molecule, a hydrogen of the water molecule making HB with the oxygen of another water molecule. A left arrow (\leftarrow) to indicate an accepting (*ie* “incoming”) hydrogen bond, the oxygen of the water molecule making HB with a hydrogen of another water molecule. We also choose the local indices of dynamics in Table 4.4. Each index $\Delta x(t)$ is defined as $\Delta x(t) = x(t + \Delta t) - x(t)$, except \tilde{D} . They depend strongly upon the choice of Δt ; we choose 1ps and 100fs for Δt .

Table 4.3: Various topological indices. Some of them are not utilized or not mentioned in this paper.

z_A	Number of adjacent molecules, defined as the number of molecules nearer than $r_C = 3.5\text{\AA}$
z_{HB}	Number of HBs of a molecule
$\overleftarrow{z}_{\text{HB}}, \overrightarrow{z}_{\text{HB}}$	Number of the accepting / donating HBs
z_V	Number of adjacent molecules, defined as the number of faces of Voronoi polyhedron
V_V	Volume of Voronoi polyhedron
S_V	Surface area of Voronoi polyhedron
z'_{HB}	Number of weak HBs, defined as the difference of z_{HB} with the threshold value of -10kJ/mol and that with -5kJ/mol .
E_B	Binding energy

Table 4.4: Various indices of structure rearrangement.

D	Local diffusion coefficient calculated from the displacement between 1 to 2ps after the moment.[RSTV 93]
Δr^2	Square displacement of the center of mass just after the moment.
$\Delta\theta$	Rotation angle just after the moment.
Δz_{HB}	Change of the number of HBs.
$\Delta \overrightarrow{z}_{\text{HB}}$	Change of the number of the donating HBs.
$\Delta \overleftarrow{z}_{\text{HB}}$	Change of the number of the accepting HBs.
$\Delta \overrightarrow{z}_{\text{HB}}^+$	Increment of the number of the donating HBs.
$\Delta \overleftarrow{z}_{\text{HB}}^+$	Increment of the number of the accepting HBs.
$\Delta \overrightarrow{z}_{\text{HB}}^-$	Decrement of the number of the donating HBs.
$\Delta \overleftarrow{z}_{\text{HB}}^-$	Decrement of the number of the accepting HBs.

A simultaneous linear correlation coefficient is already defined in Eq. 4.9. If the two sequences correlate nonlinearly, however, another type of correlation should be used. In addition to the simultaneous correlation we here utilize the mutual information $I(\{x\} : \{y\})$. The probability of taking the value x_i can be denoted as $P(x_i)$. The information of the data set is defined as

$$H(\{x\}) = -\sum_i P(x_i) \log P(x_i). \quad (4.15)$$

The information $H(\{y\})$ can also be defined for another sequential data set $\{y\}$. The joint probability $P(x_i, y_j)$ is the probability that x is x_i and y is y_j at the same time. Its information is calculated in the same manner as follows:

$$H(\{x\}, \{y\}) = -\sum_{ij} P(x_i, y_j) \log P(x_i, y_j), \quad (4.16)$$

Then the mutual information is defined as

$$I(\{x\} : \{y\}) = H(\{x\}) + H(\{y\}) - H(\{x\}, \{y\}), \quad (4.17)$$

which indicates the excess information produced by the correlation of two sets. It becomes 0 if there is no correlation between x and y . As there is any averaging operation in the definition, this index is applicable even when x does not take ordered values. Mutual information is not utilized for continuous topological indices in this work. Although there are various ways to take the time correlation, for examples, delayed correlations, correlations between distant points and many body correlations, we take only simultaneous correlations in this work.

Let us now look at these correlations in detail. The correlations among topological indices at 240K are listed in Table 4.5. The correlation between $\overleftarrow{z}_{\text{HB}}$ (the number of the accepting HBs) and $\overrightarrow{z}_{\text{HB}}$ (the number of the donating HBs) is strikingly small ($C(\overleftarrow{z}_{\text{HB}}, \overrightarrow{z}_{\text{HB}}) = 0.0397$); the number of incoming HBs does not correlate with the number of outgoing HBs. Relatively large negative correlation between z_{HB} and E_{B} simply indicates the fact that the more HBs a water molecule has, the lower its binding energy becomes.

The correlations at 300K are listed in Table 4.6. The correlation coefficient between $\overleftarrow{z}_{\text{HB}}$ and $\overrightarrow{z}_{\text{HB}}$ is still small and all other indices indicate similar tendencies to those at 240K.

Table 4.5: Various correlation between two topological indices at 240K. Upper: correlation coefficient. Lower: mutual information. H is a single information content.

	H	z_A	z_{HB}	$\overrightarrow{z}_{\text{HB}}$	$\overleftarrow{z}_{\text{HB}}$	E_B
H		1.1319	0.996	0.574	0.740	
z_A	1.319		0.0543	0.0158	0.0722	0.0974
z_{HB}	0.996	0.0533		0.6459	0.7616	-0.3378
$\overrightarrow{z}_{\text{HB}}$	0.574		0.2365		0.4014	
$\overleftarrow{z}_{\text{HB}}$	0.740					
					0.0397	-0.1558
					0.0015	
						-0.3278

Table 4.6: The correlation coefficients between two topological indices at 300K.

	z_A	z_{HB}	$\overrightarrow{z}_{\text{HB}}$	$\overleftarrow{z}_{\text{HB}}$	E_B
z_A		0.1198	0.0862	0.1084	0.0066
z_{HB}			0.6695	0.7409	-0.6182
$\overrightarrow{z}_{\text{HB}}$				0.0410	-0.3602
$\overleftarrow{z}_{\text{HB}}$					-0.5316

Table 4.7 shows the relation between topological index and its change at 240K. There are strong correlations between $(\overrightarrow{z}_{\text{HB}}, \Delta \overrightarrow{z}_{\text{HB}}^+)$ (increment of the number of the donating HBs)), $(\overrightarrow{z}_{\text{HB}}, \Delta \overrightarrow{z}_{\text{HB}}^-)$ (decrement of the number of donating HBs)), $(\overleftarrow{z}_{\text{HB}}, \Delta \overleftarrow{z}_{\text{HB}}^+)$ (increment of the number of the accepting HBs)), $(\overleftarrow{z}_{\text{HB}}, \Delta \overleftarrow{z}_{\text{HB}}^-)$ (decrement of the number of the accepting HBs)). On the other hand, $\overrightarrow{z}_{\text{HB}}$ yields small correlation with $\Delta \overleftarrow{z}_{\text{HB}}^+$ and with $\Delta \overleftarrow{z}_{\text{HB}}^-$. The negative large correlation between $\Delta\theta$ (rotation angle) and z_{HB} simply implies that the water molecule can rotate easily when the number of HBs is small. Those indices at 300K are listed in Table 4.8. Although intensive molecular motions reduce the correlations with $\Delta\theta$ or $\Delta\mathbf{r}$, overall tendencies are kept even at the room temperature.

Table 4.7: Various correlations between topological index and dynamic index at 240K. Δt is 100fs. Upper: correlation coefficient. Lower: mutual information. H is a single information content.

	H	z_A	z_{HB}	$\overrightarrow{z}_{\text{HB}}$	$\overleftarrow{z}_{\text{HB}}$	E_B
H		1.346	1.022	0.589	0.765	
$\Delta \overrightarrow{z}_{\text{HB}}$	0.1660	-0.2154	-0.2995	-0.0479	0.2712	
	0.765	0.0152	0.0454	0.1190	0.0013	
$\Delta \overleftarrow{z}_{\text{HB}}$	0.1773	-0.0859	0.0041	-0.1272	0.0575	
	0.754	0.0164	0.0313	0.0002	0.0607	
$\Delta \overrightarrow{z}_{\text{HB}}^+$	0.1033	-0.4082	-0.6353	-0.0291	0.2024	
	0.488	0.0070	0.0853	0.1802	0.0005	
$\Delta \overleftarrow{z}_{\text{HB}}^+$	0.1050	-0.3352	0.0152	-0.4730	0.0417	
	0.487	0.0060	0.0612	0.0002	0.1131	
$\Delta \overrightarrow{z}_{\text{HB}}^-$	0.1445	0.0876	0.1897	-0.0424	0.2024	
	0.487	0.0105	0.0068	0.0348	0.0009	
$\Delta \overleftarrow{z}_{\text{HB}}^-$	0.1482	0.2137	-0.0094	0.2929	0.0404	
	0.486	0.0117	0.0305	0.0001	0.0502	
Δr^2	0.0262	-0.0915	-0.0589	-0.0779	0.1580	
$\Delta\theta$	0.0729	-0.5703	-0.2908	-0.5228	0.2957	

Table 4.8: The correlation coefficients between topological index and dynamic index at 300K. Δt is 1ps.

	z_A	z_{HB}	\vec{z}_{HB}	\overleftarrow{z}_{HB}	E_B
$\Delta \vec{z}_{HB}$	0.1090	-0.0808	-0.0517	-0.0675	0.1793
$\Delta \overleftarrow{z}_{HB}$	0.1153	-0.0325	-0.0249	-0.0626	0.0344
$\Delta \vec{z}_{HB}^+$	0.0536	-0.3270	-0.4366	-0.0671	0.2850
$\Delta \overleftarrow{z}_{HB}^+$	0.0424	-0.2875	-0.0312	-0.3781	0.2385
$\Delta \vec{z}_{HB}^-$	0.1267	0.1944	0.3526	-0.0445	0.0108
$\Delta \overleftarrow{z}_{HB}^-$	0.1389	0.3362	-0.0081	0.4732	-0.1826
Δr^2	0.0301	-0.0579	-0.0442	-0.0443	0.1179
$\Delta \theta$	0.0551	-0.1240	-0.0924	-0.0901	0.2332

The relation between two indices of structural change is also interesting. Table 4.9 shows that the decrement of the number of outgoing HBs strongly causes the simultaneous increment of the number of outgoing HBs, $C(\Delta \vec{z}_{\text{HB}}^+, \Delta \vec{z}_{\text{HB}}^-) = 0.5169$, and so that the number of outgoing HBs does not much change from 2 even when bond alternations take place. There is also significant correlation between increment and decrement of the number of incoming HBs $C(\Delta \vec{z}_{\text{HB}}^+, \Delta \vec{z}_{\text{HB}}^-) = 0.2689$, which is but less than $C(\Delta \vec{z}_{\text{HB}}^+, \Delta \vec{z}_{\text{HB}}^-) = 0.5169$ because three incoming hydrogen bonds per a water molecule is possible. On the other hand, there is only small correlation between simultaneous change of the number of incoming and outgoing HBs ($C(\Delta \vec{z}_{\text{HB}}^+, \Delta \vec{z}_{\text{HB}}^+) = 0.0948$, $C(\Delta \vec{z}_{\text{HB}}^+, \Delta \vec{z}_{\text{HB}}^-) = 0.0663$, $C(\Delta \vec{z}_{\text{HB}}^-, \Delta \vec{z}_{\text{HB}}^+) = 0.0632$, $C(\Delta \vec{z}_{\text{HB}}^-, \Delta \vec{z}_{\text{HB}}^-) = 0.0989$). The large correlations with Δr^2 (square displacement of the center of mass) or $\Delta \theta$ shows that any kind of HBNR causes translation or rotation of the molecule. These tendencies are kept even at 300K, shown in Table 4.10.

There is a certain relation between the average square displacement $\overline{\Delta r^2}$ and the coordination number z_A . [RSTV 93, SGS 91] However, the direct correlation between the square displacement before averaged, Δr^2 , and the coordination number, z_A , is very small ($C(z_A, \Delta r^2) = -0.0659$ for $\Delta t = 1ps$, 0.0262 for $\Delta t = 100fs$). This is because the distribution of Δr^2 is very broad. Δr^2 is an inadequate index to perform the correlation analysis.

As a summary, the MD calculation reveals that:

- Four HBs are not equivalent.
- The number of incoming and outgoing HBs are independently controlled to be around 2. As the result, the total number of HBs per one water molecule becomes to about 4.

It should be noted that these rules are intrinsically exist even in the room temperature.

Turning now into the time dependencies of these local topological indices by power spectra, interesting tendencies can be observed. In Figs. 4.8-4.9, power spectra of various local topological indices are indicated in log-log. All indices have the smooth slope in the short time scale and flat “white” spectra in the longer time scale, as has already been found in the fluctuation of the potential energy by Sasai *et al* .[SOR 92] The crossover point of the short- and long-time behavior is 0.5cm^{-1} at 240K and 5cm^{-1} at 300K.

4.2.2 Graphical Analysis

In this section, we propose a new graphical representation of the hydrogen bond network, which leads naturally to a new concept of defects. Correlated motion of the hydrogen bonds is described in terms of the network topology and the defect.

The topology of the HBN of water can be represented by a graph, where nodes and bonds correspond to water molecules and hydrogen bonds, respectively. In liquid water, there are several water molecules which surround an individual water molecule, but not

making HBs with that central water molecule. These non-HB surrounding water molecules easily turn to create HBs with the central water molecule. We introduce here the 'virtual HB' to represent the non-HB bond between the adjacent water molecules, which is ready to change to HB. The new topological graph of the network, constructed with HBs and virtual HBs is able to describe the geometrical information for possible HB alternations, thus can treat the HB rearrangement dynamics. We use the term 'adjacency bonds' to indicate both real and virtual bonds.

Let us consider the graphical representation of HBN. The HBN, indicated in Fig. 4.10(a), can simply be represented by a directed graph, shown in Fig. 4.10(b). Each node and arrow corresponds to the water molecule and HB, respectively. Here an incoming arrow to a node indicates that a hydrogen of another water molecule makes a HB with the oxygen of that node (water molecule). An outgoing arrow from a node, a water molecule, indicates that a hydrogen of that node (water molecule) makes a HB with an oxygen of another water molecule. Dashed bonds are added to denote the virtual HBs. Each node nearly has 2 incoming and 2 outgoing HBs. Each arrow is further replaced by a bond with white and black circles at the head and the tail of the arrow, respectively. The diagram of HBN obtained after this operation is shown in Fig. 4.10(c). As we have seen in the previous section, the events of incoming bonds are nearly independent from the events of outgoing bonds; the white circles and the black circles are not mutually exchangeable. Three white circles in a node can then be put together into one white circle and three black ones to one black one, as shown in Fig. 4.10(d). Each node is separated into two seminodes.; one for a donating part of the node (black circle) and the other for an accepting part (white circle). The bonds are then no longer necessarily to be represented with 'directed' allows. By this operation, HBN is converted into an undirected infinite graph. The number of seminodes is twice of that of nodes and thus the number of edges at each seminode becomes half. Here, we use the notations of "seminode" and "edge" in the undirected graph whereas we have used "node" and "bond" in the directed graph, respectively.

Each edge is either of “occupied” or “vacant” state. An occupied edge is called a “hydrogen edge (HE)”. A vacant edge is an virtual HE. Each seminode is assumed to have not less than 2 virtual HEs. We assume that the number of HEs attached to one seminode takes the value between 1 to 3. This is a reasonable assumption because water molecules having 0 or 4 incoming / outgoing HEs are quite rare in real water. We draw the state transition among HB states at a node using the MD data in the previous section. Fig. 4.11 shows the changes of HBs at 220K. Each arrow denotes the transition probabilities to various HB states in a step. Infrequent transitions are omitted from the diagram. The large probability P_{12} and P_{32} indicates that water molecule with 1 or 3 donating HB will changed to have 2 donating HB quickly. The lower loop P_{22}^{\pm} denotes that one of the two HBs is diminished and another HB is created at a time. Most probable total number of the donating HBs is thus 2. The same is true for the accepting HBs.

We call a seminode with more or less than 2 HEs as “defect”. There are oversatisfied (having more than 2 HEs; denoted by \oplus) and dissatisfied (less than 2 HEs; \ominus) types of defects. A state transition of an edge always causes one of the three types of the motion of defect, propagation, pair creation and pair annihilation, as illustrated in Fig. 4.12. The defects occupy 9% at 220K, 22% at 240K, or 36% at 300K of the seminodes. It should be noted that the percentage of the defect decreases rapidly around 220K.

A HB annihilation probability is enumerated by the number of HBs attached to each seminode. When both seminodes are \oplus defects, the HB (and thus both defects) annihilates with a probability, say, p . When one end is \oplus defect, the HB annihilates with a probability q and the other end becomes \ominus defect. While both ends are not \oplus defects, the HB annihilates with a low probability r . p , q and r should be called as “pair annihilation probability”, “propagation probability” and “pair creation probability”, respectively. In Table 4.11, p , q and r extracted from MD data are 0.72, 0.29 and 0.10, respectively.

Table 4.11: The probabilities, P_a , of disconnecting a hydrogen bond (HB) under various states of the terminal seminodes, extracted from MD data at 220K. The terminal seminodes are two water molecules linked by the HB. The state of the terminal seminodes is specified by the numbers of HEs attached to both terminal seminodes, $\overrightarrow{z}_{\text{HB}}$ (the number of the donating HBs) and $\overleftarrow{z}_{\text{HB}}$ (the number of the accepting HBs).

$\overrightarrow{z}_{\text{HB}}$	$\overleftarrow{z}_{\text{HB}}$	P_a
1	1	0.098
1	2	0.117
1	3	0.352
2	1	0.083
2	2	0.100
2	3	0.294
3	1	0.226
3	2	0.294
3	3	0.727

It is important to know the defect dynamics that once a defect is created, it can never cease until it reaches a partner defect to annihilate with. This situation is very close to so called “domino phenomenon”; once one defect passes over a path, another defect never can pass the same path and defect stops when it meets another defect. In another word, the defect motion of the defect leaves a trace on the network structure and so that the defect’s walk is far from random. This memory effect restricts defect’s walk more as the average number of virtual HBs at a seminode is lowered. If there are only two virtual HBs at a seminode, a single defect cannot pass the seminode and is sometimes confined in a small region of the network. More detailed discussions are given in Appendix A. Such a property of defects restricts the propagation of HBNR in the structured water.

Average number of molecules, whose hydrogen bond is rearranged in short time Δt , is plotted against temperature in Fig. 4.13. At low temperature region, the number of molecules grows slowly even Δt becomes longer. This tendency is enhanced in supercooled water. It denotes the fact that the same molecule changes its hydrogen bonds again and again. Each line linearly decreases as the temperature becomes lower. When Δt is chosen as very short value, its line seems to reach zero at about 160K, which is nearly equal to T_g , *ie* glass transition temperature of water.[JHM 90] On the other hand, when Δt is longer, its line crosses with the line of shorter time around 220K and the system seems to be frozen in higher temperature. As already shown in Fig. 4.5, the total motion of the center of mass is always proportional to the total number of hydrogen bond rearrangements. If hydrogen bonds are rearranged homogeneously anywhere in the system, diffusion should occur above 160K. The actual diffusion, however, becomes too slow to look out around 220K. These paradoxical results coincide with the observation by Giguère[G 87], that is, the hydrogen bond rearrangement is localized before each hydrogen bond is really frozen as the temperature becomes lower.⁵ The self-diffusion coefficients calculated from our MD simulations are:

⁵Vilgis gave a simple explanation to Angell’s phenomenological classification of fragile and strong liquid[V 93]. He asserted that the difference between them is found in the coordination number of a molecule, where the distributions of the coordination number in strong liquids are narrower than those in fragile liquids. As mentioned before, the percentage of the defective seminode seems to approach to

$0.4216 \times 10^{-6} \text{cm}^2 \text{sec}^{-1}$ at 200K, $1.3960 \times 10^{-6} \text{cm}^2 \text{sec}^{-1}$ at 220K, $4.6837 \times 10^{-6} \text{cm}^2 \text{sec}^{-1}$ at 240K, and $28.68 \times 10^{-6} \text{cm}^2 \text{sec}^{-1}$ at 300K. These results also indicate that the system is almost frozen around 220K.

4.2.3 Lattice Model

Based on the decomposition scheme of the HBN graph and the HB state transition probabilities extracted from the trajectory calculations shown in the previous section, we are now ready to construct a lattice model of the HBN rearrangement dynamics in the supercooled water.

1. Let us choose a simple (or body centered) cubic lattice. Each node of the lattice has 6(8) neighborhoods. and the lattice bonds represent the adjacency bonds of the water.
2. Each bond has a directionality, an arrow, representing the incoming or outgoing hydrogen bond. Each node has 3(4) incoming and 3(4) outgoing arrows. we call these arrows as “adjacency edges”.⁶
3. HEs are placed on the edges of the adjacency edge network. HEs occupy some fraction of the adjacency edges.

Then the next problem is how to propagate the network change. It is desirable to reproduce the network dynamics by a model with a minimum set of parameters. We choose two sets: The first is based on the state transition probabilities of the seminodes shown in Fig. 4.11 and the other is based on that of the edges shown in Table 4.11. We call them methods A and B, respectively. We separate the donating HBs and accepting HBs at individual node, *ie* using undirected graph representation, and impose the state transitions rule described in the previous section.

zero around 220K. Referring the assertion by Tanaka[T 95], it is possible to regard the phenomenon in supercooled water at 220K as the transition from fragile liquid to strong liquid.

⁶Although all the nodes have the same number of incoming and outgoing arrows, topological randomness is intrinsically embedded in terms of the connectivity along the directed graph.

The following is the procedure to advance one simulation step.

Method A:

1. Choose randomly some adjacency edges and switch their HE occupancy from the occupied to vacant state, or conversely (we call this “flip the edge”)
2. Compare the modified network with original one. Repeat random HB flips until the transition probabilities P_{12} , P_{32} , P_{21} , P_{23} and P_{22}^{\pm} of the whole change of the HB network coincide with a set of given values.

For actual application we have used $P_{12} = 0.4$, $P_{32} = 0.3$, $P_{21} = 0.030$, $P_{23} = 0.0041$, $P_{22}^{\pm} = 0.05$ as transition probabilities; these probabilities are a little smaller than those values listed in Fig. 4.11, because this procedure becomes very time consuming as these probabilities get larger. Each simulation step contains several thousands of edge flips, and we performed 4096 steps.

Method B:

1. Randomly choose one edge.
2. Count the number of HEs attached to each end seminodes of the chosen edge.
 - (a) If the chosen edge is not occupied:
 - i. If both end seminodes are \ominus defects, flip the edge with probability p .
 - ii. If one end seminode is \ominus defect, flip the edge with probability q .
 - iii. If both are not \ominus defects, flip the edge with probability r .
 - (b) If the chosen edge is occupied:
 - i. If both end seminodes are \oplus defects, flip the edge with probability p .
 - ii. If one end seminode is \oplus defect, flip the edge with probability q .
 - iii. If both are not \oplus defects, flip the edge with probability r .

Where p , q , and r are pair annihilation, propagation and pair creation probabilities, respectively.

3. Repeat the above procedure n_n times, where n_n is the number of nodes in the lattice.

Here we assumed that the HB disconnecting probabilities p , q , and r are equivalent to the HB connecting probabilities, *viz* the state transition diagram in Fig. 4.11 is symmetric. For actual simulation, we have used 0.72, 0.29 and 0.10 for p , q , and r , respectively.

By both methods, the average number of the HBs at an individual node is kept nearly to be 2+2. It should be noted here that some features of the real water are ignored in these lattice models. Water molecules can not translate, that is, there is no diffusion of the center of mass, and the lattice structure does not change. These assumptions will breakdown at high temperature and long time dynamics of water.

To compare the magnitude of energy fluctuation, we divided the total system into sublattices, each of which includes $6 \times 6 \times 6 = 216$ nodes. We assume that the total potential energy of a sub-lattice is equal to the total number of HBs in the sublattice multiplied by a constant. Fourier transform of the potential energy fluctuation of sub-lattice thus obtained is plotted in Fig. 4.14. Both methods reproduce the $1/f^\alpha$ spectra with $\alpha = 0.6$ (f is the frequency), which is very close to the previous MD result with the exponent $\alpha = 0.75$. [SOR 92] If HBs are randomly picked up and flipped, an energy fluctuation behaves as $1/f^2$.

The distribution of HB lifetime is also analyzed. It is found that the HB lifetime calculated by MD behaves as t^α in short time and decays exponentially in long time (not shown in figures). This behavior of HB lifetime was already pointed by Stanley *et al* [SPSH 90]. As shown in Fig. 4.15, our lattice model well reproduces this HB life time distribution. Of course, if each HB flips with a single relaxation time, HB lifetime distribution must be exponential in all time scale.

In order to make a further analysis, we introduce the heterogeneity index for HBNR. The frequencies of HBNRs at nodes during n steps are counted and then averaged over the nodes. The average frequency in n steps is expressed by \overline{m}_n and its spatial standard deviation by σ_n . The heterogeneity index is defined as

$$H_n = \frac{\sigma_n}{\overline{m}_n}. \quad (4.18)$$

\overline{m}_n is expected to grow proportionally to n . If the HBNRs are homogeneous process, σ_n is proportional to $n^{\frac{1}{2}}$ and thus H_n decays with $n^{-\frac{1}{2}}$. If HBNR are heterogeneous, the decay is slower than $n^{-\frac{1}{2}}$ as shown in Appendix B. The heterogeneity index obtained by MD calculations is plotted against time in Fig. 4.16(a). At high temperatures (260-300 K), the heterogeneity index initially decays slower than the homogeneous case, with the exponent of $\alpha < 0.5$, but turns to be homogeneous for the time longer than 10ps. At lower temperatures (200-220 K), the index has three slopes. The curve decays slowly in the middle time domain, meaning that there is very long-lived heterogeneity. The time scale where the heterogeneity index shows the slope with the exponent of $\alpha = 0.5$ is almost the same as the time scale when various local topological indices indicate white power spectra. The heterogeneity index is also calculated for a sublattice with $6 \times 6 \times 6$ nodes in the lattice model, and is shown in Fig. 4.16(b). Our models can reproduce the gentle slope as the MD curve in short time, $\alpha < 0.5$, indicating the temporal correlation of HBs is described by our models. They can not, however, reproduce the decay in long time dynamics, because translational motions, which causes large scale structural rearrangements of the HB network, are missing in the lattice models. For example, if a closed ring⁷ is formed by the seminodes and the adjacency edges, the external defect can never intrude into the ring. The frequency of hydrogen bond rearrangement becomes, therefore, always lower in the closed ring. Such a structure is, however, broken after a long time in the real system.

⁷Note that this ring differs from the ring of Speedy's proposal. He did not pay attention to the direction of the hydrogen bond and that the ring structure exists everywhere in the network. [S 84] On the other hand, the ring defined here is made of seminodes with two adjacency edges only. Such a structure is rarely found in the hydrogen bond network.

4.2.4 Discussion

We have analyzed the HBNR dynamics by performing MD calculations and constructing the lattice model. The simple lattice model based on state transition diagram was shown to well reproduce all of the HB lifetime, the HBNR pattern (in Hamming matrix) and the energy fluctuation, obtained from MD calculation of supercooled water. Change of the propagation rule or of the lattice structure is expected not to make qualitative difference of the results. The properties found in the present system are expected to be found in many other systems whose dynamics is coupled to defects as in the spinglass.

The analysis of the heterogeneity index indicated that the HBNRs are very heterogeneous. The HBNR was shown to be the motions of defects. The defect walks along the undirected graph, which is reduced from the three-dimensionally percolated directed graph. Even when the directed graph is constructed homogeneously and well percolated, the spatial edge (*ie* HB) connection among seminodes in the undirected graph can be very heterogeneous. The motion of defects on the undirected graph is thus heterogenized by the global network topology. Moreover, that the traces of the defect movements on the hydrogen bond network remain for a considerable time, inevitably localize the HBNR. When defects exist at some locations of the network, they rearrange HB connections in that local area (*ie* a subsystem of water). After defects leave that area, the local network is rarely rearranged. A subsystem, therefore, exhibits the energy fluctuation of $1/f^\alpha$ type, and yields domain structures in the distance matrix.[TO 89, SOR 92]

These observations lead to the conclusion that the existence of the defects and the network topology produce the spontaneous spatiotemporal fluctuation of the HBNR. The hydrogen bond network consequently becomes heterogeneous. The heterogeneity of the hydrogen bond network is, thus, not the origin of the heterogeneous HBNR, but the result from the latter.

As mentioned before, the defect cannot go through the seminode with few adjacent nodes. Suppose hydrophobic molecules are solved in water. Water molecules in the first

coordinate of the solute are the case. Reduction of the number of adjacent HB formers leads to the decrement of HB rearrangements. In special case, all water molecules contact with guest molecules in the clathrate hydrate. If the guest molecule is hydrophobic, the hydrogen bond network is hardly rearranged. While if the guest molecule is somewhat polarized, the guest molecule also composes the hydrogen bond network. Such a coupling between the guest molecule and the lattice gives rise to cause complicated HBNR dynamics. Koga *et al* showed that the lifetime of hydrogen bonds indicates similar shape as in liquid water.[KT 95, SPSH 90] It is interesting to apply our lattice model to aqueous solutions.

Table 4.12: The probabilities of the \oplus defects to be created (r), annihilated (p), and propagated (q) at various temperature. Δt is 1ps.

T	p	q	r
220K	0.730	0.296	0.100
240K	0.719	0.355	0.161
260K	0.715	0.422	0.240
280K	0.739	0.496	0.339

The probabilities of defect motion, p , q , and r at various temperatures are listed in Table 4.12. The pair annihilation probability p is always large but does not indicate temperature dependence, while the pair creation probability q becomes larger as the temperature is raised. As is already seen in the previous section, overall tendencies of correlation coefficients (see Tables 4.6, 4.8, and 4.10) are conserved even at the room temperature. You may think the defect motion at the room temperature can be also reproduced by our lattice model. At the supercooled region, the number of HEs at a seminode is almost 1 to 3. This fact simplifies the rule of defect motions. At higher temperature, however, the state transition rules indicated in Fig. 4.11 becomes too complicated to apply the similar logics.

The picture presented in this work is valid only for the short-time dynamics of supercooled water. Large displacements of molecules, which rearrange the topology of adjacency bonds (*ie* reconstruct the lattice) are missing in our model. These large displacements make HBNR more homogeneous, resulting to the $t^{-\frac{1}{2}}$ slope of the heterogeneity index for very long time dynamics, as seen in Fig. 4.16. As the temperature becomes lower, however, correlated HBNR becomes dominant. The heterogeneity index curve indicates that heterogenization contends with homogenization below 240K.

Real energy fluctuation observed in MD result is slower than that of lattice dynamic model. There will be slower layers in the hierarchy of real dynamics which are not taken in the model. As the water molecules have only four neighborhoods nearby, there won't be so many configuration of water molecules in local structures. In this story, the state of water is classified only by the number of hydrogen bonds. But even if all the second neighbor molecules are taken into consideration, possible network patterns will not become too many to count. Classifying the local topology by taking higher order topological indices into account will lead to more reliable approximations, where the information theory gives useful measure for the task.

There found to exist localized collective motions, involving large network rearrangement, in liquid water even at the room temperature.[TO 89] In the current model, however, such

collective motions can not be treated because our present model only deals with adjacent correlations. It is important to construct the models which are applicable in all temperature range.

4.3 Some Other Analyses and Remarks

4.3.1 Survey of the Potential Hypersurface

Let us now consider a configuration of liquid water as a phase point on the potential hypersurface. The geometry of the potential energy hypersurface may be characterized by the number of adjacent inherent structures around an inherent structure, distance and barrier height between them, or the curvature of the hypersurface.

The shape of the potential energy surface can be revealed by examining the quenching of the phase point by Eq. 2.1. If the undulation of the potential surface is relatively mild and smooth, the shape of the basin is approximated by a parabola. In this case, the potential energy change along the quenching yields an exponential decay.⁸ If the potential surface has abnormal pleats near the bottom of a basin, such an approximation is no longer valid. The quenching of the phase point passes through a deep, narrow, and folded groove before reaching a distant minimum

The potential energy profile in the quenching process is plotted in Figs. 4.17 and 4.18. At 240K, energy decays smoothly and no point of inflection exists. On the other hand, there are several points of inflection in the quenching process at 300K. The numbers over the potential energy profile denotes the number of instantaneous normal modes with imaginary frequency, which increases around each point of inflection. It implies that the trajectory of quenching is approaching to the saddle point and may bifurcate or kink near the point. The visualization of the quenching process indicates that large collective motions occur near each point of inflection. The potential energy profile of inherent structures along the

⁸Here, the time step of quenching is fixed as a constant value.

real trajectory thus becomes abnormally rough by such hierarchical structural relaxations.⁹

The potential energy profile in the quenching process from successive instantaneous structures is shown in Fig. 4.19 and 4.20. At the low temperature, quenching leads to the bottom of the basin immediately. On the other hand, a lot of stumbling occur in the quenching process from the structure at high temperature. It should be pointed that the potential energy fluctuation of slightly quenched structures is small compared to the original trajectory or deeply quenched structures. Three Euclidean distance matrices are shown in Fig. 4.21. First one is made from the original trajectory (potential energy profile is indicated by the label (0) in Fig. 4.20), the second is from the slightly quenched trajectory (indicated by (3) in the same figure), and the last is from inherent structures (*ie* completely quenched trajectory, indicated by (50) in the same figure). Slight quenching reveals distinct island structures in the distance matrix, while deep quenching makes fine structures in it. It is one expression of the multivalley structure of the potential surface.

These results show that the *de facto* potential energy hypersurfaces along trajectories are smoother than those along the reaction coordinates connecting adjacent inherent structures. The system does not feel a curvature of the bottom of a basin, but may rather feel the moderate undulation of the plateau. On the other hand, the rules of HBNR described in Section 4.2.1 prevent from rearranging the connectivity of the hydrogen bonds freely, *ie* there are many structures which are geometrically close to those along the trajectory but energetically separated by the high energy barrier. The phase space around the trajectory is narrowed by these forbidden structure rearrangements. In other words, the structure rearrangements in liquid water is not “energy-driven mechanism” but rather “entropy-driven mechanism”. This condition has similarity to the binary mixture of hard sphere liquid near the glass transition point.

⁹LaViolette and Stillinger has revealed a similar stepwise potential energy profile in the quenching process of the simple liquids.[LS 86] They attributed it to the high vibrational anharmonicity of the potential hypersurface and suggested that the hierarchical structural relaxation occurs in the quenching process.

4.3.2 Probabilistic Automaton, Spinglass and Water

A probabilistic cellular automaton is a useful model of collective dynamics and phase transition of a system. Our lattice model described in Section 4.2.3 is a probabilistic automaton, where the state of a hydrogen bond at $t + \Delta t$ is determined by the state of surrounding hydrogen bonds in some probabilities. Although the number of incoming and outgoing adjacency bonds at a node is all the same, the network has topological randomness in our model. A PCA with fixed spatial randomness yields a new universality class where the critical exponents are different from the homogeneous system without randomness.[N 88] It is, however, still unknown whether our PCA with the topological randomness belongs to another universality class or not.

Turning now into comparison with spinglass. Let us now compare water with spinglass systems.

The following characteristics are observed in the real spinglass system:

1. Linear magnetic susceptibility and specific heat have a cusp at the spinglass transition temperature T_g .
2. Slow dynamics around T_g .
3. Hysteresis below T_g .

Many lattice models are also proposed, where intrinsic randomness is installed in the short range interaction. Edwards and Anderson's mean field approximation model reproduced the characteristic behavior of thermodynamic properties. On the other hand, Sherrington and Kirkpatrick's model revealed the ultrametric structure of the potential hypersurface. There are interesting coincidence of these spinglass properties with the behavior of liquid water around $T_a = -45^\circ\text{C}$. A spin flip in the spinglass model corresponds to a hydrogen bond creation/annihilation in the hydrogen bond network. As the spin flip probability varies by the circumstance, wait time distribution of spin flip becomes $1/f^\alpha$. Marginal

stability of the spinglass phase is also observed in the hydrogen bond network. The spin configuration can be largely modified with small energy by flipping spins in appropriate order. While, available spin configurations, *ie* reachable region of phase space, are altered by a small change in network topology.

Sasai, Stanley and others have proposed lattice models of liquid water, which are intended to reproduce the phase diagram. Their models have, however, not yet to include the intrinsic topological randomness of the network, which is essential in the short time dynamics of liquid water. The water dynamics might be well characterized by using the spinglass dynamics.

4.3.3 Comparison with Random Bond Percolation

Let us now look at the pattern of network rearrangement by comparing the network structure at time t and itself at time $t + \Delta t$. If there is a hydrogen bond between molecules i and j at time t , and if the hydrogen bond also exists at another time $t + \Delta t$, it is called “survived”.¹⁰ Illustrating the survived hydrogen bond after 20ps in Fig. 4.22, many chain-like clusters can be observed.

The diameter of a connected graph with size n is defined as

$$D = \max(p_{ij}), \quad (4.19)$$

where p_{ij} denotes the path length between nodes i and j of the connected graph. D expresses the shape of the connected graph; if the graph is a straight chain, D is equal to the chain length, and if it is branched, D is small.

The distributions of the diameter of the survived cluster at various observation time are calculated from MD simulations and plotted against the number of nodes in a graph (‘cluster size’) n in Fig. 4.23. It shows that small survived graphs (‘ σ -clusters’) tend to form chain-like structure.

¹⁰This definition does not require the bond to exist throughout the two observation time.

For comparing with liquid water, various lattices are chosen and bonds are randomly placed on the lattice in the manner of random bond percolation model for various bond occupation probabilities p below percolation threshold.¹¹ This lattice model is called “Random Bond Lattice Model (RBLM)”. The diameter distributions for RBLM are calculated and plotted against the ‘cluster size’ n in Fig. 4.24. We can see that the distributions are almost independent of p or lattice. There are many chain-like clusters. These diameter distributions obtained from the random bond lattice model are similar to that of the σ -clusters in MD calculation.

The cluster size distributions obtained from the random bond lattice model are plotted in Fig. 4.25. For larger p , we find larger clusters. Shape of the cluster in liquid water should be compared with these “reference” systems. The size distribution of the σ -clusters (in MD) is shown in Fig. 4.26 for two temperatures. At the lower temperature, the survived hydrogen bonds percolate even after 25.6ps.

Instead of the “survived clusters”, we have examined the changes of the network in MD by comparing the network structure at time t with later structure at $t + \Delta t$. An “altered” cluster (α -cluster) is defined as the cluster of hydrogen bonds being altered to be connected or disconnected after Δt . Here we denote the α -cluster with the size = n “ α_n -cluster”. The size distribution of α -clusters is shown in Fig. 4.27. There is no distinct difference in this distribution between liquid water and random bond percolation model.

Let us examine the shape distribution of the clusters in more detail. The diameter distributions of the size $n = 6$ cluster in the random bond lattice model (RBLM) are shown in Fig. 4.28. The distribution does not depend on the value of p or the type of lattice. More than half of these clusters are with $D = 4$, and about 40% with $D = 5$. The diameter distribution of the size $n = 6$ σ -cluster (σ_6 -cluster) in liquid water is shown in Fig. 4.30. The distribution is similar to that of RBLM with the diamond lattice. On the other hand, the diameter distribution of α -cluster shows some difference from RBLM distribution; the

¹¹Bond percolation thresholds p_C are 0.179 for body-centered cubic lattice, 0.249 for simple cubic lattice, and 0.388 for diamond lattice.

portion of $D = 5$ cluster reduces and that of $D = 3$ cluster increases. The same tendency is observed for size $n=7,8$ α -clusters. (Figs. 4.31-4.36) This fact that the α -cluster has smaller D value indicates that the network rearrangement take place in compact area, as already mentioned in Section 4.2.1, *ie* the hydrogen bonds are rearranged cooperatively. The analysis of α -cluster is for the short-time dynamics. There seems, however, not to exist the robust chain-like long-lived backbone in the hydrogen bond network of liquid water. It is not conclusive yet, since we have only examined it through the cluster shape distribution. The higher-order topological indices must be introduced in order to analyze the long-time and long-ranged fluctuation. We might find more sharp difference from the random bond lattice model there.

The snapshot of the hydrogen bond network is well represented by RBLM, as found by Stanley *et al* . It is, however, more important to extract the dynamic heterogeneity from the water dynamics, Our lattice model in Section 4.2.3, not RBLM, can deal with it. Further study is required for such analyses.

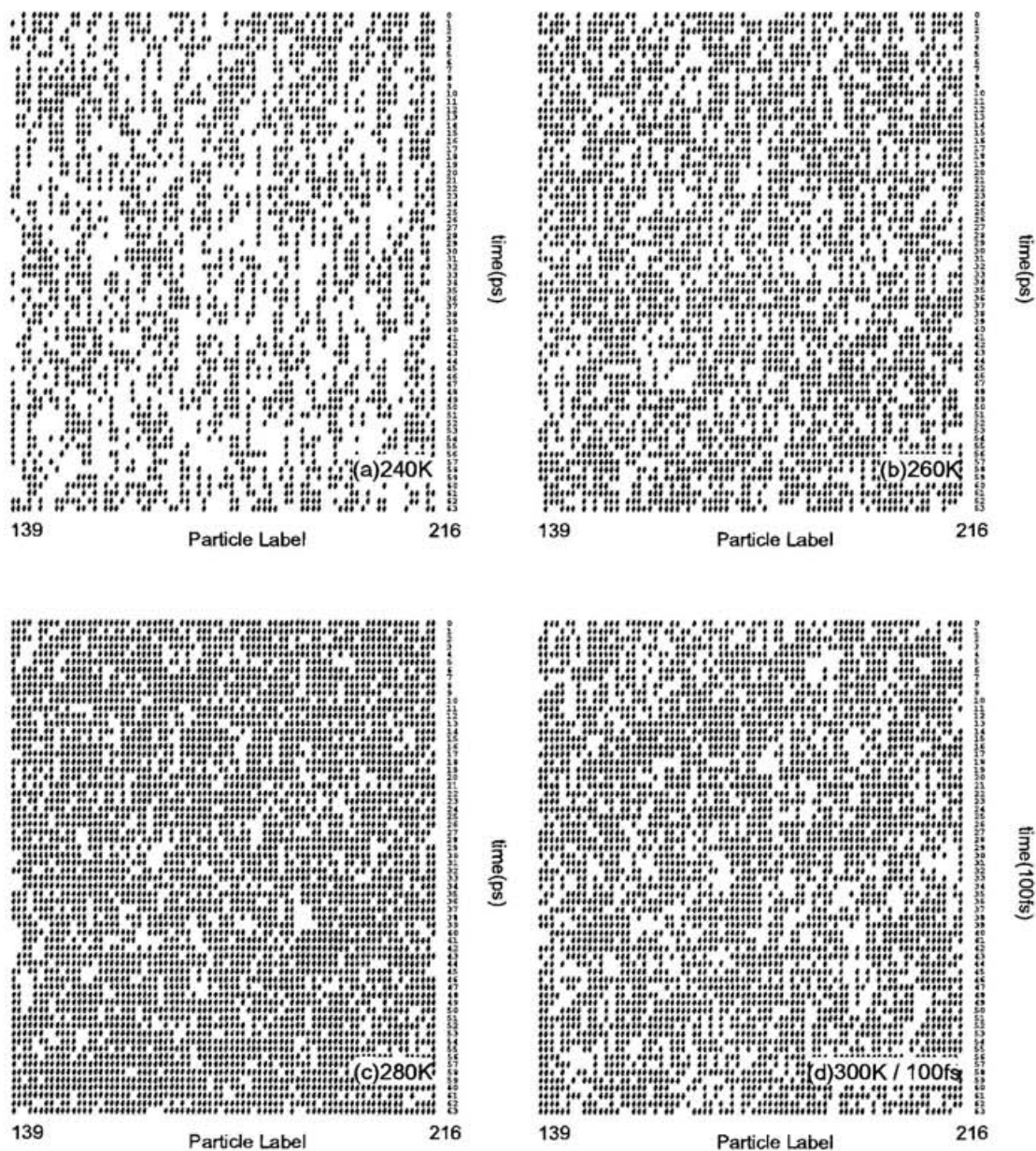


Figure 4.1: The hydrogen bond rearrangement map at (a) 240K, (b) 260K, (c) 280K, and (d) 300K. '#' is put when any hydrogen bond of a water molecule i is rearranged (i e connected or disconnected) at time t . As molecules are arbitrarily labeled, there is no spatial information in abscissa. Not all molecules are indicated. Note that the time scale is different in Fig. (d).

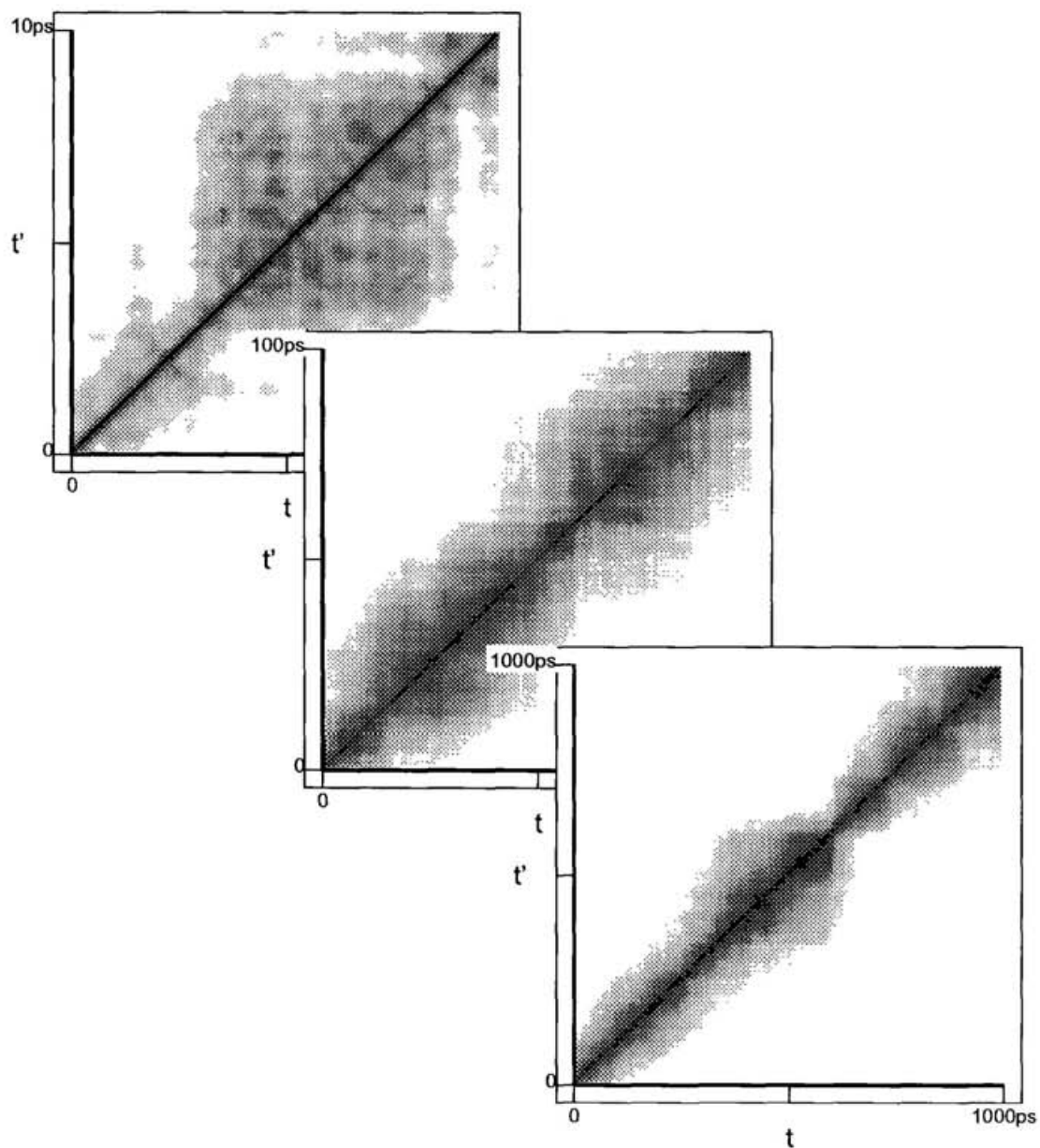


Figure 4.2: The distance matrices of liquid water at 248K for various time ranges are indicated. 64 molecules are in the system.

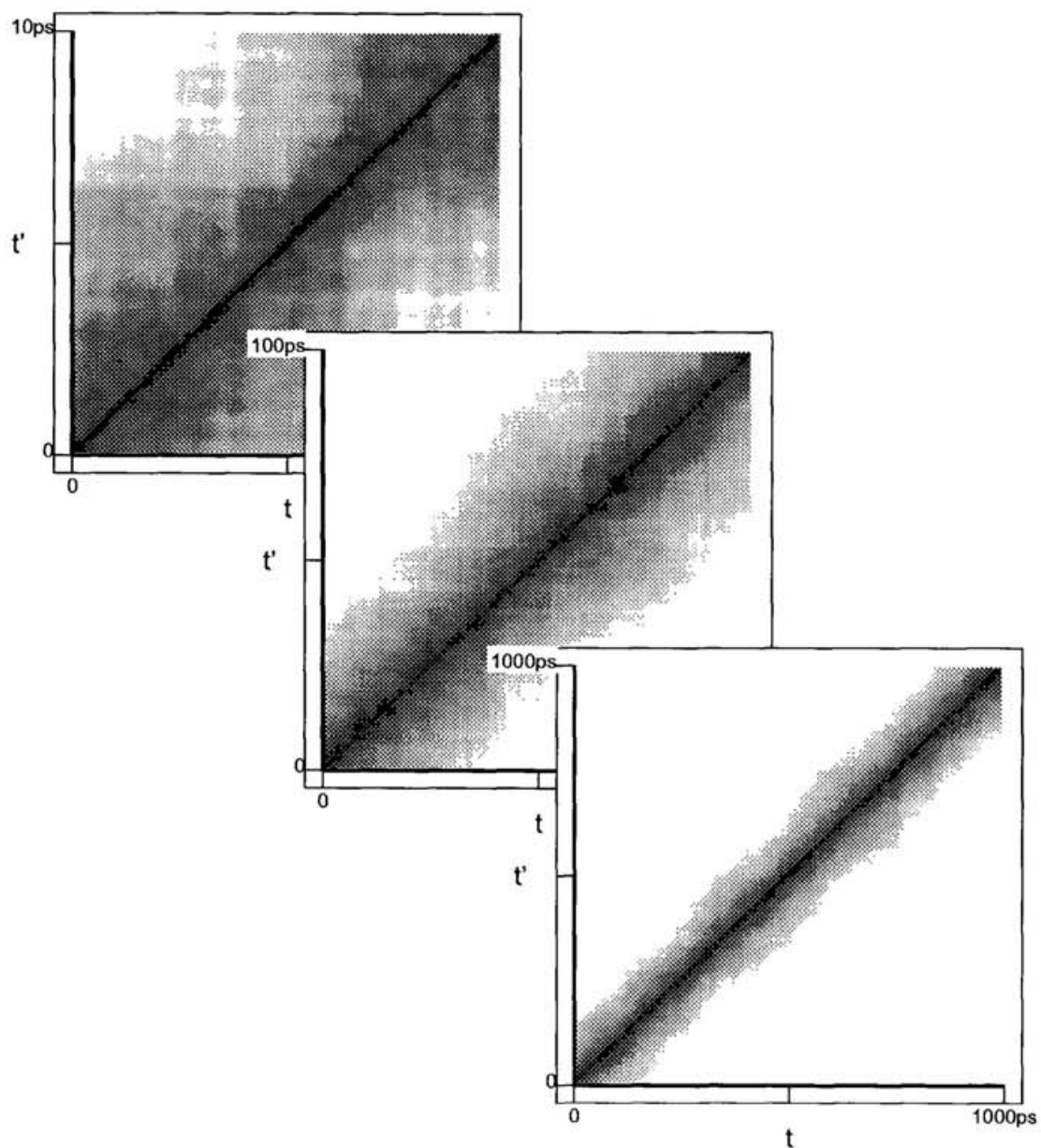


Figure 4.3: The distance matrices of liquid water at 273K for various time ranges are indicated. 64 molecules are in the system.

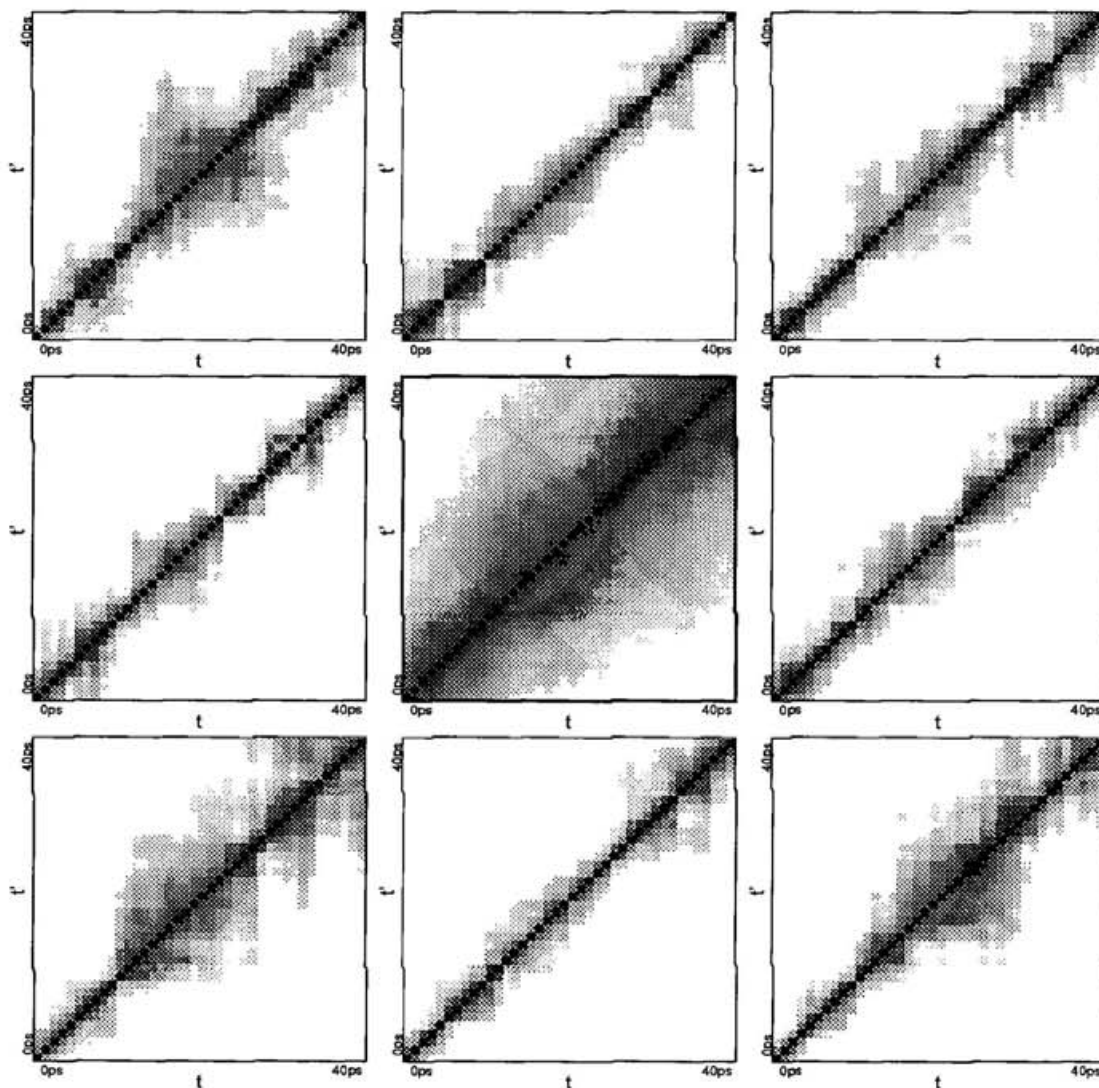


Figure 4.4: The distance matrices of liquid water during 40ps at 240K. 216 molecules are in the total system. Center is the total distance matrix, surroundings are partial distance matrix of 1/8 system.

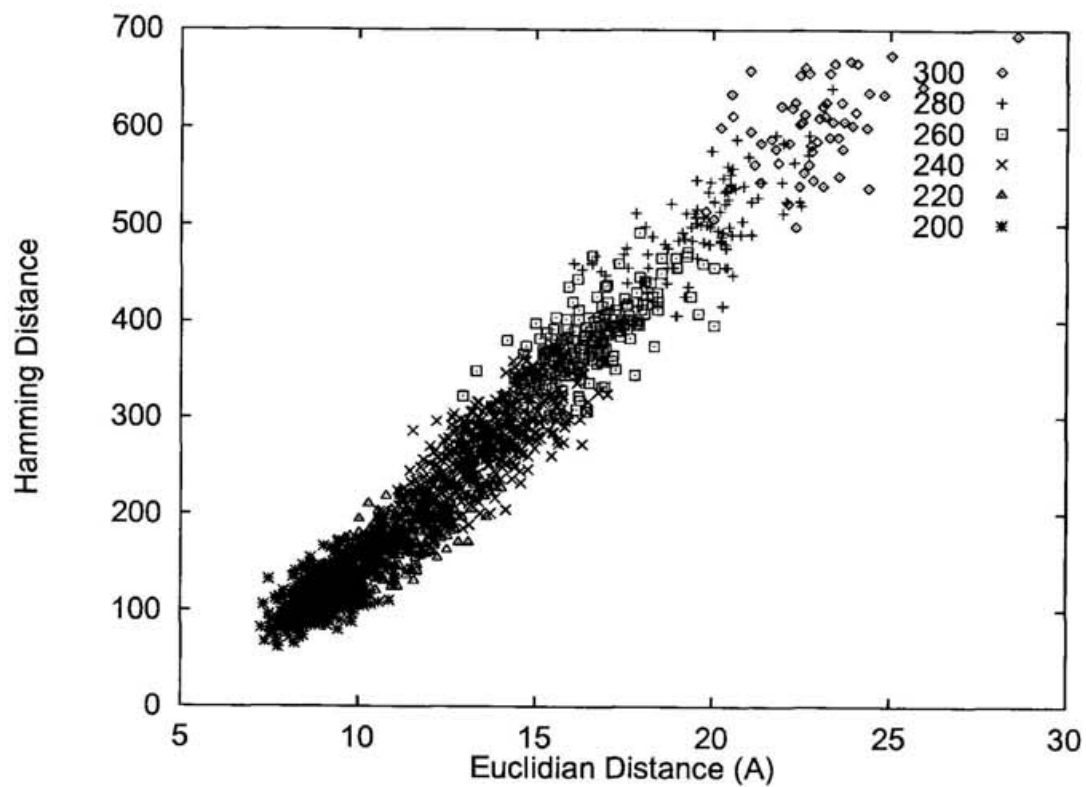


Figure 4.5: The Hamming distance is plotted against Euclidean distance. They are calculated from successive MD configurations in 1ps interval.

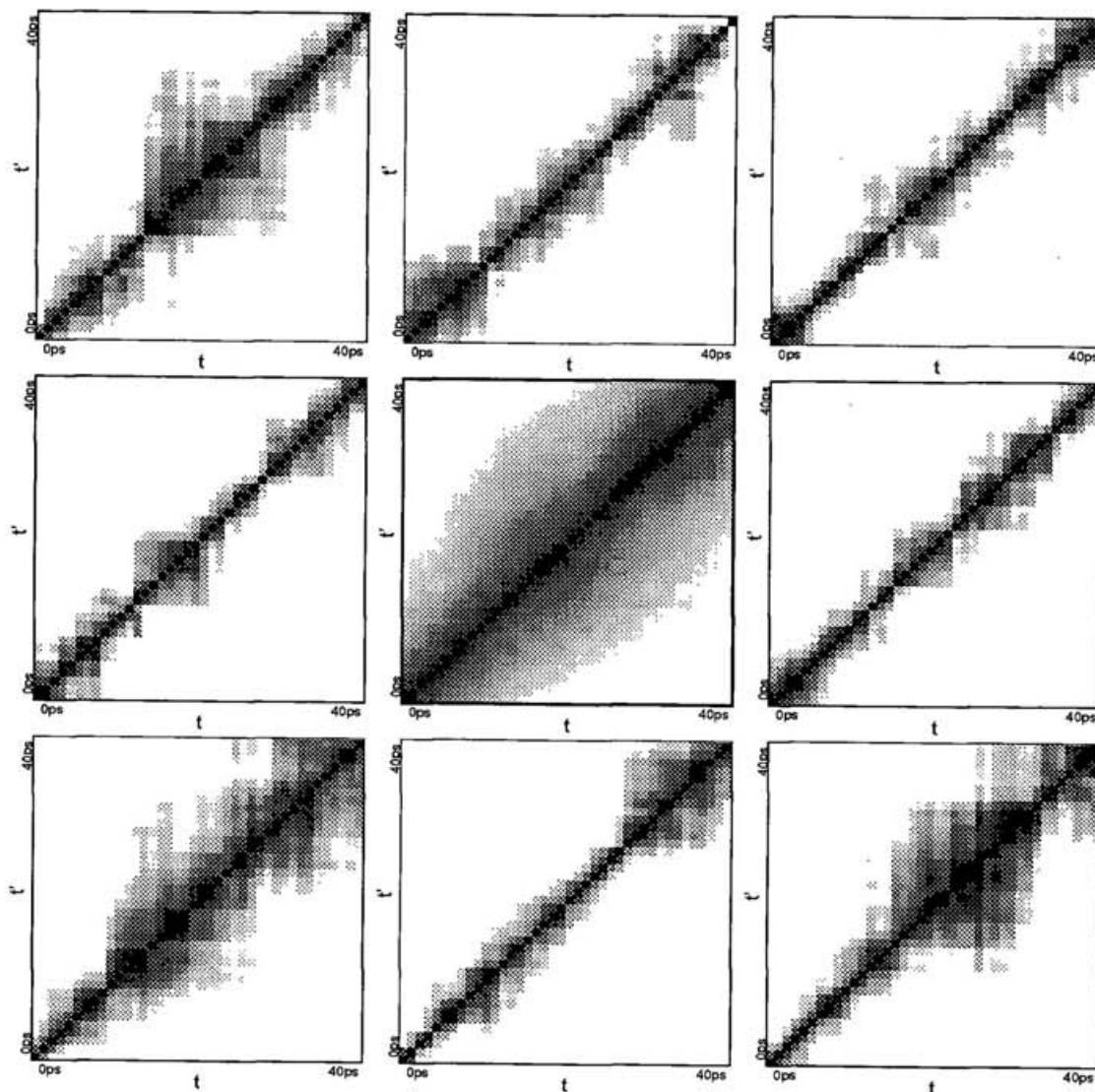


Figure 4.6: The Hamming distance matrices of liquid water during 40ps at 240K, made from the same trajectory as 4.4. 216 molecules are in the total system. Center is the total distance matrix, surroundings are partial distance matrix of 1/8 system.

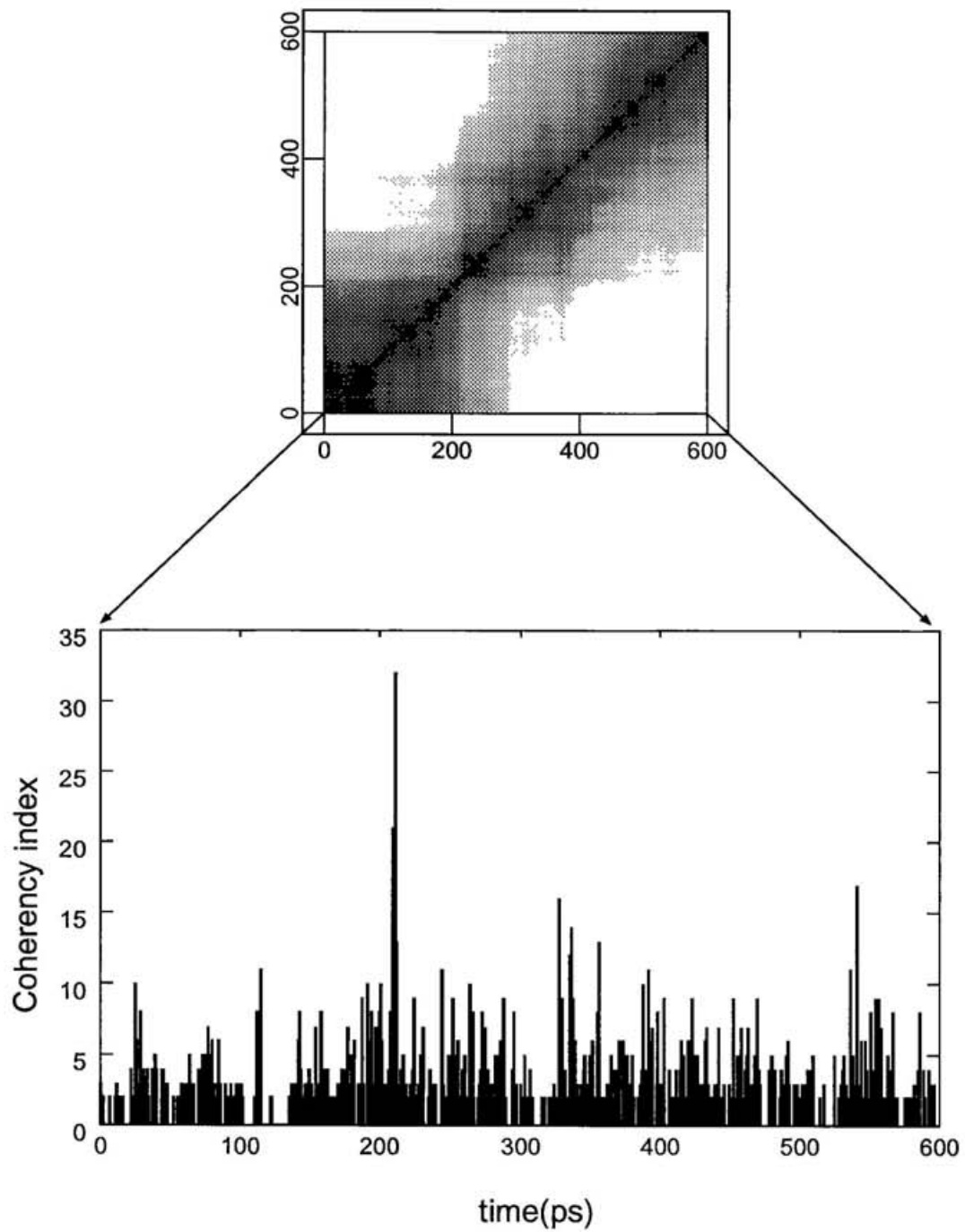


Figure 4.7: The coherency index of 64 water molecules at 240K for 600ps is indicated with the distance matrix.

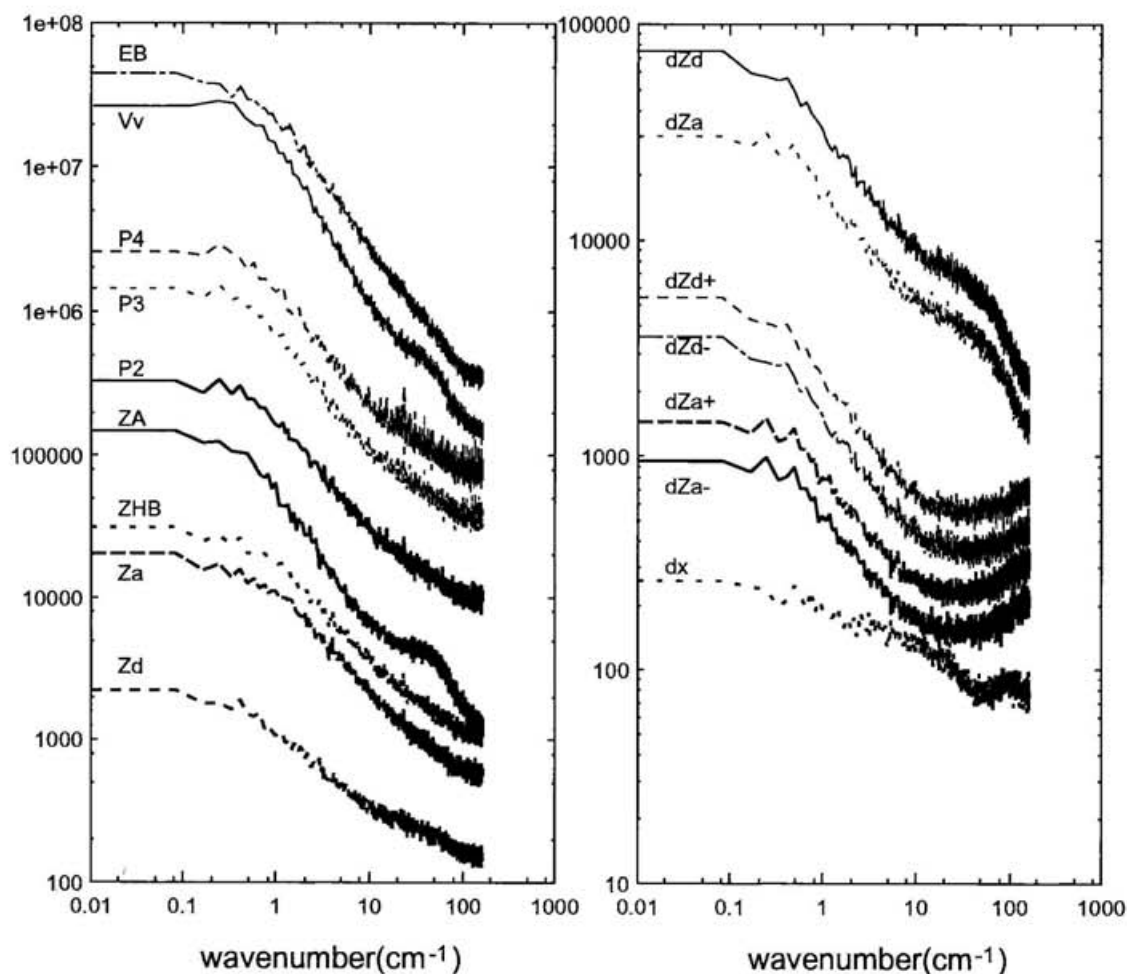


Figure 4.8: The power spectra of various local topological indices at 240K. The labels correspond to: ZA: Number of adjacent molecules, defined as the number of molecules nearer than $r_C = 3.5\text{\AA}$; ZHB: number of HBs of a molecule; Zd: number of the donating HBs; Za: number of the accepting HBs; EB: binding energy; P2, P3, P4: number of n th neighbor along the network; Vv: volume of Voronoi polyhedron; dZd+, dZd-: increment / decrement of the number of the donating HBs; dZd+, dZa-: increment / decrement of the number of the accepting HBs; dZd:=(dZd-)+(dZd+); dZa:=(dZa-)+(dZa+); dx: square displacement of the center of mass just after the moment. Vertical axes are arbitrarily shifted. 216 molecules are in the system.

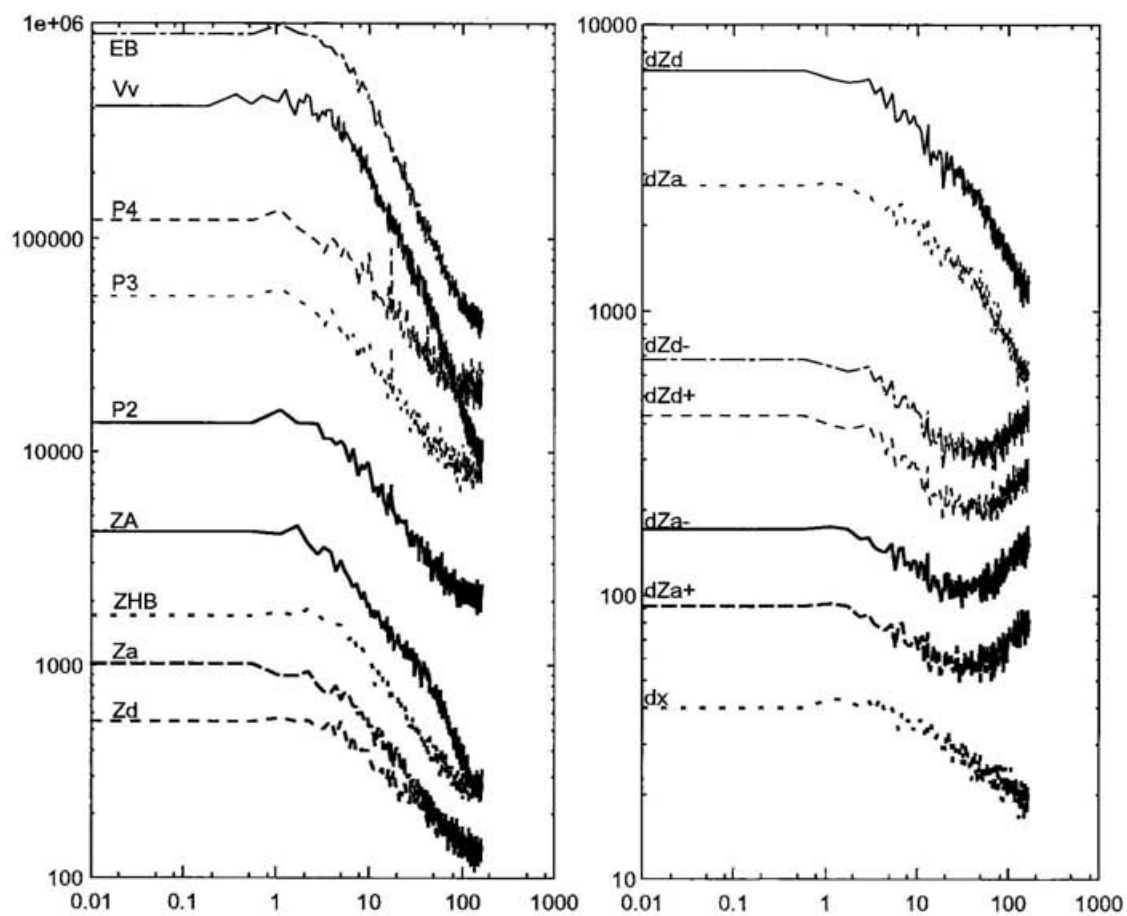


Figure 4.9: The power spectra of various local topological indices at 300K. Labels are the same as in Fig. 4.8. Vertical axes are arbitrarily shifted.

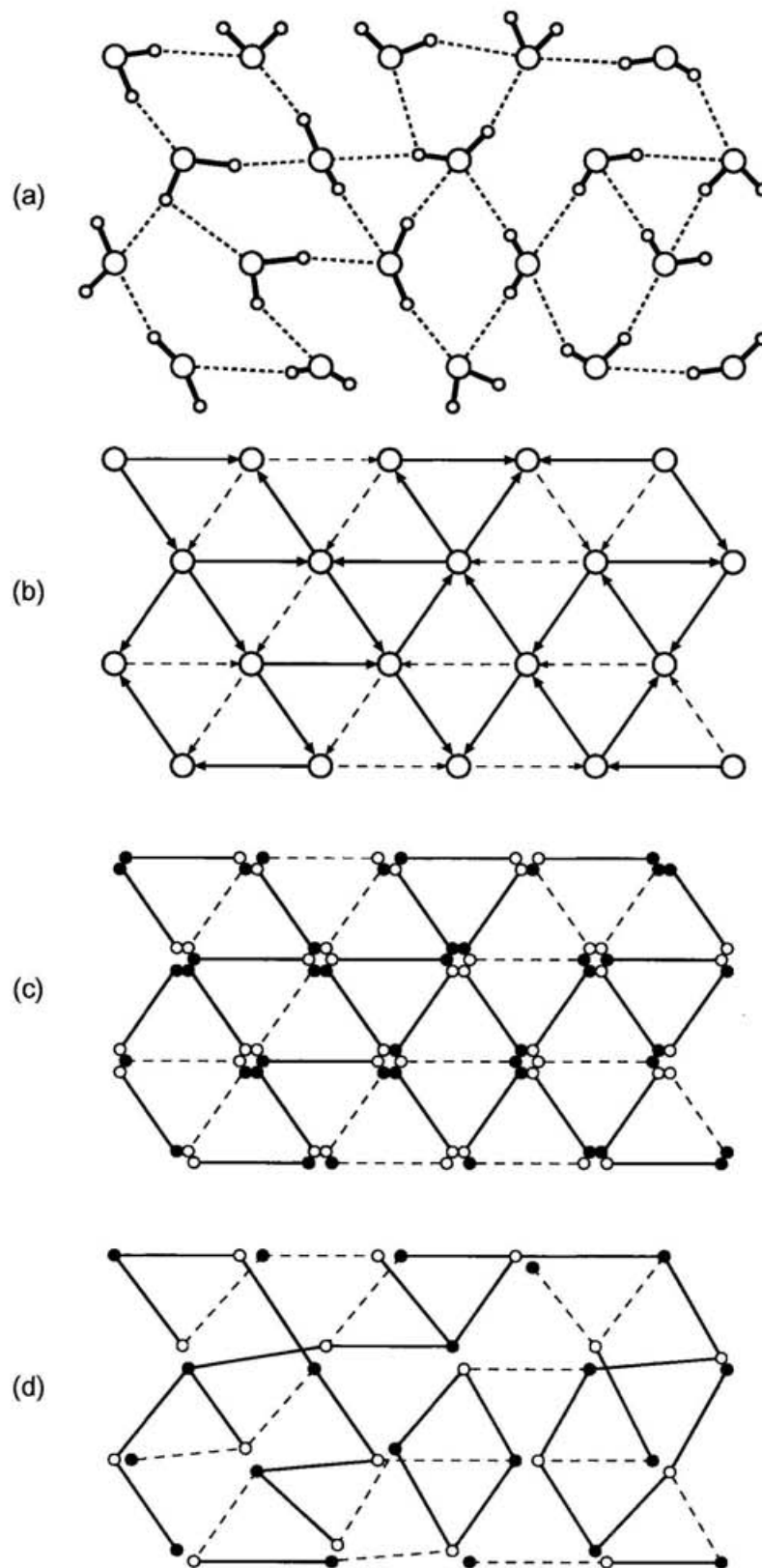


Figure 4.10: The separation scheme of the HB network. (a) The original HBN in liquid water; (b) The same network represented by digraph (*i.e.* directed graph). Virtual HBs are added; (c) Arrows are replaced by the bond with black and white circles; (d) Black and white circles are gathered and the network reduces to an undirected graph.

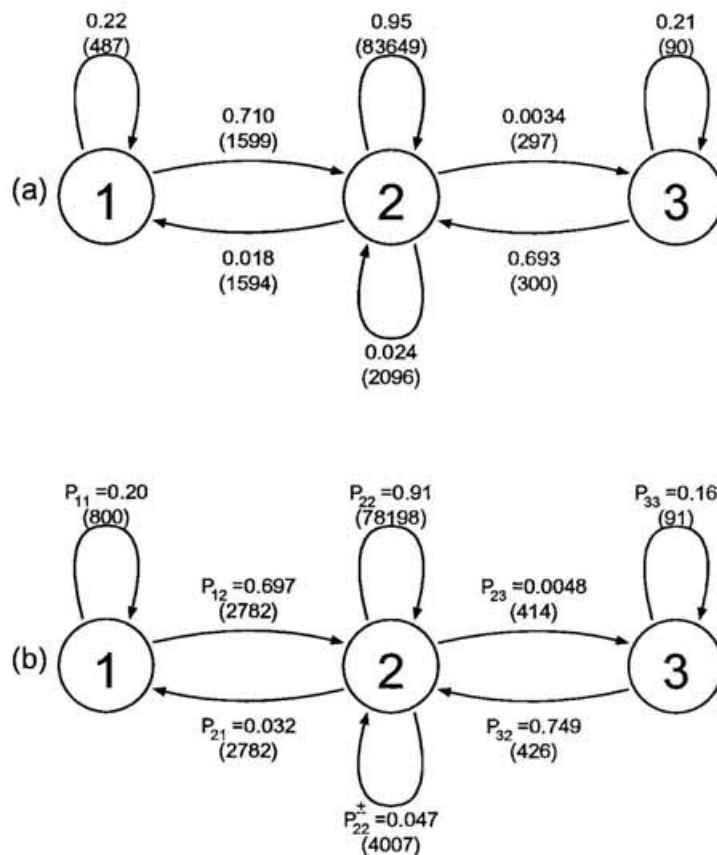


Figure 4.11: The state transition diagram of a node at (a)200K, (b)220K, extracted from the MD data. The state (i) of the node is specified by the number (i) of the donating HBs from that node. P_{ij} denotes the transition probability from state i to state j . P_{22}^{\pm} is the probability that one HB is detached and another is connected at the same time. The numbers in parentheses are raw occurrence number in the simulation. Δt is 1ps.

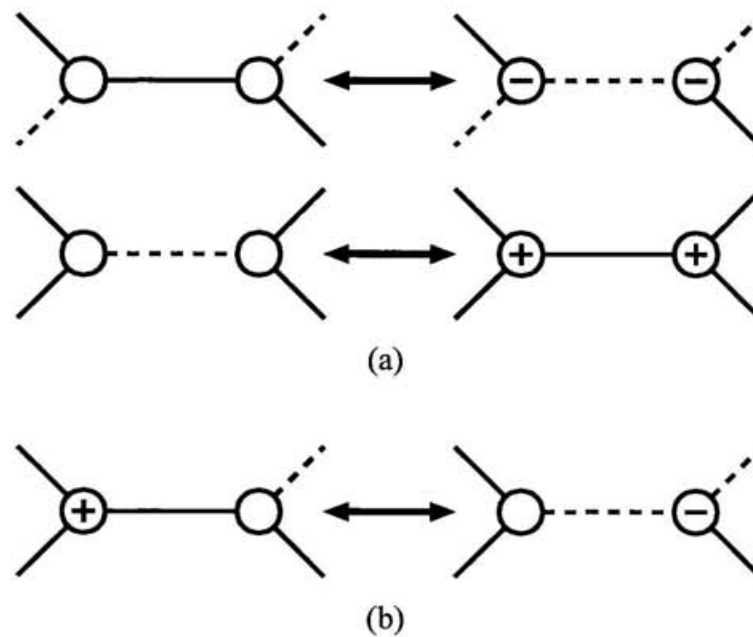


Figure 4.12: Three types of defect motion. (a) creation and annihilation of defect pair; (b) propagation of a defect. Dashed line denotes the virtual HE and solid line the HE. “+” and “-” indicate the oversatisfied and dissatisfied types of the defect, respectively.

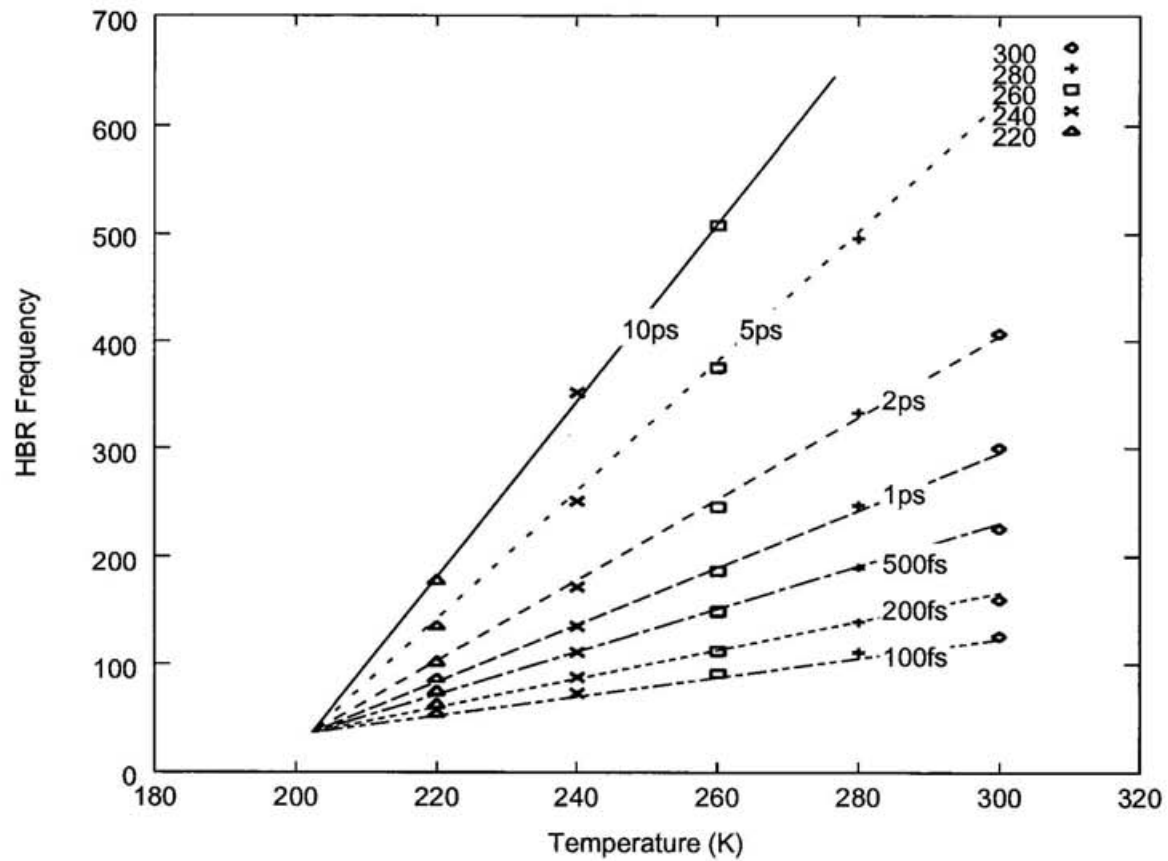


Figure 4.13: The number of hydrogen bonds which are connected or disconnected in the short time Δt , indicated on the lines, are plotted against temperature. 216 molecules are in the system.

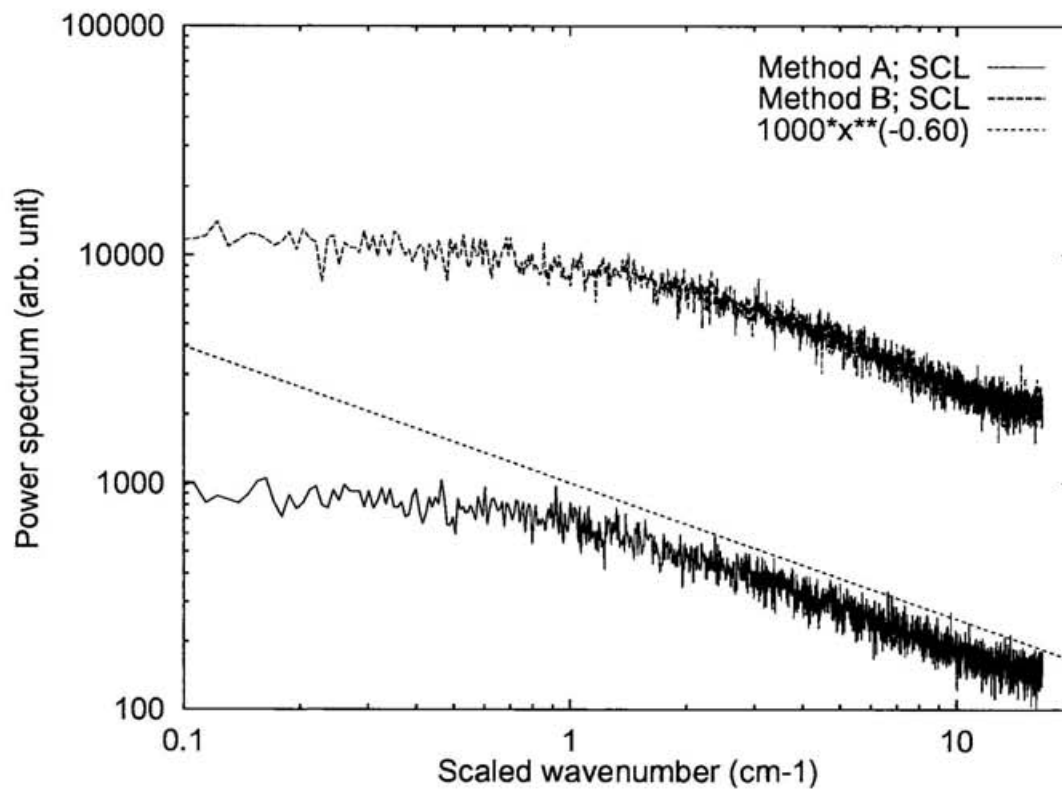


Figure 4.14: The energy fluctuations in the model lattice systems are plotted in log-log scale. Upper lines are obtained by method B and lower by method A.

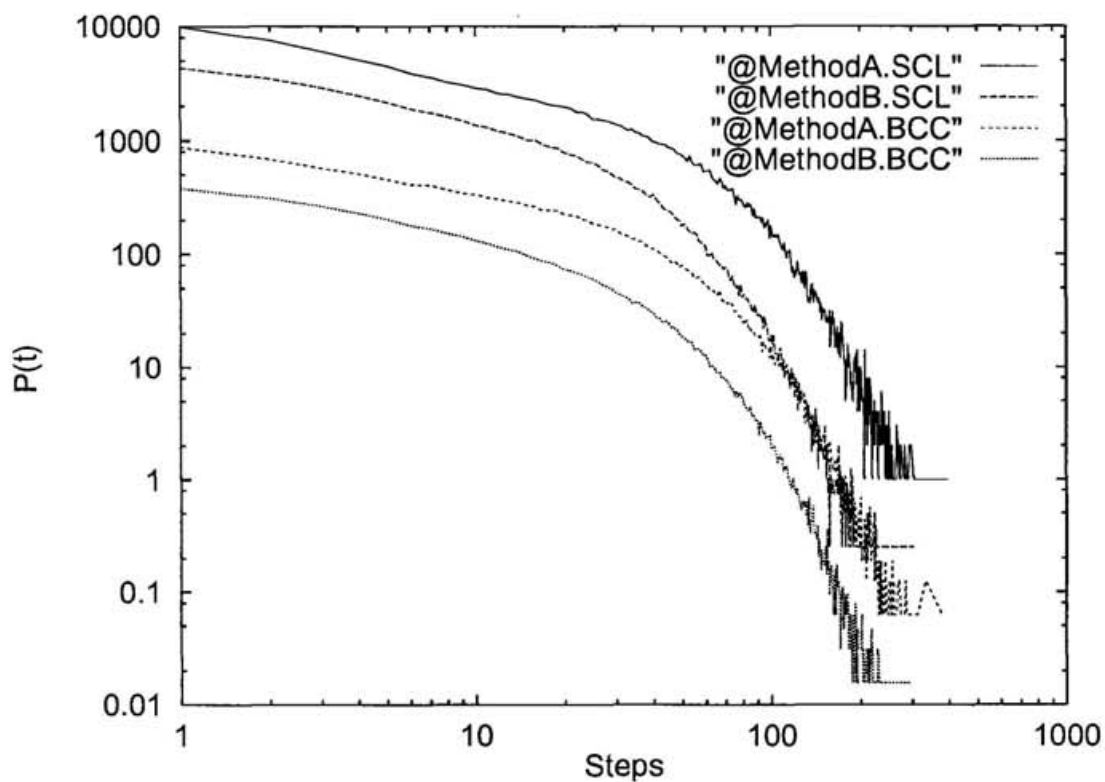


Figure 4.15: The HB lifetime distribution obtained for the models under various setting. From top: Result by method A with simple cubic lattice (SCL); method B with SCL; method A with body centered cubic lattice (BCC); method B with BCC. Vertical axis is in arbitrary unit.

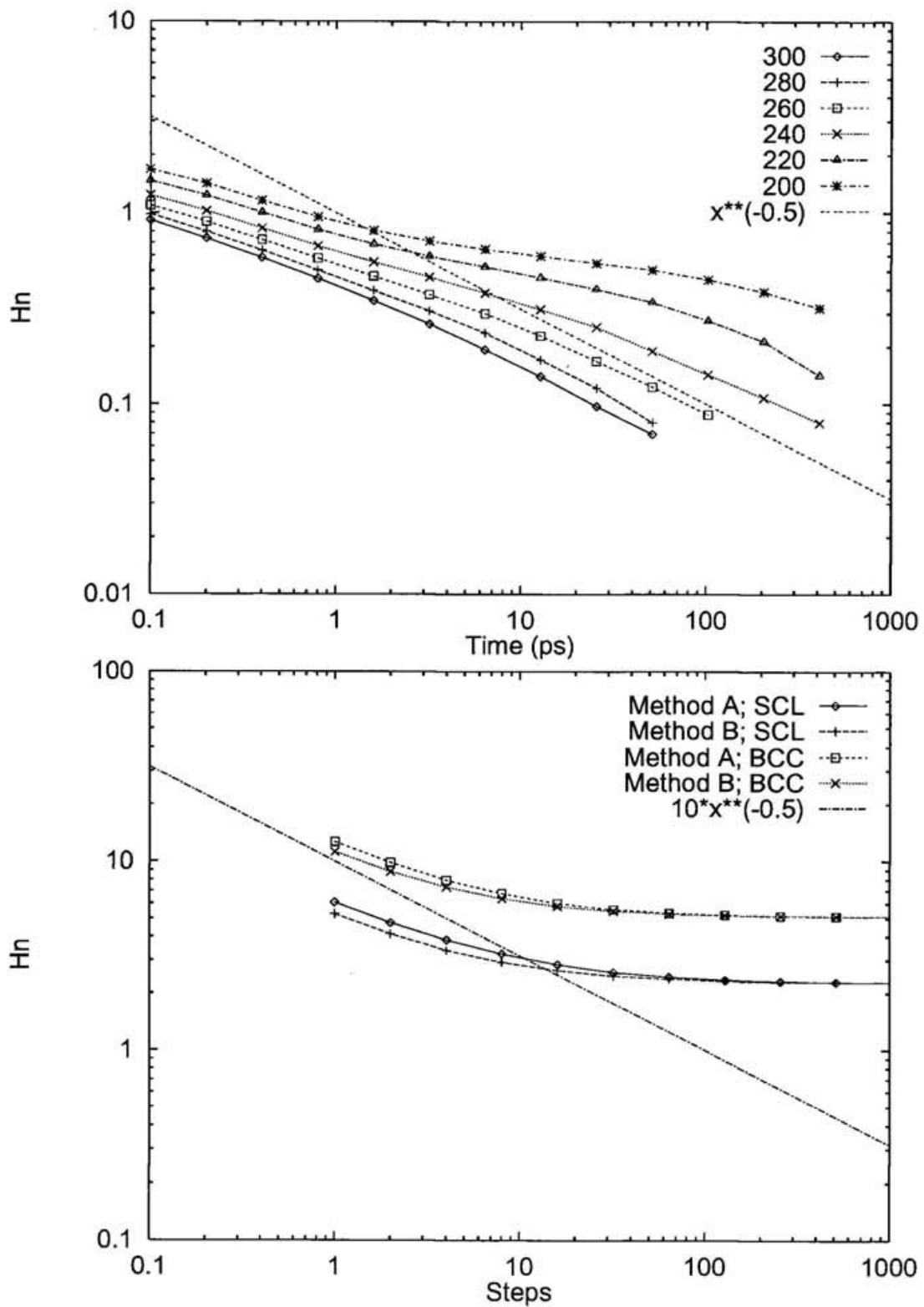


Figure 4.16: The heterogeneity index defined in Eq. 4.18. (a) MD results; (b) Lattice model. Straight dotted lines indicate $n^{-\frac{1}{2}}$ ($t^{-\frac{1}{2}}$) for eye guide.

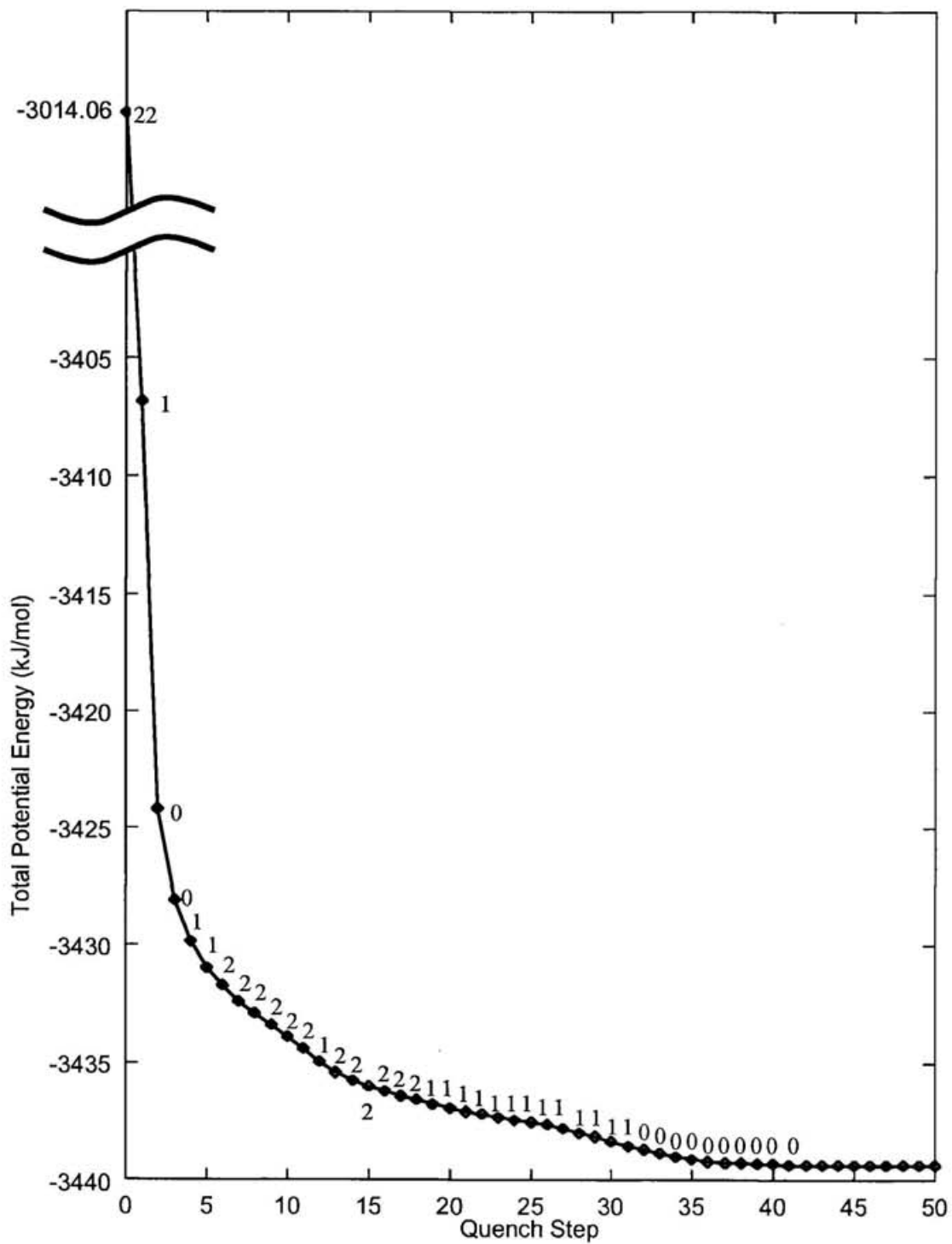


Figure 4.17: The potential energy profile in the quenching process from an instantaneous structure at 240K. The number above the line denotes the number of instantaneous normal modes with imaginary frequency. 64 molecules are in the system.

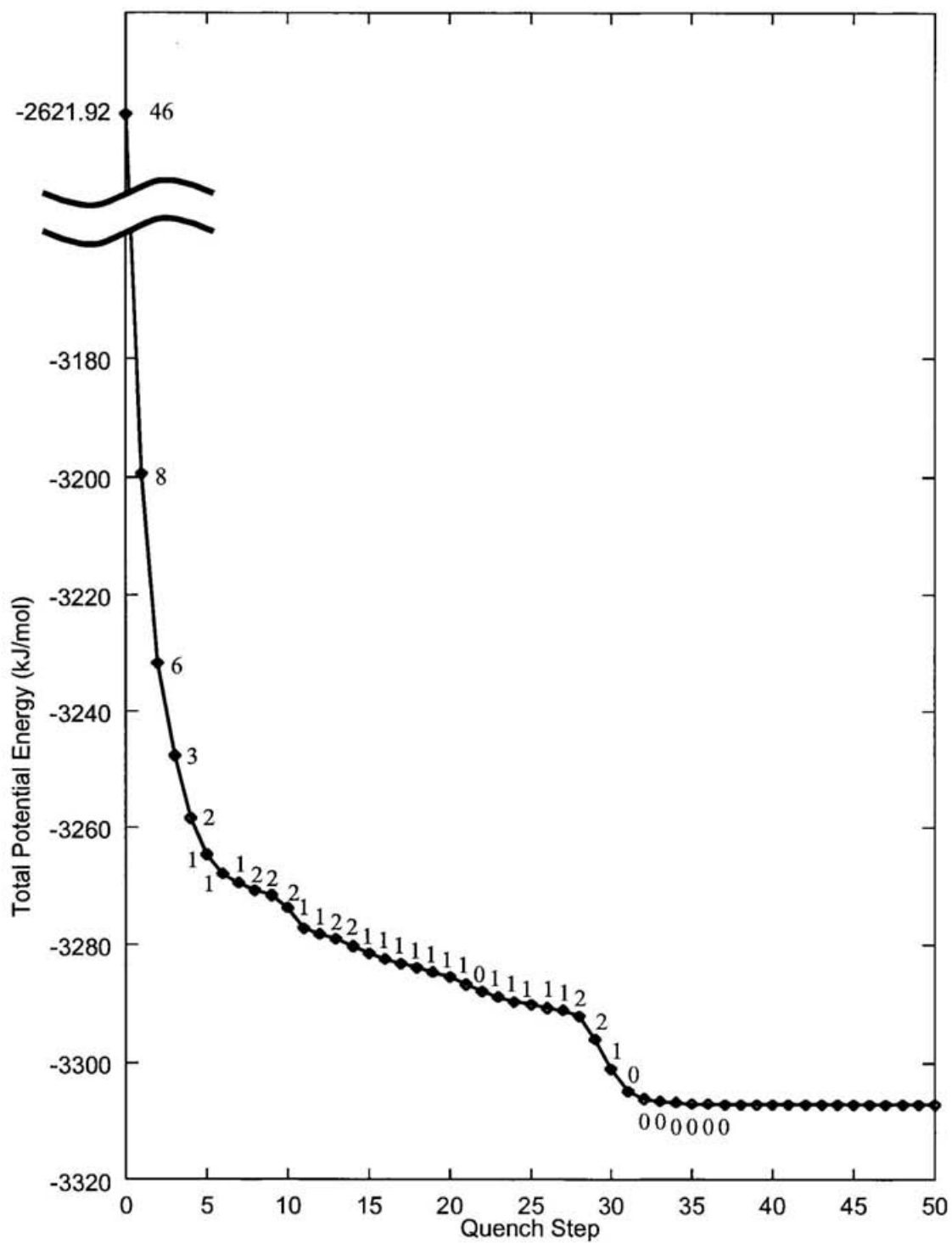


Figure 4.18: The potential energy profile in the quenching process from an instantaneous structure at 300K. The number above the line denotes the number of instantaneous normal modes with imaginary frequency. 64 molecules are in the system.

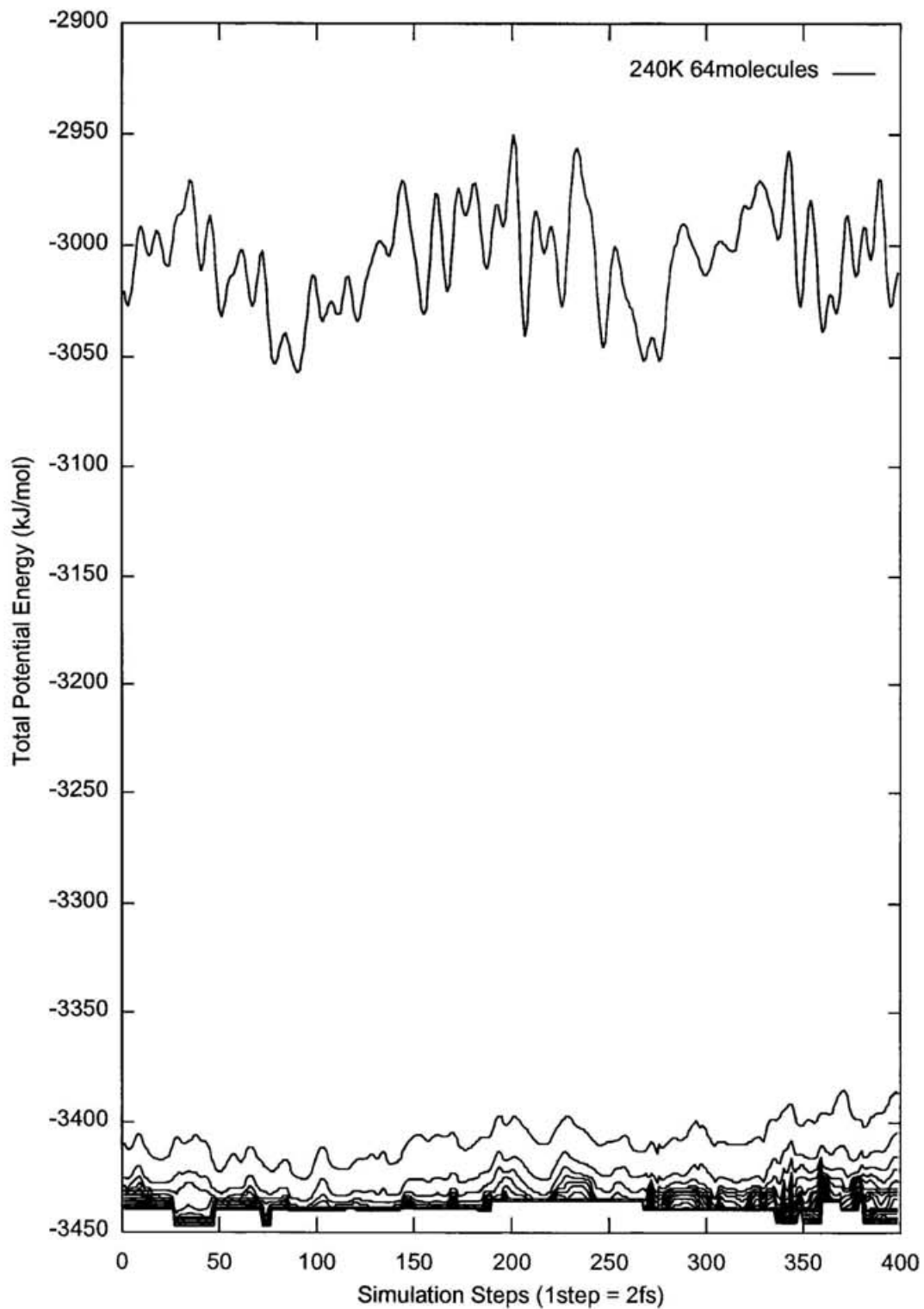


Figure 4.19: The potential energy profile in quenching processes from successive instantaneous structures at 240K. The ordinate is real simulation steps by 2fs and the abscissa is the potential energy profile along the steepest descent path. Potential is plotted at intervals of several virtual steps.

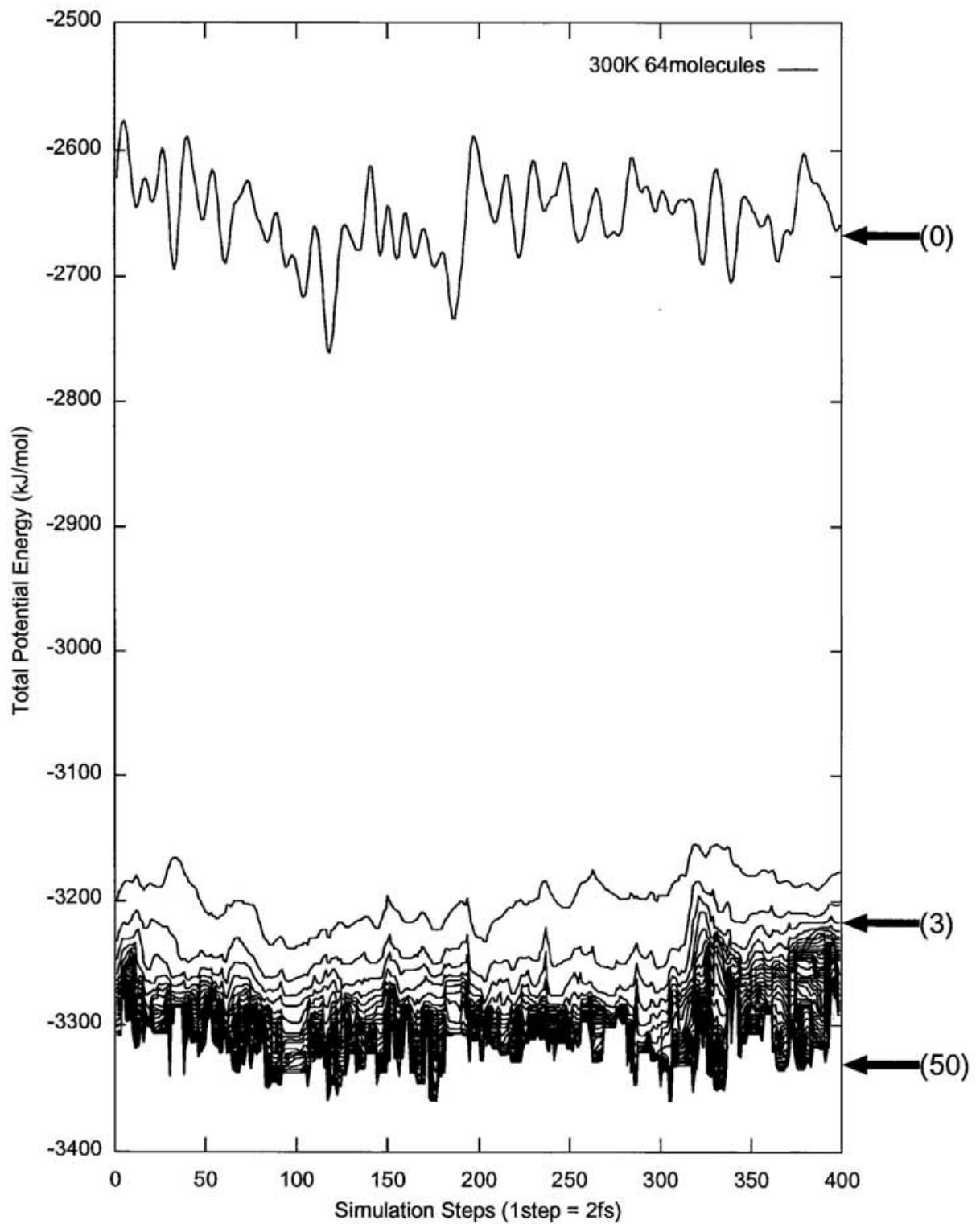


Figure 4.20: The same graph as Fig. 4.19 but at 300K. The numbers beside the graph correspond to the labels in the distance matrix, Fig. 4.21

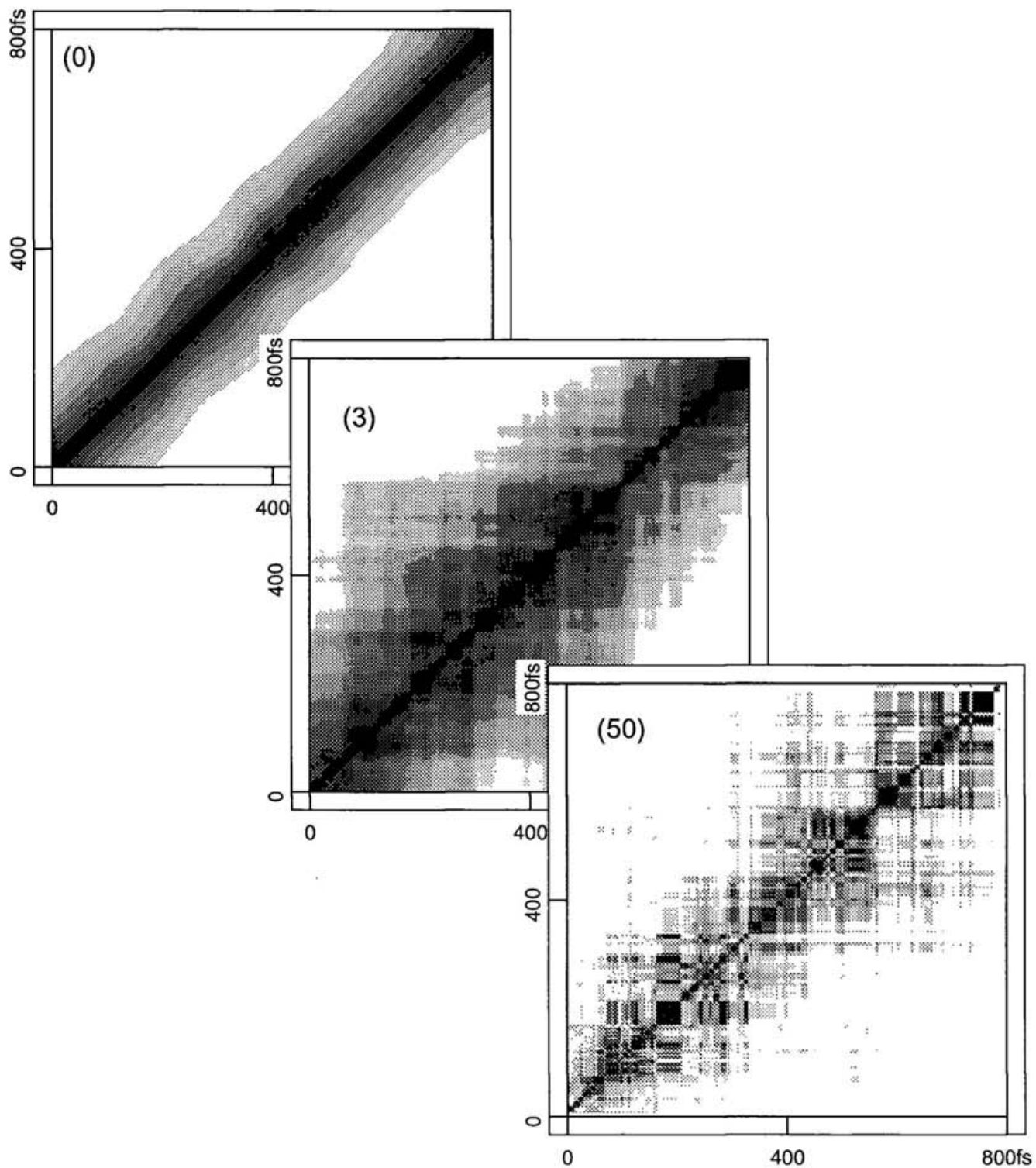


Figure 4.21: Various distance matrices in the quenching process; (0) before quenching; (3) slightly quenched trajectory (50) deeply quenched trajectory. The degree of grayness in the figure indicates the similarity between two configurations; the darker mark means that the configurations are closer in distance.

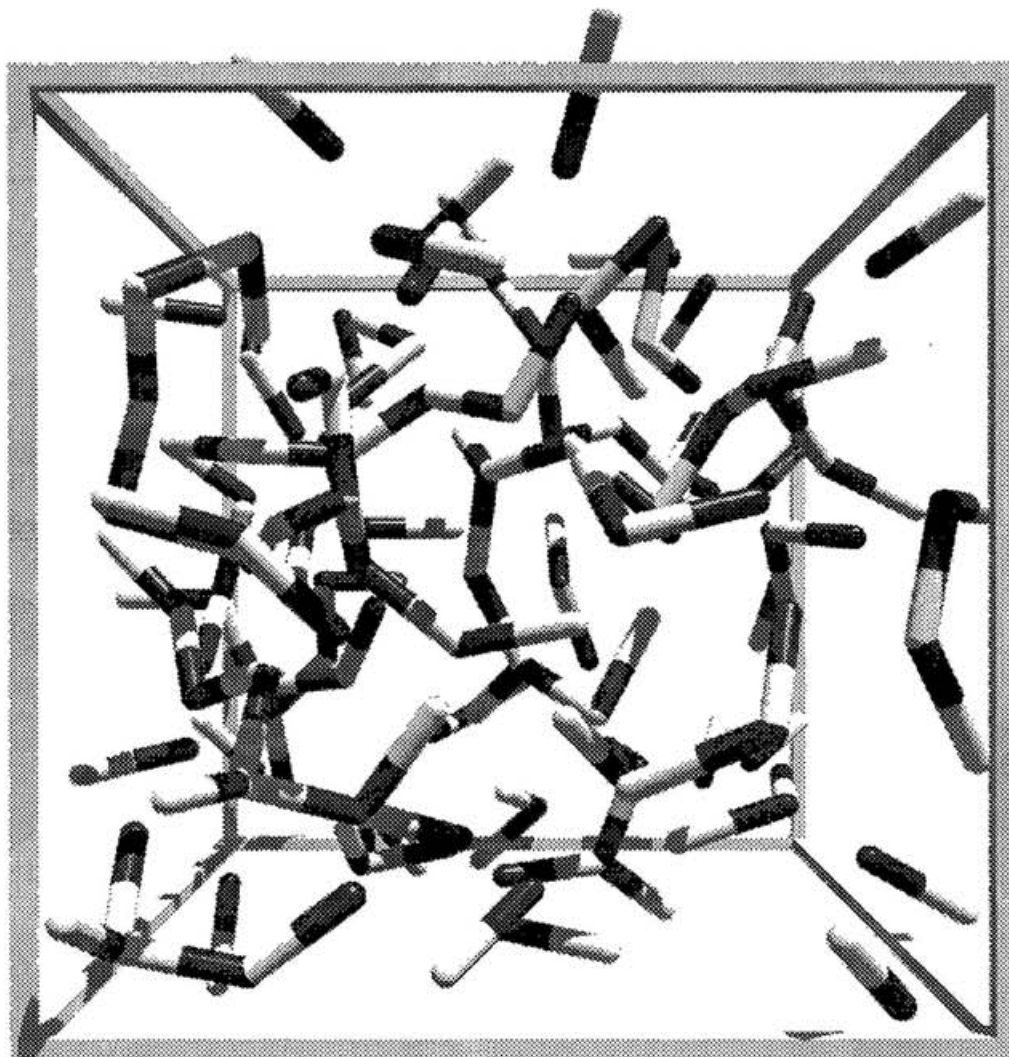


Figure 4.22: The illustration of survived hydrogen bond clusters at 240K. The hydrogen bonds connecting the same pair of molecules as 20ps before are indicated. Water molecules are omitted. Each bond is colored in two tones to distinguish its direction.

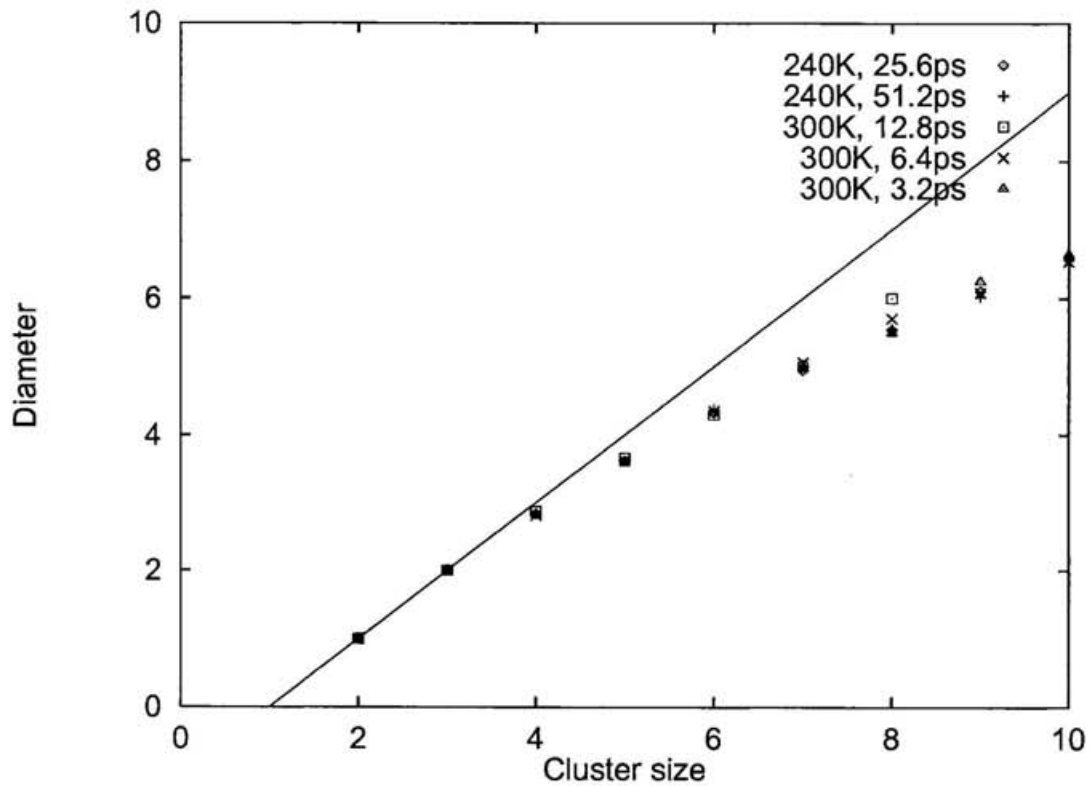


Figure 4.23: The average diameter of σ -clusters in liquid water at various observation time and temperatures. Solid line indicates the upper limit of diameter. Temperature and Δt are labeled in the graph.

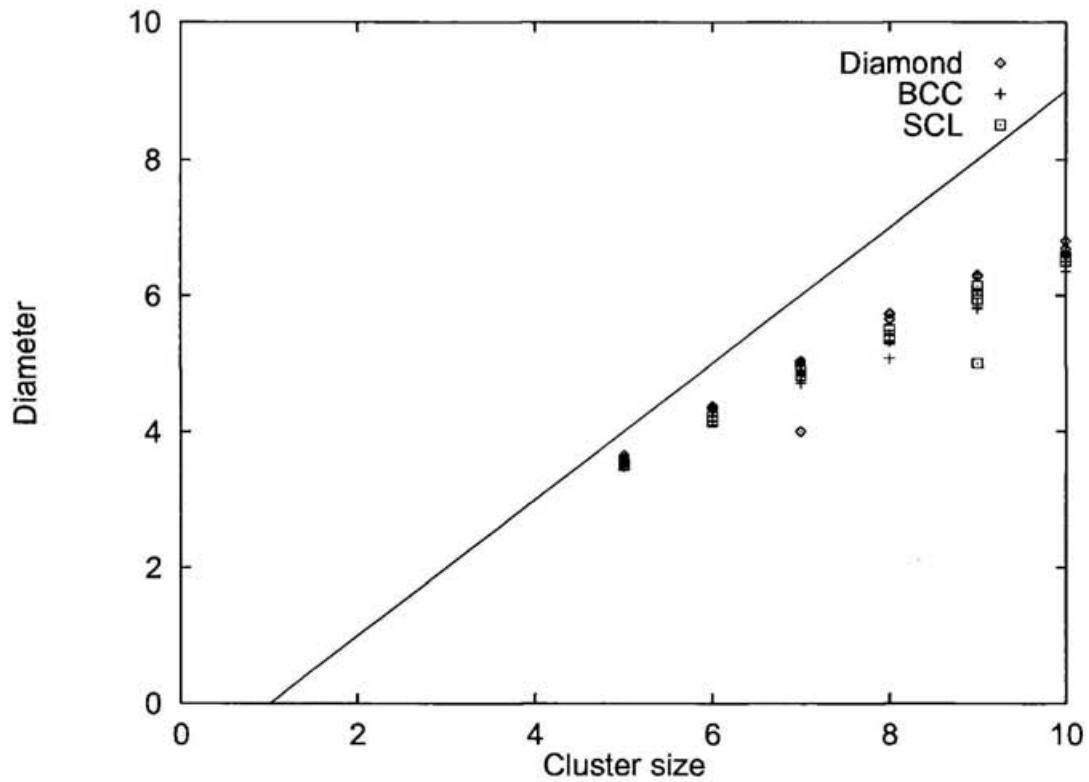


Figure 4.24: The average diameter of clusters in random bond lattice model with various lattices. Solid line indicates the upper limit of diameter. Various p are chosen below p_c , the bond percolation threshold.

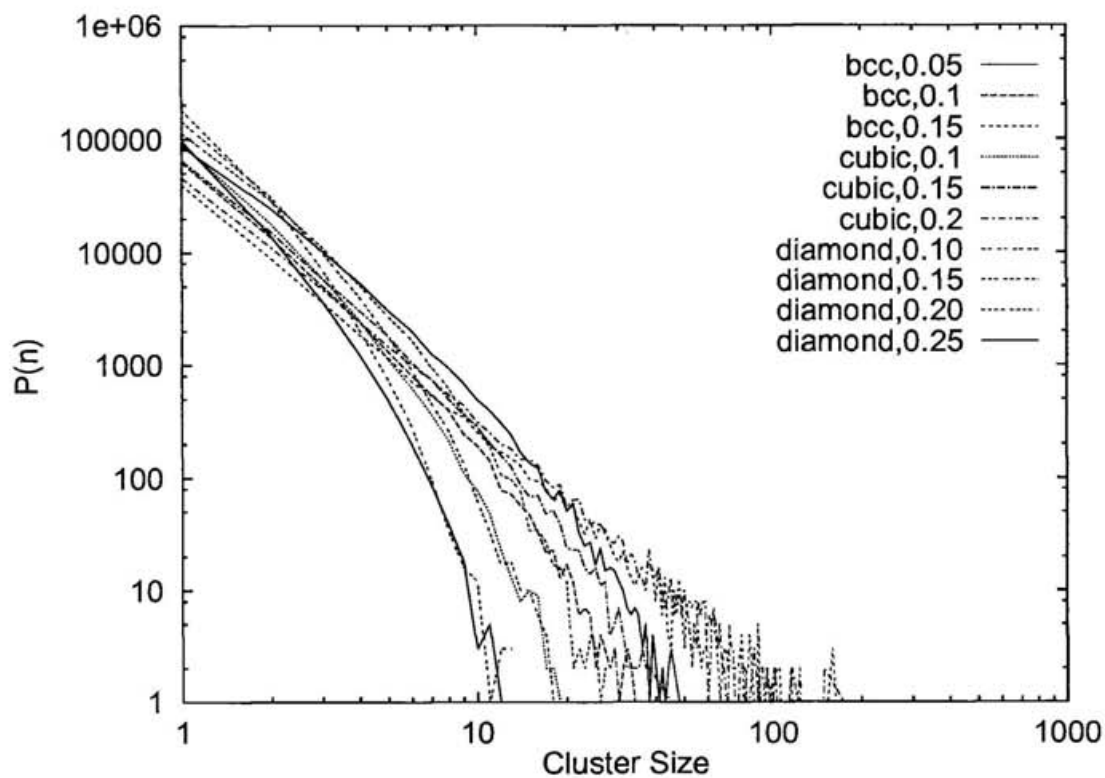


Figure 4.25: The cluster size distribution of the random bond lattice model with various lattices. bcc: body centered cubic lattice; cubic: simple cubic lattice; diamond: diamond lattice. Each number denotes p , the bond occupancy probability.

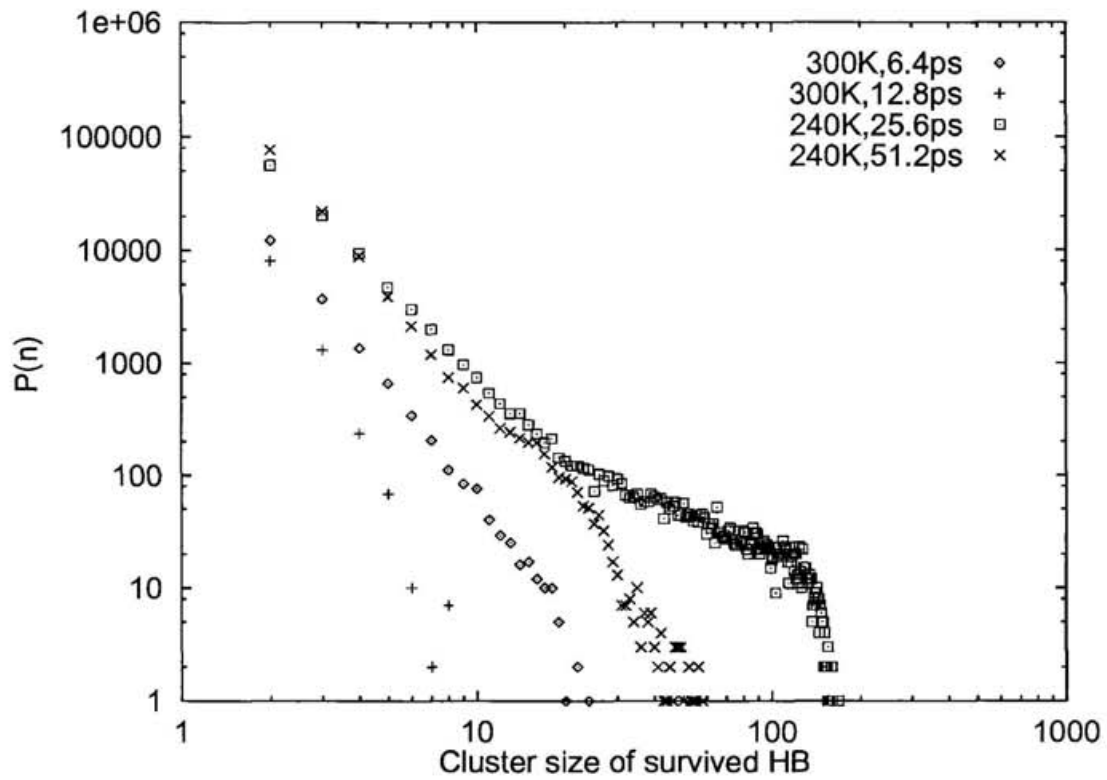


Figure 4.26: The size distribution of the σ -clusters in liquid water. Temperature and Δt are labeled in the graph. Square dots indicate that the bond occupancy probability is above the percolation threshold and that the system is percolated. The cluster size distribution is, however, truncated around $n=150$ because of the limitation by finite lattice size.

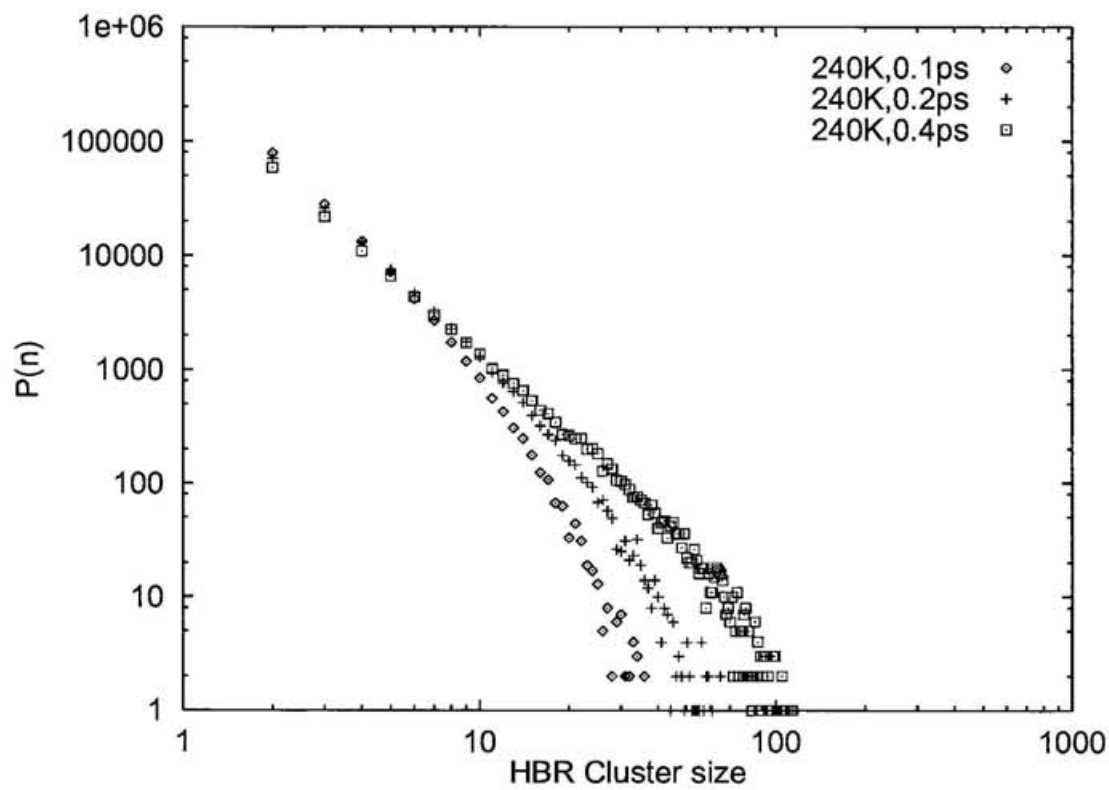


Figure 4.27: The size distribution of the α -clusters in liquid water. Temperature is 240K. Δt is 0.1ps, 0.2ps, and 0.4ps.

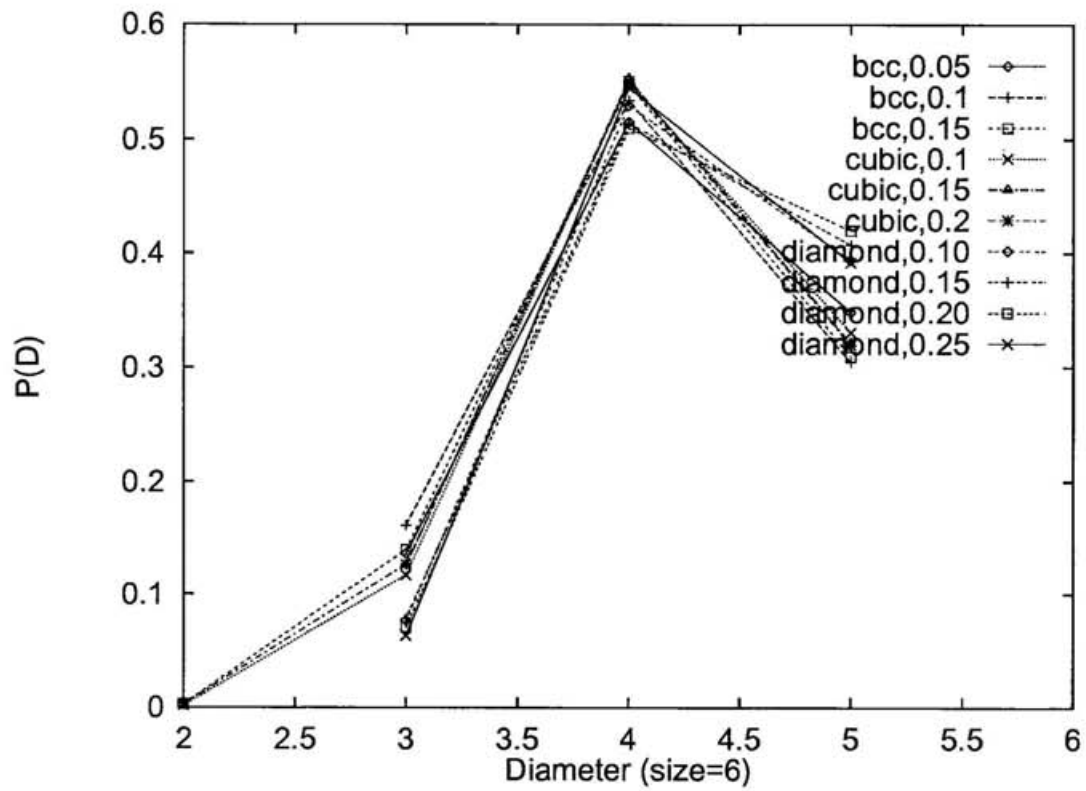


Figure 4.28: The diameter distribution of the size=6 cluster in random bond lattice model with various lattices.

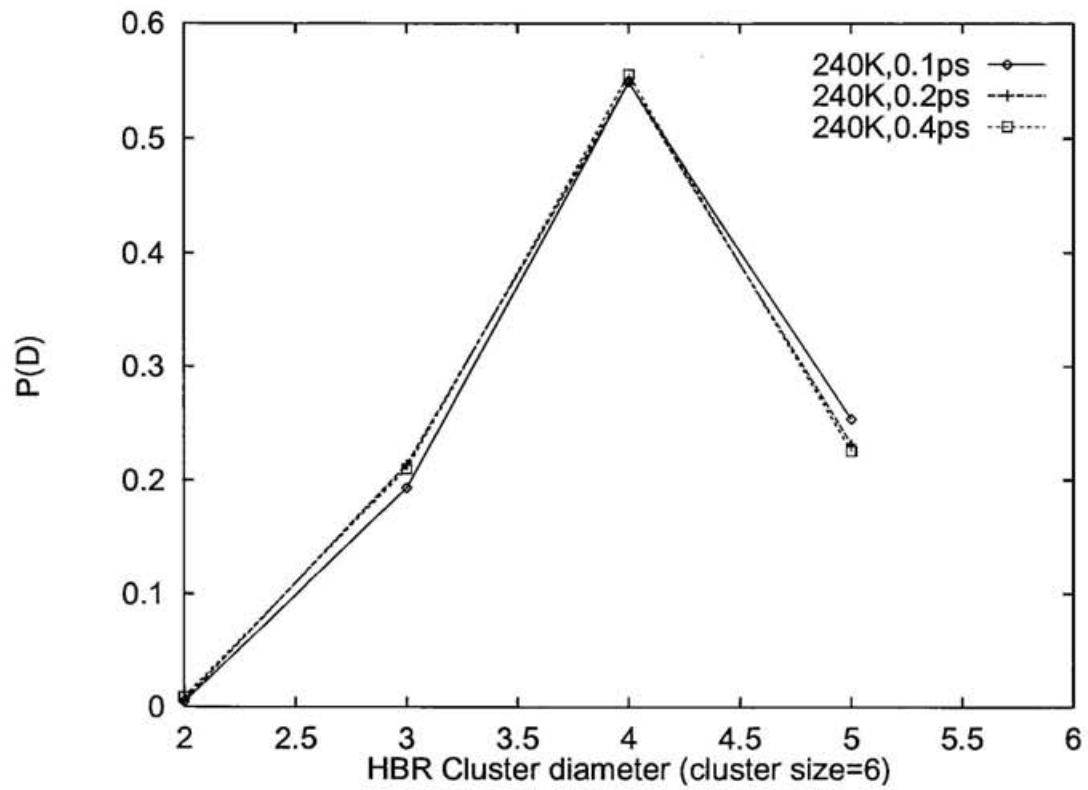


Figure 4.29: The diameter distribution of the α_6 -clusters in liquid water. Temperature and Δt are labeled in the graph.

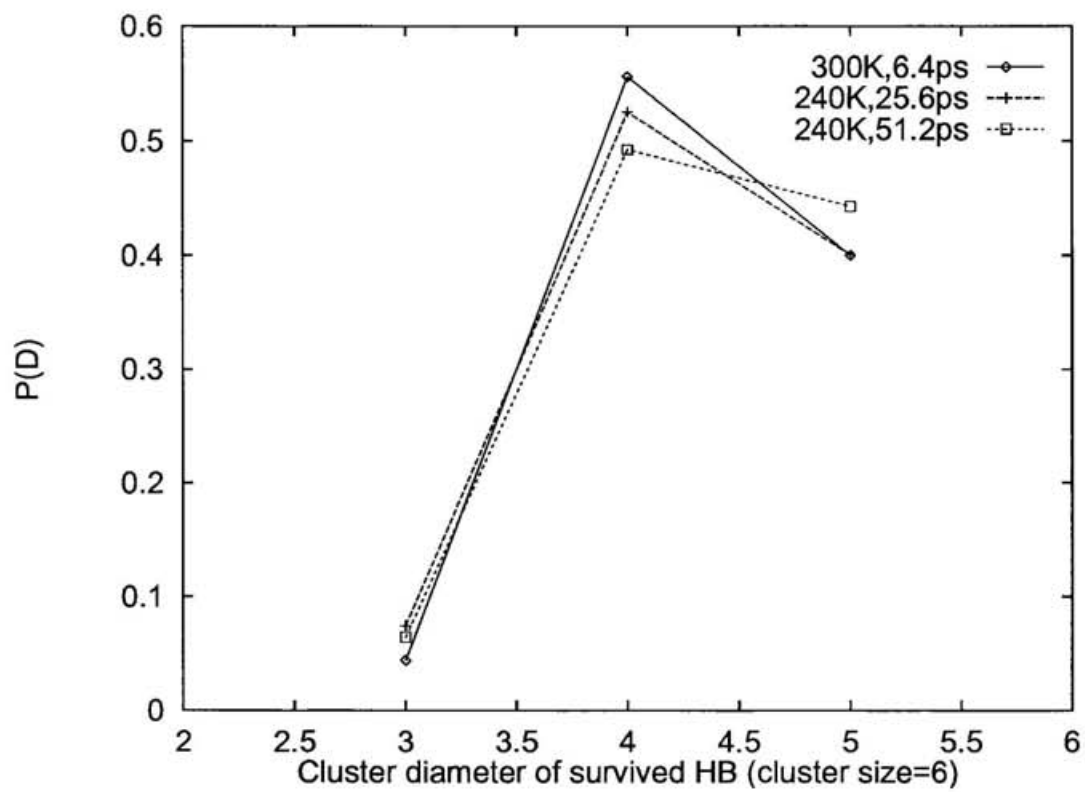


Figure 4.30: The diameter distribution of the σ_6 -clusters in liquid water. Temperature and Δt are labeled in the graph.

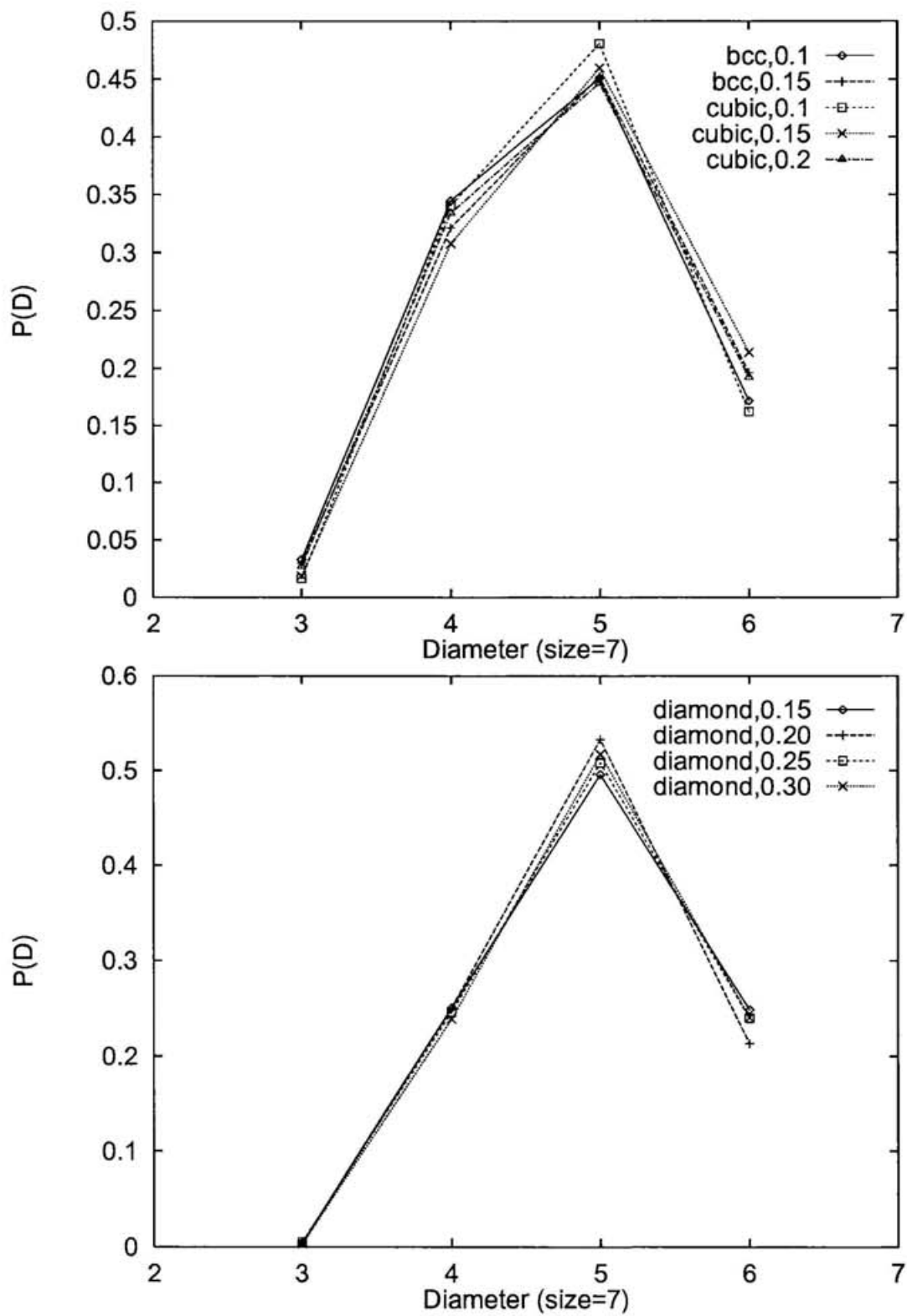


Figure 4.31: The diameter distribution of the size=7 cluster in random bond lattice model with various lattices.

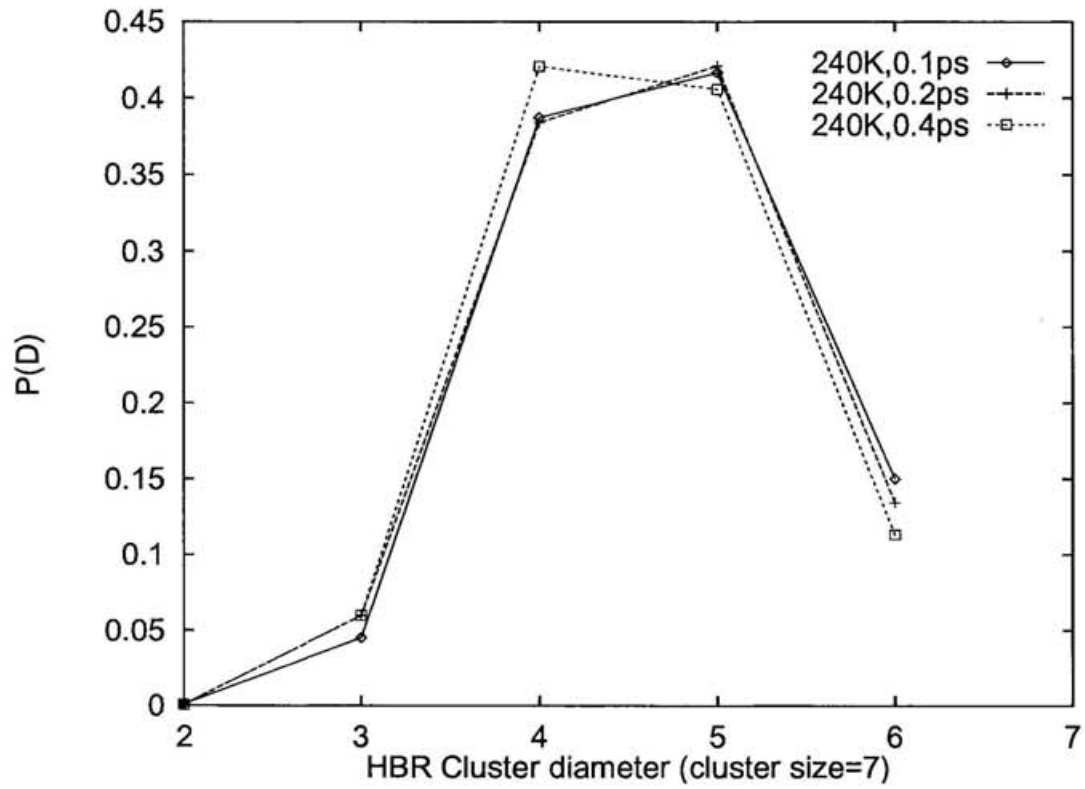


Figure 4.32: The diameter distribution of the α_7 -clusters in liquid water. Temperature and Δt are labeled in the graph.

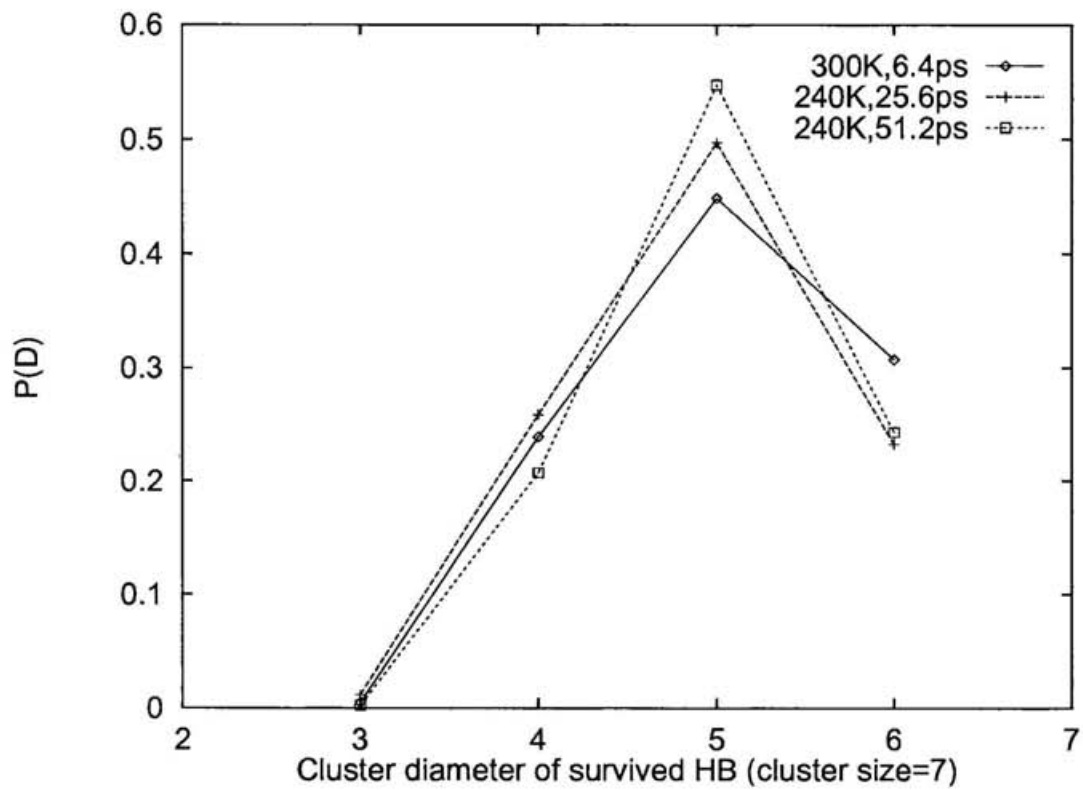


Figure 4.33: The diameter distribution of the σ_7 -clusters in liquid water. Temperature and Δt are labeled in the graph.

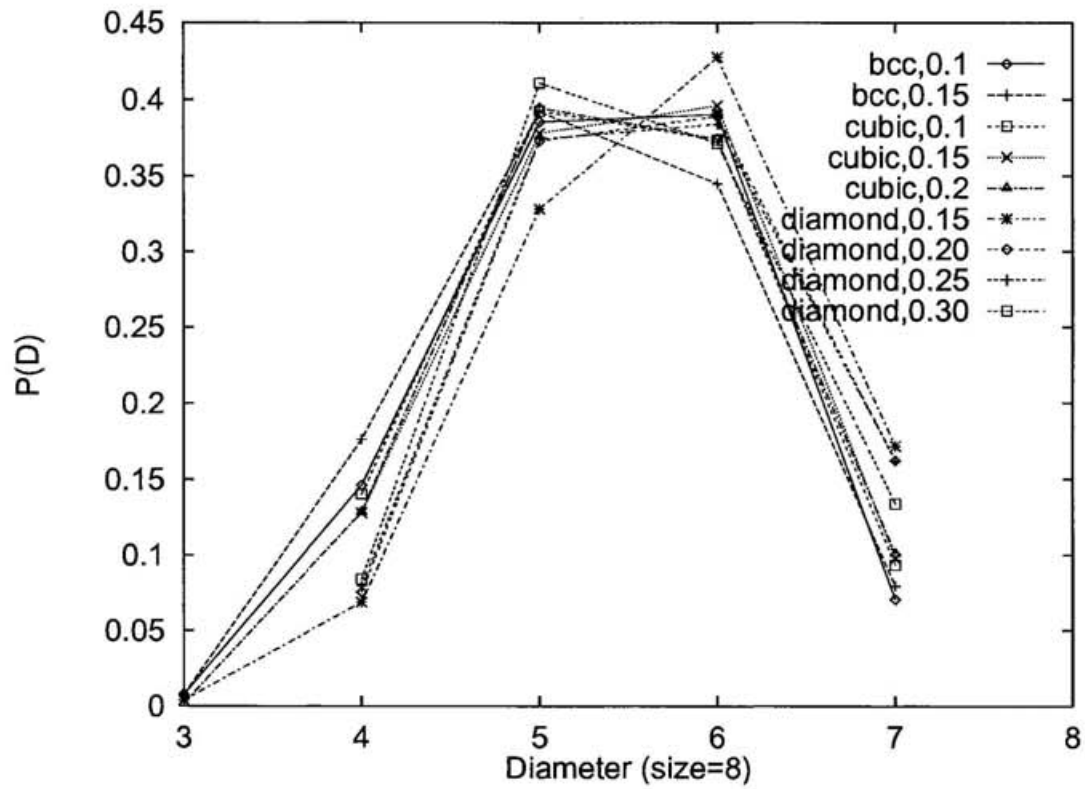


Figure 4.34: The diameter distribution of the size=8 cluster in random bond lattice model with various lattices.

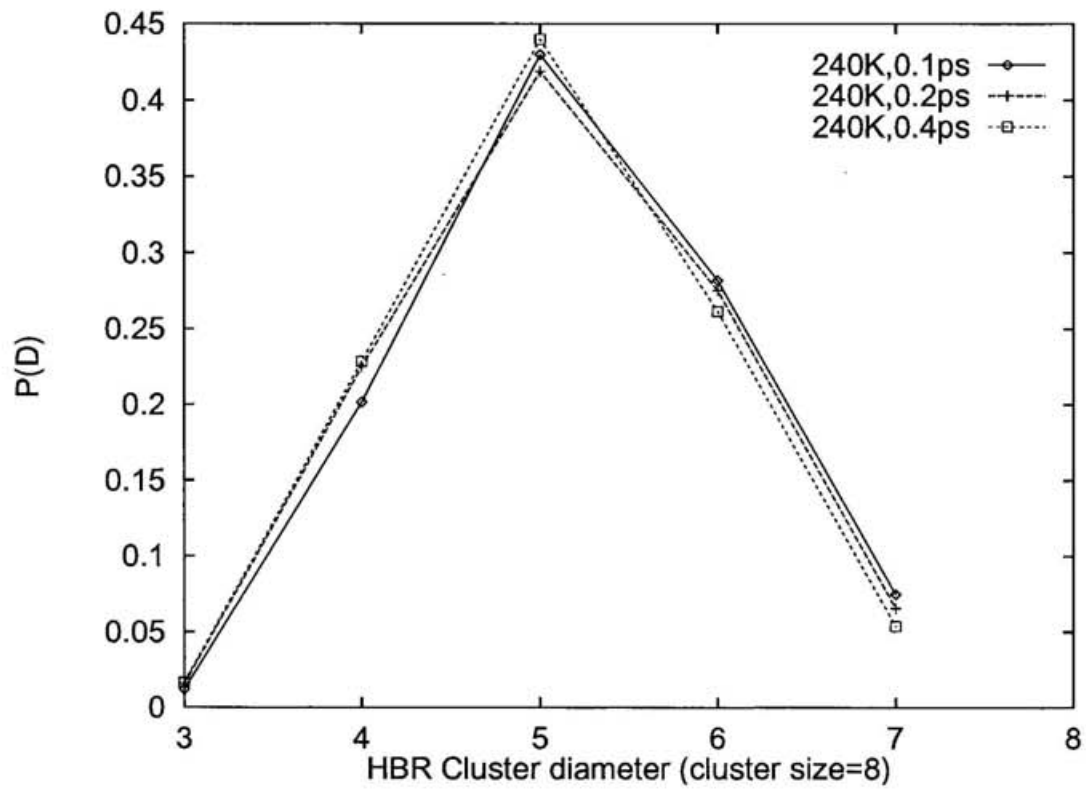


Figure 4.35: The diameter distribution of the α_8 -clusters in liquid water. Temperature and Δt are labeled in the graph.

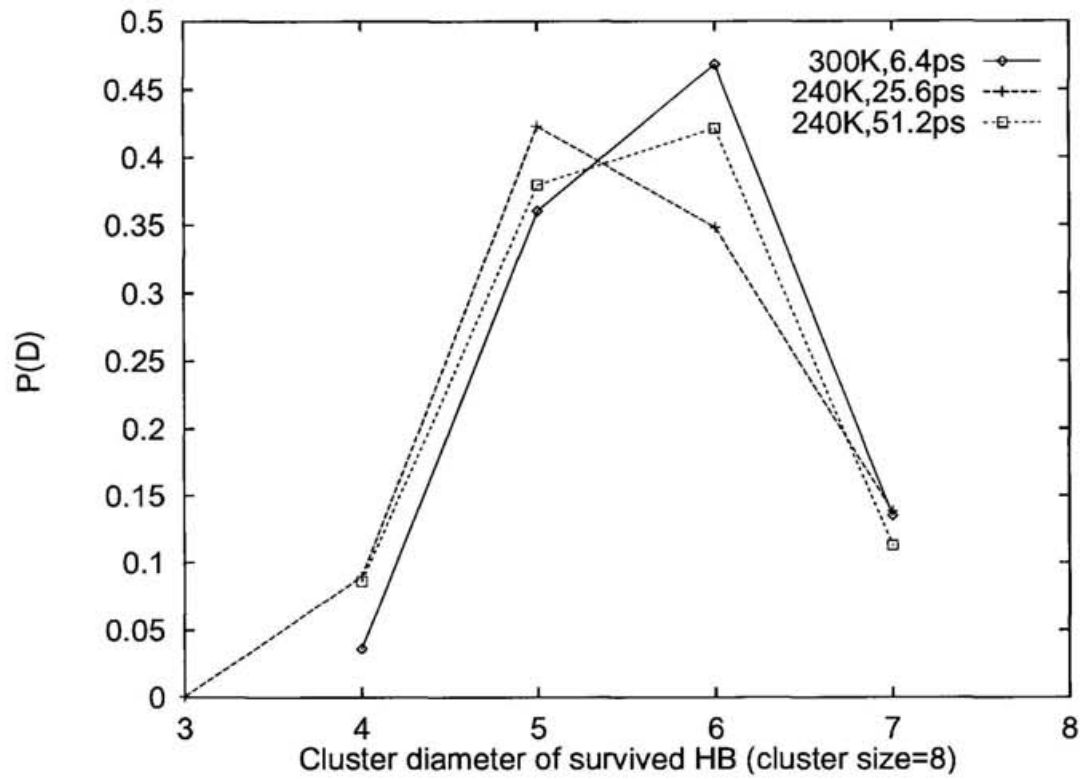


Figure 4.36: The diameter distribution of the σ_8 -clusters in liquid water. Temperature and Δt are labeled in the graph.

Chapter 5

Conclusions

In this thesis, the topological randomness in liquid water was examined in terms of distortion in hydrogen bond network and the dynamics of hydrogen bond network rearrangement was analyzed by network topology. A number of topological and dynamical indices were introduced and the correlations between them were carefully examined. We have shown that there exist characteristic correlations in the local structure and its change. The local rule of the hydrogen bond network rearrangement led naturally to a new concept of defects. Based on the local rule, the lattice dynamic model was created and various dynamic properties of the hydrogen bond network were reproduced by the model.

If enough correlations are known, the dynamics of a system can be represented in terms of correlations. (The representation is not necessary to be deterministic. Perfectly probabilistic representation can be a choice, if it is simple enough.) The basis for the correlation function can be arbitrarily chosen. An appropriate choice of the basis reduces uncertainty with low-order approximation. The spatial correlation of liquid is generally well approximated by the radial distribution function, while the van Hove function provides us with rich information of spatiotemporal correlations. But they are not necessarily the best choice. The topological indices are another choice for the dynamic network system like liquid water because multi-body correlations are easily included.

How can we predict the motion of a molecule? One extreme case is the deterministic description; full variables are traced and no ambiguity is left in time axis. The state

of a system at any time is described by the variables. The other extreme case is the expression by the time development of one variable; any information of motion is convoluted in the time correlation function of the variable. In the experiments, as it is easier to raise the time resolution than the scale resolution, many information is served in the spectral form. In the computer simulation, however, we can choose any level between the extremes. The deterministic description is too fine to treat the whole output at once. we need not predict the far future precisely in such a strongly chaotic system like liquid water. Comprehensibility is attainable by reducing variables. It is rather desirable to denote moderate future by moderately small number of variables. The spatial correlation is rather intelligible than the time correlation because the spatial correlation can be recognized as a pattern. It is therefore desirable to leave complexity in spatial correlations and make the time correlations simpler.

There are a lot of layers between order and disorder in physical phenomena. Both the perfect disorder and the perfect order are nothing but the perfect boredom. The complexity of a system should therefore be defined as the number of independent correlations in the system.

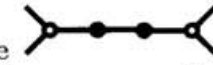



In this thesis, the short time and short range correlations are extracted from MD results and realized in the lattice model, which is Markovian in time. Larger scale and longer time correlations, however, still remain unknown. Extracting the higher order correlation will draw more strict sketch of the hydrogen bond network dynamics in liquid water.

Appendix A

Defect Motion on Sparse Network

In liquid water, coordination number of each molecule is fairly smaller than simple liquid. Let us suppose the case that hydrogen bond network is more sparse. Such a case may correspond to water in stretched or much supercooled state, where the number of adjacent molecules is smaller.

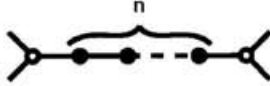
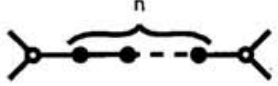
If each node has less than 6 adjacency bonds (in digraphic expression), the undirected graph consists of $z_a = 2$ and $z_a = 3$ seminodes. All possible motion along the $z_a = 2$ and $z_a = 3$ seminodes are shown in Fig. A.1. In any case, a defect cannot pass through the $z_a = 2$ seminode. Increasing the number of $z_a = 2$ seminodes will cause segmentation of the wandering region of defects.

Here we indicate that the two graphs are identical; the graph with $z=2$ and $z=3$ nodes, and the graph with all $z=3$ nodes and two kinds of bonds. The percolation threshold can be calculated as well. The node with 2 bonds ($z=2$) is represented by black circle \bullet and the node with 3 bonds ($z=3$) by white circle \circ , respectively. The chain of black circle  can be replaced by a “defect-opaque” bond represented by a wave line . With the replacement, network is reconstructed from all $z=3$ nodes and opaque  and transparent  bonds. Total number of nodes is N and the ratio of black circle is p_2 . The ratio of white circle \circ becomes $p_3 = 1 - p_2$, then total number of bonds is $\frac{N}{2}(3 - p_2)$. Choose a node in a random manner. The probability

that the node you choose is black \bullet and two adjacent nodes are both white \circ is

$$p_2 \cdot p_3^2. \quad (\text{A.1})$$

We define n -chain as the linear chain composed by n connected black nodes and termi-

nated both end with two white nodes, ie . In the same manner, the probability that the node you choose is one of n -chain  is


$$n p_2^n p_3^2. \quad (\text{A.2})$$

Each n -chain includes $n + 1$ bonds. Total number of bonds included in the chain is

$$N \cdot 2p_2p_3^2 + N \cdot 3p_2^2p_3^2 + \cdots + N(n+1)p_2^n p_3^2 + \cdots = N(1+p_3)p_2, \quad (\text{A.3})$$

On the other hand, total number of chains is

$$N \cdot p_2p_3^2 + N \cdot p_2^2p_3^2 + \cdots + Np_2^n p_3^2 + \cdots = Np_3p_2. \quad (\text{A.4})$$


If each chain is replaced by an “opaque” bond , total number of bonds reduces to

$$\frac{N}{2}(3-p_2) - N(1+p_3)p_2 + Np_2p_3, \quad (\text{A.5})$$

while the ratio of the opaque bond  against total number of bonds becomes

$$\frac{Np_2p_3}{\frac{N}{2}(3-p_2) - N(1+p_3)p_2 + Np_2p_3} = \frac{2}{3}p_2. \quad (\text{A.6})$$

Network with black circles is reconstructed to the network with opaque bonds at last.

For example, the bond percolation threshold of the $z_a = 3$ network is $p_C = 0.6527$ for honeycomb lattice and $p_C = 0.6666$ for Bethe lattice. When the transparent bond  percolates, defect disclosed. The critical ratio of black circle is

$$p = 1 - \frac{2}{3}p_2 > p_C \cong \frac{2}{3}, \quad (\text{A.7})$$

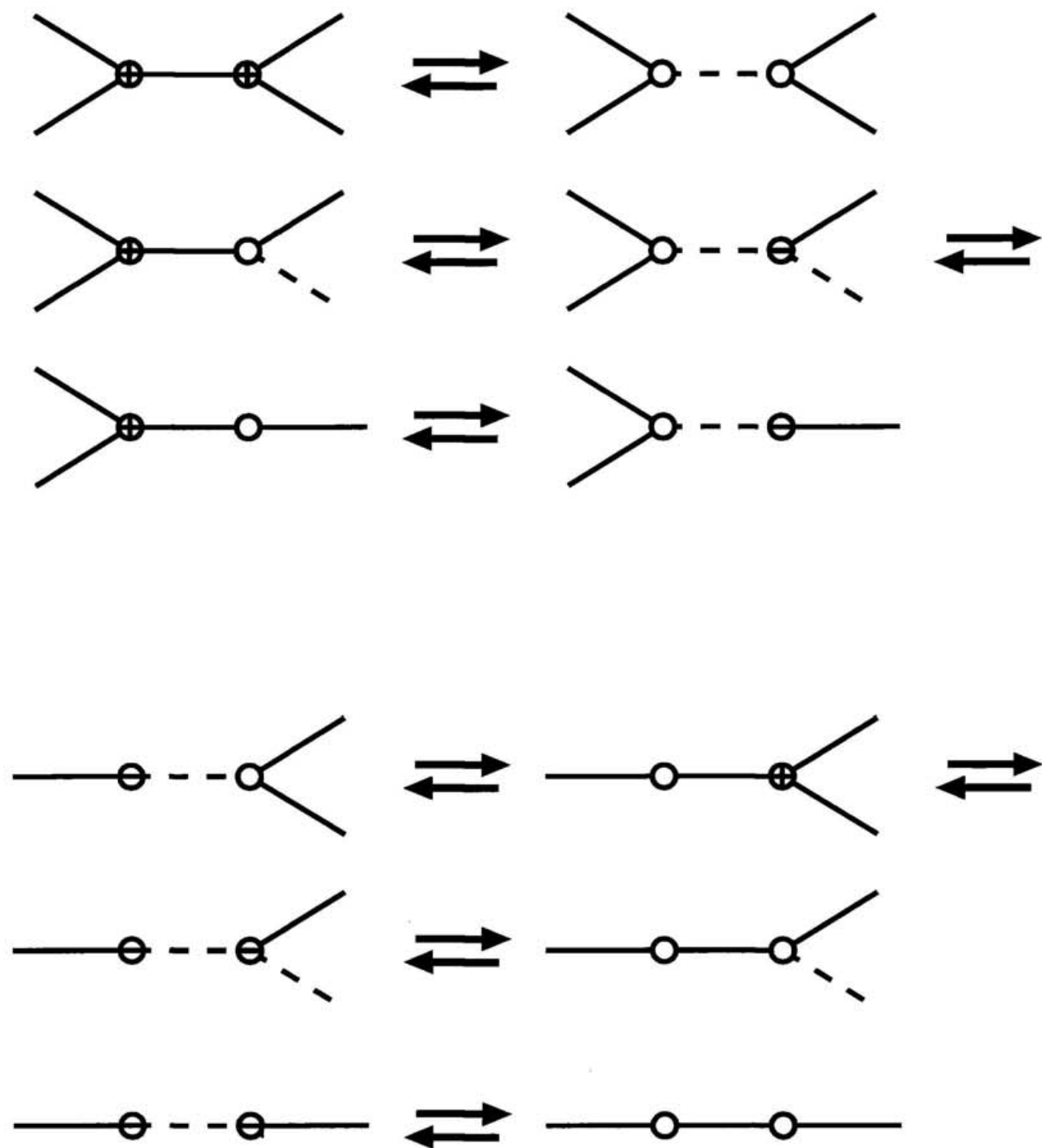


Figure A.1: Possible motions of a defect on the network. The oversatisfied defect seminode, dissatisfied defect seminode, normal seminode, hydrogen edge, and adjacency edge are indicated by a \oplus circle, a \ominus circle, a white circle, solid line, and dashed line, respectively.

and that

$$p_2 < 0.5 \tag{A.8}$$

That is, defect is enclosed when the ratio of black circle ● exceeds that of white node ○ .

Appendix B

Heterogeneity Index

The heterogeneity index of random events occur on the network is calculated as follows. Suppose there are N bonds in the system. The i th event occurs at a randomly chosen bond. It is convenient to define the variable $x_i(a)$, which is 1 if an event occurs at the bond a at i th trial.

After n trials, average occurrence of events at a bond is simply denoted as

$$\bar{m}_n(a) = \sum_{i=1}^n x_i(a) = \frac{n}{N}. \quad (\text{B.1})$$

Spatial fluctuation of the occurrence of events is evaluated by the dispersion as:

$$\begin{aligned} \sigma_n^2 &= \frac{1}{N} \sum_{a=1}^N \left(\sum_{i=1}^n x_i(a) - \frac{n}{N} \right)^2 \\ &= \left\langle \left(\sum_{i=1}^n \left(x_i(a) - \frac{1}{N} \right) \right)^2 \right\rangle \\ &= \left\langle \sum_{i=1}^n \left(x_i(a) - \frac{1}{N} \right) \cdot \sum_{j=1}^n \left(x_j(a) - \frac{1}{N} \right) \right\rangle \\ &= \left\langle \sum_{i=1}^n \left(x_i(a) - \frac{1}{N} \right)^2 + 2 \sum_{i=1}^n \sum_{i \neq j}^n \left(x_i(a) - \frac{1}{N} \right) \left(x_j(a) - \frac{1}{N} \right) \right\rangle, \end{aligned}$$

where the second term of the last formula becomes 0 because each event is independent.

$$\begin{aligned} &= \left\langle \sum_{i=1}^n \left(x_i(a)^2 - 2 \cdot x_i(a) \cdot \frac{1}{N} + \frac{1}{N^2} \right) \right\rangle \\ &= \left\langle \frac{n}{N} - 2 \cdot \frac{n}{N} \cdot \frac{1}{N} + \frac{n}{N^2} \right\rangle \\ &= n \cdot \frac{1}{N} \left(1 - \frac{1}{N} \right) \end{aligned} \quad (\text{B.2})$$

It comes that $\frac{\sigma_n}{\bar{m}_n}$ is proportional to time $n^{-\frac{1}{2}}$. While if the events does not occur fairly in space, $\bar{m}_n(a)$ differs for each bond and that $\frac{\sigma_n}{\bar{m}_n}$ converge to non-zero value after a long time.

Appendix C

Simulation Methods and Algorithms

In this section, some useful algorithms and programs are explained.

C.1 Voronoi Polyhedra Tessellation

Suppose there is a set S consists of N sites $\{p_1 \cdots p_N\}$. Here the procedure to determine the Voronoi polyhedra is sketched.

1. Each vertex of the Voronoi polyhedron is equidistance r to four “constructor” sites, $\{p_i, p_j, p_k, p_l\}$. When the sphere at vertex v with radius r is denoted by $S(v)$, no other site should exist in the $S(v)$. When four sites are arbitrarily chosen, a vertex v is determined algebraically. If the $S(v)$ does not include any other sites, v is a Voronoi vertex. All Voronoi vertices are stored with its coordinate and label of four constructor sites.
2. Each edge of the Voronoi polyhedron is terminated by a pair of Voronoi vertices which has three common constructor sites. All edges are stored with the label of two terminator vertices and three three constructor sites.
3. Each face of the Voronoi polyhedron is enclosed by several edges which has two common constructor sites. All faces are stored with the label of two constructor

sites, list of enclosing edges in cyclic order, and the distance from the face to a constructor.

4. The Voronoi polyhedra $V(p)$ is made of the set of Voronoi faces with common constructor site p .

The volume of a Voronoi polyhedron is now easily calculated. Note that if the density is too low, or the sites are too much clustered, a site sometimes form Voronoi face with itself in the image cells under the periodic boundary condition. In addition, small edges or faces are sometimes reduced to a vertex to clarify the outline shape of the polyhedron.

C.2 Voronoi Grid Tessellation

It is sometimes convenient to take statistics in partial system rather than the whole system. Instantaneous physical properties of the partial system is given by averaging them over the molecules in the partial system. The number of the molecules in the partial system, however, alters time by time and that the time dependence of the property cannot be determined uniquely. Moreover, if the cell size of partial system is smaller than unit volume, the cell sometimes becomes empty. To avoid such trouble, the content ratio c_i of a molecule i in the small partial system is defined in terms of Voronoi polyhedra as

$$c_i = \frac{\text{Partial volume of the Voronoi polyhedron of the molecule } i \text{ included in the system}}{\text{Volume of the Voronoi polyhedron of the molecule } i}. \quad (\text{C.1})$$

When a molecule come into the cell, c_i continuously grows from 0 to 1.

The local average of a physical quantity X , defined per a molecule, is then easily defined with c_i as

$$\langle X \rangle = \frac{\sum_N X_i c_i}{\sum_N c_i}, \quad (\text{C.2})$$

where summation is performed over all molecules.

Partial Voronoi polyhedron is defined as the intersection of the cell of the partial system and the Voronoi polyhedron. The shape of the cell is usually a convex polyhe-

dron. As the Voronoi polyhedron is always convex, the intersection also becomes a convex polyhedron.[PI 85]

Practically, the intersection convex polyhedron is simply attained by the following procedure:

1. Pick up the all vertices, edges and faces concerned with the Voronoi polyhedra $V(p)$.
2. Consider a set of sites which are mirror images of the site p by each face of the cell, *ie* each face of the cell bisects one of the additional sites and site p .
3. Intersection of the Voronoi polyhedron and the convex cell is attained by adding these additional constructor sites and remake the list of Voronoi elements (*ie* vertices, edges, and faces).

By keeping the whole list of vertices, edges, and faces of the original Voronoi polyhedron $V(p)$, this procedure can be executed by only a few additional calculations.

C.3 Number of n-rings in the Network

The number of ring in the network is sometimes useful order parameter (e.g. melting of ice). Here we introduce an algorithm to count the number of ring in the network by algebraic method.

The number of 3-member ring in the network is algebraically given by the following theorem.[T 89]

Theorem: When the adjacency matrix of graph G is expressed as A , the total number of triangles made of edges in G is equal to

$$\frac{1}{6}\text{tr}(A^3), \quad (\text{C.3})$$

where $\text{tr}(A^3)$ denotes the sum of the diagonal element of A^3 .


The i th diagonal element, say $a_{ii}^{(3)}$, of A^3 denotes the number of cyclic paths starting from the node i and return to i after 3 hops along the network. By summing up $a_{ii}^{(3)}$, each triangle is counted 6 times, because there are three start points and two directions for counting one triangle cyclic path, say “3-cycle”.



The number of 4- or 5-membered ring can be counted up in a somehow complex way. Here we show the procedure to count the number of 4- or 5-membered rings in which the specified node belongs, instead of total number of 4- or 5-membered rings.

• Four membered rings

The total number of 4-cycle is counted with $\text{tr}(A^4)$ in the same way as the number of triangles. The number of 4-ring is taken by subtracting the number of reduced quadrilaterals from the total 4-cycles. There are two types of reduced quadrilateral,



and . d_i denotes the adjacency number of the vertex V_i . If the $\{i, j\}$ th element of A^n is denoted by $a_{ij}^{(n)}$, d_i is equal to $a_{ii}^{(2)}$.

The number of reduced 4-cycles passing the initial vertex V_i two times is d_i^2 , which includes both  and . On the other hand, the number of reduced 4-cycles that passes the initial vertex only once is

$$\sum_{a.v.} (d_j - 1), \quad (\text{C.4})$$

where the summation is performed over the adjacent vertices of V_i .



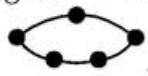
The number of 4-ring is thus expressed by elements of adjacency matrix as

$$N = (a_{ii}^{(4)} - d_i^2 - \sum_{a.v.} (d_j - 1))/2, \quad (\text{C.5})$$


where the last 2 indicates the symmetry.



• Five membered rings



The total number of 5-cycle is counted with $\text{tr}(A^5)$, but it also counts the number of





the whiskered triangles  and the heavy triangles  other than the right pentagon .

Here we enumerate all cases that a vertex belongs to a 5-cycle. White circle denotes the initial vertex.

Case 1; the initial vertex is on the the right 5-ring  :
Symmetry number is 2.


Case 2; the initial vertex is a quadruply connected vertex of the whiskered triangle  or the heavy triangle  :

The path of 3-cycle  and 2-cycle  can be chosen independently.

The number of  passing the vertex V_i is $a_{ii}^{(3)}/2$, while the number of  is $a_{ii}^{(2)}$. Thus the total number of  and  is


$$\frac{a_{ii}^{(3)} \cdot a_{ii}^{(2)}}{2}. \tag{C.6}$$

Symmetry number is 4.

Case 3; The initial vertex is on the triangle of the whiskered triangle  :
The whisker grows from a adjacent vertex of the initial vertex. Therefore, the number of the whiskered triangle is

$$\sum_{a.v.} [a_{ij}^{(2)} \cdot (a_{jj}^{(2)} - 2)]. \tag{C.7}$$


Symmetry number is 2.

Case 4; The initial vertex is on the doubly connected vertex of the heavy triangle  :

The total number of the heavy triangle is the same as the number of normal triangle in this case, thus

$$\frac{a_{ii}^{(3)}}{2} \tag{C.8}$$

Symmetry number is 2.

Case 5; The initial vertex is on the whisker of the whiskered triangle  :

The total number of the whiskered triangle is counted by summing up the total number of the triangles, which are passing an adjacent vertex of the initial vertex but not passing the initial vertex.

$$\sum_{a.v.} \left[\frac{a_{jj}^{(3)}}{2} - a_{ij}^{(2)} \right] \quad (C.9)$$

Symmetry number is 2.

Here the symmetry number is the number of route passing all the vertex of the polygon.

The number of 5-ring is given by subtracting the number of these reduced polygons from $a_{ii}^{(5)}$:

$$N = \frac{a_{ii}^{(5)} - 4 \cdot \frac{a_{ii}^{(3)} \cdot a_{ii}^{(2)}}{2} - 2 \sum_{a.v.} [a_{ij}^{(2)} \cdot (a_{jj}^{(2)} - 2)] - 2 \cdot \frac{a_{ii}^{(3)}}{2} - 2 \sum_{a.v.} \left[\frac{a_{jj}^{(3)}}{2} - a_{ij}^{(2)} \right]}{2} \quad (C.10)$$

The number of larger rings can be counted in a similar way. As you can guess, however, the way to count 6- or higher membered ring is too complex.¹

C.4 Block Diagonalization of the matrix

In the network analysis, it is important to know the network connectivity. For example, the size distribution of connected graph in the percolative system show us the existence of spatial correlation.

¹In the real analysis of the hydrogen bond network, this algorithm is not useful by some reason. First, the definition of the number of n -ring is not independent to the number of $n-1$ -ring, *ie* the n -ring should not be the composition of n' -ring and n'' -ring. Therefore, we must mark from small ring to large ring checking not to count then twice. Second, as the system is not so large, larger ring sometimes go across the periodic boundary. To avoid this, the coordinate as well as the topology of the network should be in mind.

The simplest way to separate the disconnected graph into connected clusters is to multiply the adjacency matrix many times. $a_{ij}^{(\infty)}$ is non-zero if the vertices i and j are connected, *ie* there is more than one path between node i and j , and is zero if not connected.

However, this algorithm takes much time by the order of $O(N^4)$, where N stands for the total number of vertices, since it includes multiplication of matrix. In addition, if an edge is added to or removed from the graph, we must perform the whole protocols again.

We here introduce the progressive construction method. This method is useful especially when treating dynamically reconstructing network.

This method is based on the following facts:

- Addition of an edge affects the connectivity of at most two clusters to which the terminal vertices belong.
- Removal of an edge divides the cluster to which the edge belongs into at most two fragments.

The procedure is

1. Number all vertices. A connected graph (cluster) is identified by the lowest label of the composing vertices. Each vertex V_i has an attribute of ID of the cluster to which it belongs, g_i . If there is no bond between nodes, g_i is identical to i .
2. If an edge is added between vertices V_i and V_j , compare g_i and g_j and align all g of the vertices in the two groups to the lowest value. This requires time proportional to average cluster size, which is usually independent to N for random bond lattice model.
3. If an edge is removed from a cluster, the cluster may be divided into two fragments. Connection matrix of the fragments is made by repeating step 2 again and again. This requires time proportional to square average cluster size, but independent to N .

Consequently, this algorithm only takes of order $O(N)$ to construct the whole network.

C.5 Visualization

Computer graphics technology helps us to understand the informations embedded in the structure. According to the study on pattern recognition, human sight can detect the difference of two textures where the second order statistical values² are different. It is more sensitive for localized mobile patterns. Such an intuition is sometimes useful, because we have only a few tools to sift out localized motions in space and time, like wavelet transformation.

The following serves as an example:

The density fluctuation in liquid water is easily understood by visualizing the cavity distribution. Fig. C.1 is made from a snapshot of the system with 216 water molecules at 298K, by coloring the unoccupied space. Each water molecule is simply expressed by a sphere with a radius of 2.5Å. There is a large cavity in the middle of the cell. Such cavities are also visualized as the contour surface of the distance field

$$\phi(\mathbf{r}) = \min |\mathbf{r} - \mathbf{r}_i|, \quad (\text{C.11})$$

where \mathbf{r}_i is the position of i th molecule.

Another way to visualize the density fluctuation is exemplified here. In Fig. C.2, the Voronoi polyhedra whose volume more than 120% or less than 83% of the average volume are shown. Total number of molecules in the system is 216. The molecules with large local volume are gathering. The time dependence of the local volume is discussed in Section 4.2.1.

²Statistical values (average, standard deviation, etc.) of two-point correlations(distance, difference of the density, etc.)

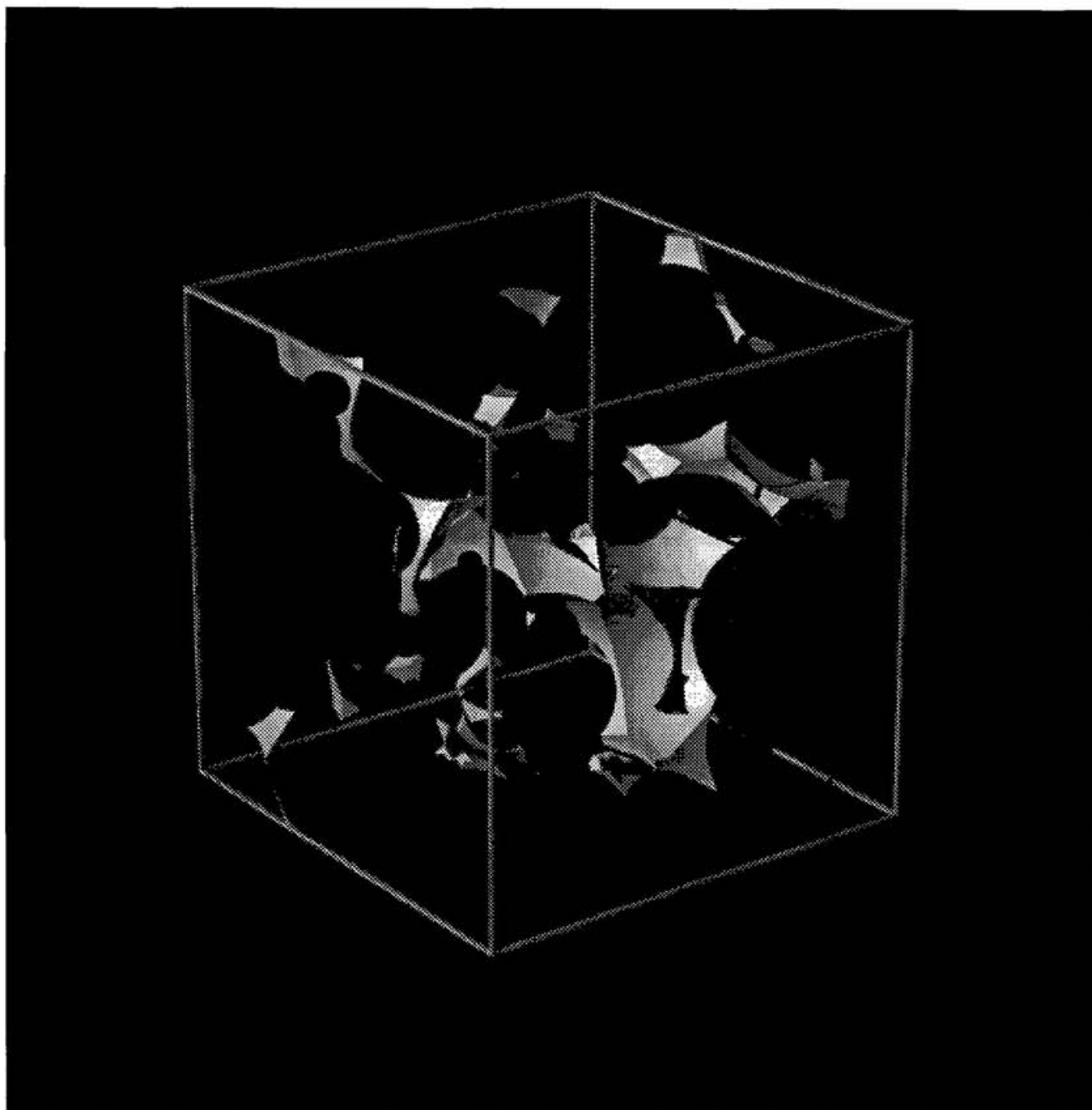


Figure C.1: The cavity in liquid water is visualized. Spherical regions with radii= 2.5\AA , which represent the volume occupied by water molecules, are cut out from the simulation cubic cell and the left unoccupied volume is colored.

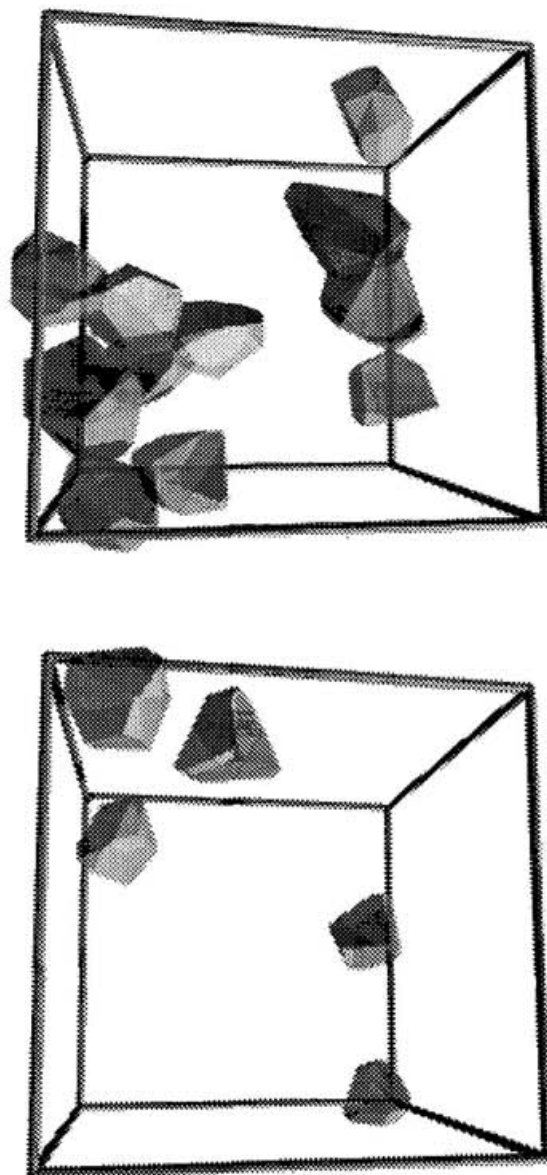


Figure C.2: The local density is indicated by the Voronoi polyhedra. Upper: the polyhedra whose volume is more than 120% of the average value; lower: those smaller than 83%. The two figures are drawn from the same configuration. The configuration is taken from the quenched structure from 298K. The number of water molecules is 216.

Bibliography

- [A 80] H.C. Andersen, *J. Chem. Phys.*, **72**, 2384 (1980)
- [A 82] C.A. Angell, *Water: A Comprehensive Treatise Volume 7 "Water and Aqueous Solutions at Subzero Temperatures"* edited by F. Franks, , (1982)
- [A 93] C.A. Angell, *J. Phys. Chem.*, **97**, 6339 (1993)
- [AR 84] C.A. Angell and V. Rodger, *J. Chem. Phys.*, **80**, 6245 (1984)
- [AS 90] J.E. Adams and R.M. Stratt, *J. Chem. Phys.*, **93**, 1332 (1990)
- [AST 73] C.A. Angell, J. Shuppert, and J.C. Tucker, *J. Phys. Chem.*, **77**, 3092 (1973)
- [B 64] J.D. Bernal, *Proc. Roy. Soc.*, **A280**, 299 (1964)
- [B 72] G.M. Bell, *J. Phys. C*, **5**, 889 (1972)
- [B 78] S.W. Benson, *J. Am. Chem. Soc.*, **100**, 5640 (1978)
- [BF 33] J.D. Bernal and R.H. Fowler, *J. Chem. Phys.*, **1**, 515 (1933)
- [BGWH 86] J.P. Bergsma, B.J. Gertner, K.R. Wilson, and J.T. Hynes, *J. Chem. Phys.*, **86**, 1356 (1986)
- [BL 70] G.M. Bell and D.A. Lavis, *J. Phys. A*, **3**, 427 (1970)
- [BR 87] A.C. Belch and S.A. Rice, *J. Chem. Phys.*, **86**, 5676 (1987)
- [BS 76] G.M. Bell and D.W. Salt, *Trans. Faraday Soc. II*, **72**, 76 (1976)
- [BSGM 84] R.L. Blumberg, H.E. Stanley, A. Geiger, and P. Mausbach, *J. Chem. Phys.*, **80**, 5230 (1984)
- [BTS 81] L. Bosio, J. Teixeira, and H.E. Stanley, *Phys. Rev. Lett.*, **46**, 597 (1981)

- [CFSOS 94] M. Cho, G.R. Fleming, S. Saito, and I. Ohmine, R.M. Stratt, *J. Chem. Phys.*, **100**, 6672 (1994)
- [CFW 81] J.N. Cape, J.L. Finney, and L.V. Woodcock, *J. Chem. Phys.*, **75**, 2366 (1981)
- [CPJ 89] J.Y. Cavaille, J. Perez, and G.P. Johari, *Phys. Rev. B*, **39**, 2411 (1989)
- [CT 59] M.H. Cohen and D. Turnbull, *D.J. Chem. Phys.*, **31**, 1164 (1959)
- [DME 92] J. Dings, J.C.F. Michielsen, and J. van der Elsken, *Phys. Rev. A*, **45**, 5731 (1992)
- [EK 83] R. Elber and M. Karplus, *Chem. Phys. Lett.*, **87**, 2833 (1983)
- [EK 87] R. Elber and M. Karplus, *Science*, **235**, 318 (1987)
- [F 58] H.S. Frank, *Proc. Roy. Soc.*, **A247**, 481 (1958)
- [F 70] J.L. Finney, *Proc. R. Soc. London, Ser. A*, **319**, 479 (1970)
- [F 72a] F. Franks, *Water: A Comprehensive Treatise Volume 1 "The Physics and Physical Chemistry of Water" edited by F. Franks*, , (1972)
- [F 72b] H.S. Frank, *in Ref. [F 72a]*, , 515 ()
- [FIG 74] P.D. Flemming III and J.H. Gibbs, *J. Stat. Phys.*, **10**, 157 (1974)
- [FW 57] H.S. Frank and W.-Y. Wen, *Discussions Faraday Soc.*, **24**, 133 (1957)
- [G 71] C.W. Gear, *The numerical initial value problem of ordinary differential equations; Prentice Hall: Englewood Cliffs*, , (1971)
- [G 86] E. Grunwald, *J. Am. Chem. Soc.*, **108**, 5719 (1986)
- [G 87] P.A. Giguère, *J. Chem. Phys.*, **87**, 4835 (1987)
- [G79] M.J. Gillan, *Mol. Phys.*, **38**, 1781 (1979)
- [GBWLH 86] B.J. Gertner, J.P. Bergsma, K.R. Wilson, S. Lee, and J.T. Hynes, *J. Chem. Phys.*, **86**, 1377 (1986)
- [GLS 86] J.L. Green, A.R. Lacey, and M.G. Sceat, *J. Phys. Chem.*, **90**, 3958 (1986)
- [GLS 88] J.L. Green, A.R. Lacey, and M.G. Sceat, *J. Phys. Chem.*, **90**, 2958 (1988)
- [GS 82] A. Geiger and H.E. Stanley, *Phys. Rev. Lett.*, **49**, 1749 (1982)

- [GSR 79] A. Geiger, F.H. Stillinger, and A. Rahman, *J. Chem. Phys.*, **70**, 4185 (1979)
- [GWH 88] B.J. Gertner, K.R. Wilson, and J.T. Hynes, *J. Chem. Phys.*, **90**, 3537 (1988)
- [H 63] J. Hallett, *Proc. Phys. Soc., London*, **82**, 1046 (1963)
- [H 83] C.-K. Hu, *J. Phys. A*, **16**, L321 (1983)
- [H 92] F. Hirata, *J. Chem. Phys.*, **96**, 4619 (1992)
- [HA 78] I.M. Hodge and C.A. Angell, *J. Chem. Phys.*, **68**, 1363 (1978)
- [HR 79a] C.S. Hsu and A. Rahaman, *J. Chem. Phys.*, **70**, 5234 (1979)
- [HR 79b] C.S. Hsu and A. Rahaman, *J. Chem. Phys.*, **71**, 4974 (1979)
- [HR 81] F. Hirata and P.J. Rossky, *Chem. Phys. Lett.*, **83**, 329 (1981)
- [HRP 83] F. Hirata, P.J. Rossky, and B.M. Pettitt, *J. Chem. Phys.*, **78**, 4133 (1983)
- [HS 76] J.B. Hasted and M. Shashidi, *Nature*, **262**, 777 (1976)
- [HS 90] D.E. Hare and C.M. Sorensen, *J. Chem. Phys.*, **93**, 25 (1990)
- [HS 93] T.H. Head-gordon and F.H. Stillinger, *J. Chem. Phys.*, **98**, 3313 (1993)
- [J 93] G.P. Johari, *J. Chem. Phys.*, **98**, 7324 (1993)
- [JCMIK 83] W.L. Jorgensen, J. Chandrasekhar, J.D. Madura, R.W. Impey and M.L. Klein, *J. Chem. Phys.*, **79**, 926 (1983)
- [JHM 90] G.P. Johari, A. Hallbrucker, and E. Mayer, *J. Chem. Phys.*, **92**, 6742 (1990)
- [KH88] M. Kinoshita and M. Harada, *Mol. Phys.*, **65**, 599 (1988)
- [KL94] M. Kinoshita and F. Lado, *Mol. Phys.*, **83**, 351 (1994)
- [KT 95] K. Koga and H. Tanaka, *in press*, , (1995)
- [L68] F. Lado, *J. Chem. Phys.*, **49**, 3092 (1968)
- [L89] E. Lomba, *Mol. Phys.*, **68**, 87 (1989)
- [LC96] A. Luzar and D. Chandler, *Nature*, **379**, 55 (1996)
- [LDC 94] R. Lamanna, M. Delmelle, and S. Cannistraro, *Phys. Rev. E*, **49**, 2841 (1994)

- [LH 82] E.W. Lang and H.-D. Lüdemann, *Angew. Chem., Int. Ed. Engl.*, **21**, 315 (1982)
- [LMD 91] J.K. Labanowski, I. Motoc, and R.A. Dammkoehler, *Computers Chem.*, **15**, 47 (1991)
- [LMV85] S. Labik, A. Malijevsky, and P. Vonka, *Mol. Phys.*, **56**, 709 (1985)
- [LR 93] J.-C. Li and D.K. Ross, *Nature*, **365**, 327 (1993)
- [LS 86] R.A. LaViolette and F.H. Stillinger, *J. Chem. Phys.*, **85**, 6027 (1986)
- [MBCLT 93] M.-C. Bellissent-Funel, K.F. Bradley, S.H. Chen, J. Lal, and J. Teixeira, *Physica A*, **201**, 277 (1993)
- [MHT 92] K. Mizoguchi, Y. Hori, and Y. Tominaga, *J. Chem. Phys.*, **97**, 1961 (1992)
- [MKP 81] P.H.E. Meijer, R. Kikuchi, and P. Papon, *Physica A*, **109**, 365 (1981)
- [MKvR 82] P.H.E. Meijer, R. Kikuchi, and E. van Royen, *Physica A*, **115**, 124 (1982)
- [MSG 87] P. Mausbach, J. Schnitker, and A. Geiger, *J. Tech. Phys.*, **28**, 67 (1987)
- [MW 38] J. Morgan and B.E. Warren, *J. Chem. Phys.*, **6**, 666 (1938)
- [N 84] S. Nosé, *Mol. Phys.*, **52**, 255 (1984)
- [N 88] A.J. Noest, *Phys. Rev. B*, **38**, 2715 (1988)
- [NK 91] W. Nadler and T. Krausche, *Phys. Rev. A*, **44**, R7888 (1991)
- [NS 62] G. Némethy and H.A. Sheraga, *J. Chem. Phys.*, **36**, 3382 (1962)
- [NY 86] S. Nosé and F. Yonezawa, *J. Chem. Phys.*, **84**, 1803 (1986)
- [O 86] I. Ohmine, *J. Chem. Phys.*, **85**, 3342 (1986)
- [O 95] I. Ohmine, *J. Phys. Chem.*, **99**, 6767 (1995)
- [OT 90] I. Ohmine and H. Tanaka, *J. Chem. Phys.*, **93**, 8138 (1990)
- [OT 93] I. Ohmine and H. Tanaka, *Chem. Rev.*, **93**, 2545 (1993)
- [OTW 88] I. Ohmine, H. Tanaka, and P.G. Wolynes, *J. Chem. Phys.*, **89**, 5852 (1988)
- [P 51] J.A. Pople, *Proc. Roy. Soc.*, **A205**, 163 (1951)

- [P 92] P.H. Poole et al., *Nature*, **360**, 324 (1992)
- [PESS 93] P.H. Poole, U. Essmann, F. Sciortino, and H.E. Stanley, *Phys. Rev. E*, **48**, 4605 (1993)
- [PH 87] H.A. Posch and W.G. Hoover, *J. Chem. Phys.*, **87**, 6665 (1987)
- [PI 85] F. P. Preparata and M. I. Shamos, *Computational Geometry: An Introduction*, (1985)
- [PSES 93] P.H. Poole, F. Sciortino, U. Essmann, H.E. Stanley, *Phys. Rev. E, Stat. Phys. Plasmas Fluids Relat. Interdiscip. Top.*, **48**, 3799 (1993)
- [PSGSA 94] P.H. Poole, F. Sciortino, T. Grande, H.E. Stanley, and C.A. Angell, *Phys. Rev. Lett.*, **73**, 1632 (1994)
- [R 83] D.C. Rapaport, *Mol. Phys.*, **48**, 23 (1983)
- [R 92] K. Romanowska, *Int.J. Quantum Chem.*, **43**, 175 (1992)
- [RH 91] T.P. Radhakrishnan and W.C. Herndon, *J. Phys. Chem.*, **95**, 10609 (1991)
- [RLC 77] J. Rouch, D.C. Lai, and S.H. Chen, *J. Chem. Phys.*, **66**, 5031 (1977)
- [RLCS 86] G.W. Robinson, J. Lee, K.G. Casey, and D. Statman, *Chem. Phys. Lett.*, **123**, 483 (1986)
- [RM 73] D.H. Rasmussen and A.P. McKenzie, *J. Chem. Phys.*, **59**, 5003 (1973)
- [RS 71] A. Rahman and F.H. Stillinger, *J. Chem. Phys.*, **55**, 3336 (1971)
- [RS 73] A. Rahman and F.H. Stillinger, *J. Am. Chem. Soc.*, **95**, 7943 (1973)
- [RSTV 93] G. Ruocco, M. Sampoli, A. Torcini, and R. Vallauri, *J. Chem. Phys.*, **99**, 8095 (1993)
- [RSV 92] G. Ruocco, M. Sampoli, and R. Vallauri, *J. Chem. Phys.*, **96**, 6167 (1992)
- [S 80] F.H. Stillinger, *Science*, **209**, 451 (1980)
- [S 84] R.J. Speedy, *J. Phys. Chem.*, **88**, 3364 (1984)
- [S 90] M. Sasai, *J. Chem. Phys.*, **93**, 7329 (1990)

- [S 93] M. Sasai, *Bulletin Of The Chemical Society of Japan*, **66**, 3362 (1993)
- [S 94] A.K. Soper, *J. Chem. Phys.*, **101**, 6888 (1994)
- [SA 76] R.J. Speedy and C.A. Angell, *J. Chem. Phys.*, **65**, 851 (1976)
- [SAEHPF 94] H.E. Stanley, C.A. Angell, U. Essmann, M. Hemmati, P.H. Poole, and F.Sciortino, *Physica A*, **205**, 122 (1994)
- [SF 89] F. Sciortino and S.L. Fornili, *J. Chem. Phys.*, **90**, 2786 (1989)
- [SGS 91] F. Sciortino, A. Geiger, and H.E. Stanley, *Nature*, **354**, 218 (1991)
- [SGS 92] F. Sciortino, A. Geiger, and H.E. Stanley, *J. Chem. Phys.*, **96**, 3857 (1992)
- [SM 85] R.J. Speedy and M. Mezei, *J. Phys. Chem.*, **89**, 171 (1985)
- [SMJ 87] R.J. Speedy, J.D. Madura, and W.L. Jorgensen, *J. Phys. Chem.*, **91**, 909 (1987)
- [SOR 92] M. Sasai, I. Ohmine, and R. Ramaswamy, *J. Chem. Phys.*, **96**, 3045 (92)
- [SPSH 90] F. Sciortino, P. H. Poole, H.E. Stanley, and S. Havlin, *Phys. Rev. Lett.*, **64**, 1686 (1990)
- [SR 74] F.H. Stillinger and A. Rahman , *J. Chem. Phys.*, **60**, 1545 (1974)
- [SSM 94] J.-P. Shih, S.-Y. Sheu, and C.-Y. Mou, *J. Chem. Phys.*, **100**, 2202 (1994)
- [SSS 93] S. Sastry, F. Sciortino, and H.E. Stanley, *J. Chem. Phys.*, **98**, 9863 (1993)
- [ST 80] H.E. Stanley and J. Teixeira, *J. Chem. Phys.*, **73**, 3404 (1980)
- [SW 82] F.H. Stillinger and T.A. Weber, *Phys. Rev. A*, **25**, 978 (1982)
- [SW 83a] F.H. Stillinger and T.A. Weber, *J. Phys. Chem.*, **87**, 2833 (1983)
- [SW 83b] F.H. Stillinger and T.A. Weber, *Phys. Rev. A*, **28**, 2408 (1983)
- [T 86] M. Tanaka, *J. Phys. Soc. Jpn.*, **55**, 3108 (1986)
- [T 89] T. Takenaka, *Senkeidaisuutekigurafuriron*, , 46 (1989)
- [T 95] H. Tanaka, *to be published*, , (1995)
- [TL 78] J. Teixeira and J. Leblond, *J. Phys. Lett.*, **39**, L83 (1978)

- [TO 87] H. Tanaka and I. Ohmine, *J. Chem. Phys.*, **87**, 6128 (1987)
- [TO 89] H. Tanaka and I. Ohmine, *J. Chem. Phys.*, **91**, 6318 (1989)
- [V 93] T.A. Vilgis, *Phys. Rev. B*, **47**, 2882 (1993)
- [W 47a] H. Wiener, *J. Am. Chem. Soc.*, **69**, 17 (1947)
- [W 47b] H. Wiener, *J. Am. Chem. Soc.*, **69**, 2636 (1947)
- [W 72] G. Walrafen, *Water: A Comprehensive Treatise Volume 1 "The Physics and Physical Chemistry of Water" edited by F. Franks*, , 151 (1972)
- [WC 91] G.E. Walrafen and Y.C. Chu, *J. Phys. Chem.*, **85**, 8909 (1991)
- [WFHW 86] G.E. Walrafen, M.R. Fisher, M.S. Hokmabadi, and W.-H. Yang, *J. Chem. Phys.*, **85**, 6970 (1986)
- [WI 66] J.D. Worley and I.M.Klotz, *J. Chem. Phys.*, **45**, 2868 (1966)
- [WL 88] K. Wilson and R.D. Levin, *Chem. Phys. Lett.*, **152**, 435 (1988)
- [WT 87] M.S. Watanabe and K. Tsumuraya, *J. Chem. Phys.*, **87**, 4891 (1987)
- [XLMHS 93] Y. Xie, K.F. Ludwig, Jr., G. Morales, D.E. Hare, and C.M. Sorensen, *Phys. Rev. Lett.*, **71**, 2050 (1993)